



**National
Oceanography Centre**
NATURAL ENVIRONMENT RESEARCH COUNCIL

National Oceanography Centre

Internal Document No. 12

Airflow distortion at instrument sites on the
RRS *James Clark Ross* during the WAGES project

B I Moat & M J Yelland

2015

National Oceanography Centre, Southampton
University of Southampton Waterfront Campus
European Way
Southampton
Hants SO14 3ZH
UK

Author contact details
Tel: +44 (0)23 8059 7739
Email: ben.moat@noc.ac.uk

© National Oceanography Centre, 2015

DOCUMENT DATA SHEET

AUTHOR MOAT, B I & YELLAND, M J	PUBLICATION DATE 2015
TITLE Airflow distortion at instrument sites on the RRS <i>James Clark Ross</i> during the WAGES project.	
REFERENCE Southampton, UK: National Oceanography Centre, Southampton, 85pp. (National Oceanography Centre Internal Document, No. 12) (Unpublished manuscript)	
ABSTRACT <p>Wind speed measurements obtained from anemometers mounted on ships are prone to systematic errors caused by the distortion of the airflow around the ship's hull and superstructure. This report describes the results of simulations of the airflow around the RRS <i>James Clark Ross</i> made using the computational fluid dynamics (CFD) software VECTIS. The airflow distortion at anemometer sites used during the WAGES project has been quantified at a wind speed of 10 m/s for relative wind directions of 0 (bow-on), 10, 20, 30, 50, 70, 90 and 110 degrees off the bow. The anemometers used in this study were located in the bows of the ship. Temperature sensors were located on the port side of the monkey island.</p> <p>For bow-on flows the anemometers in the bows of the ship experienced relatively small flow distortion. At these sites the flow was decelerated by about 1% of the free stream wind speed. Over the full range of relative wind directions the flow to the R3 sonic is generally accelerated with the largest wind speed biases at flows directly over the beam. The vertical displacement of the airflow increases from around 1 to 2 m for flows directly over the bow, to around 5m for flows over the ships beam as the blockage of the airflow by the ship becomes greater.</p> <p>The airflow distortion at the temperature sensor locations above the monkey island was typically greater than the well-exposed foremast locations. These locations experienced wind speed biases from 6% increase for an airflow directly over the bow, to large decelerations of 55 % when the instruments were in the large recirculation region for flows directly over the starboard side.</p>	
KEYWORDS	
ISSUING ORGANISATION National Oceanography Centre University of Southampton Waterfront Campus European Way Southampton SO14 3ZH UK	
<i>Not generally distributed - please refer to author</i>	

Page intentionally left blank

1. INTRODUCTION	3
2. DESCRIPTION OF THE <i>R.R.S. JAMES CLARK ROSS</i> MODELS	3
3. THE INSTRUMENT LOCATIONS	4
4. CFD RESULTS.....	6
4.1 Introduction	6
4.2 The free stream flow	6
4.3 The vertical displacement and angle of flow at the sensor locations	6
4.4 Wind speed bias	7
5. SUMMARY.....	9
6. ACKNOWLEDGEMENTS.....	13
7. REFERENCES	13
8. FIGURES	14
9. APPENDIX A: Figures showing sections of data on 2-D planes.....	50
10. APPENDIX B: Summary table of results for each wind direction.....	79
11. APPENDIX C: FEMGV and VECTIS commands.	85

LIST OF TABLES

Table 1. Instrument positions in the VECTIS co-ordinate system for a bow-on flow and flows over the starboard side. The z value is the height of the anemometer above the sea surface. A schematic of the locations is shown in Figures 2 and 3.	5
Table 2. Instrument positions in the VECTIS co-ordinate system for effective port flows. The z value is the height of the anemometer above the sea surface. A schematic of the locations is shown in Figures 2 and 3.	5
Table 3. The percentage wind speed bias at the sensor location accounting for the height the airflow was raised (i.e. at height $z - \Delta z$). The values in brackets indicate the wind speed error using a free stream velocity from a location 2 seconds upstream of the anemometer site, i.e. $z - \Delta z_{t=2}$ (after Yelland et al., 2002). A negative relative wind direction indicates a flow over the port side.	10
Table 4. The percentage wind speed bias at the sensor location z . A negative relative wind direction indicates a flow over the port side.	10
Table 5. The variation of the vertical displacement (Δz , meters) with changes in relative wind direction. The values in brackets indicate the vertical displacement at a location 2 seconds upstream of the anemometer site, i.e. $\Delta z_{t=2}$ (after Yelland et al., 2002). A negative relative wind direction indicates a flow over the port side.	11
Table 6. The variation of the angle of the flow to the horizontal (tilt) at the sensor site (degrees). A negative relative wind direction indicates a flow over the port side.	11
Table 7. The variation in the horizontal twist ($\tan^{-1}(v/u)$) of the flow at the sensor site (degrees). A negative twist indicates a flow, which has moved anti-clockwise due to the presence of the ship. A negative relative wind direction indicates a flow over the port side.	12
Table B.1. Summary of the effects of flow distortion. The values in brackets indicate the vertical displacement and the wind speed bias using a vertical displacement calculated from 2 seconds upstream, $\Delta z_{t=2}$, of the anemometer site (after Yelland et al., 2002).	79

AIRFLOW DISTORTION AT INSTRUMENT SITES ON THE *R.R.S. JAMES CLARK ROSS* DURING THE WAGES PROJECT

B. I. Moat and M. J. Yelland

December 2014

1. INTRODUCTION

Wind speed measurements from ship-based anemometers are biased by the distortion of the airflow by the ship's hull and superstructure. For example, previous computational fluid dynamics (CFD) modelling has shown that anemometers located on the foremast platform of the RRS *Charles Darwin* experience a flow distortion of up to 14 % of the freestream or undisturbed wind speed for flows directly over the bow (Yelland et al. 1998). The effect is less severe for wind speed measurements made from the foremast platform of the RRS *Discovery* as the ship is more streamlined in shape (Yelland et al. 2002). This report describes an investigation of the airflow around the *R.R.S. James Clark Ross*. The study used a CFD model to simulate the airflow over the ship in order to quantify the effects of airflow distortion on wind speed measurements made at various instrument sites. Corrections are derived for instrument sites used during the WAGES project between May 2010 and August 2013.

The VECTIS code is described in Section 2 and the WAGES instrument positions are detailed in Section 3. The effects of flow distortion are dependent on the anemometer location and vary with changes in relative wind direction (Yelland et al., 2002). Therefore the airflow over the ship was simulated for flows directly over the bow (a wind direction of 0 degrees), and at 10, 20, 30, 50, 70, 90 and 110 degrees over the starboard bow. Effective anemometer positions were created to enable the wind speed bias for winds over the port bow to be calculated from the VECTIS simulations of the airflow over the starboard bow: since the ship is roughly symmetrical, an instrument position on the starboard side of the ship could be mirrored to an "effective" positions on the port side. The wind speed bias, the angles of deflection of the flow and the vertical displacement of the flow were calculated for all the sensor locations, and the results are discussed in Section 4.

2. DESCRIPTION OF THE *R.R.S. JAMES CLARK ROSS* MODELS

VECTIS (Ricardo, 2013) is a commercial three-dimensional Reynolds Averaged Navier-Stokes solver, which has been used successfully since 1994 to model the airflow over many research ships (Yelland et al. 1998; 2002; Moat and Yelland, 2008). These VECTIS simulations (version 2013.3) only reproduce the steady state mean flow characteristics using the standard k- ϵ (Launder and Spalding, 1974) turbulence closure model to parameterise the turbulence. Except when the anemometer is in the wake of an upstream obstacle, VECTIS simulations of the airflow over detailed ship geometries are accurate to within 2 % (Yelland et al., 2002) for well-exposed anemometer locations on

research ships. The full-scale 3-dimensional geometry is the same as that used in the previous CFD study (Berry et. al. 2001). It was created using the software package FEMGV (Version 7.2 - TNO Diana, 2010). The geometry was exported from FEMGV in ABAQUS format and converted into a VECTIS surface definition file using VECTIS translators (APPENDIX B). The numerical representation of the geometry was very detailed (Figure 1) and reproduced the actual geometry to within 0.1 m. The general ship dimensions are 99 m in overall length and 18.9 m in breadth. A computational domain was defined around the geometry with the ship in the centre. The width of the domain increased with the ship's orientation to the flow to prevent spurious increases in wind speed created by the blockage of the ship in the domain. For flows directly over the bow the computational volume was 660 m long ($-330 \text{ m} < x < 330 \text{ m}$), 400 m wide ($-200 \text{ m} < y < 200 \text{ m}$) and 150 m high ($0 \text{ m} < z < 150 \text{ m}$). For relative wind directions at 10, 20 and 30 degrees the width was changed to 1000 m wide ($-500 \text{ m} < y < 500 \text{ m}$). For relative wind directions at 50, 90 and 110 degrees the width was changed to 1600 m wide ($-800 \text{ m} < y < 800 \text{ m}$). In general, the ratio of the frontal area of the ship to the area of the inlet gave a blockage by the ship of less than 0.01.

The number of computational cells within the domain was around 5 to 6 million. The time taken for each simulation to converge was about 24 hours using 8 3.3 GHz Xeon cores on a Linux workstation. This fast convergence time was obtained using the steady-state rather than the time-marching solver (Moat and Yelland, 2006). The cell sizes varied throughout the computational domain with high-resolution cells in the vicinity of the foremast (cells of around 0.10 m) and much lower resolution cells in areas well away from the ship where the flow did not vary very rapidly.

The vertical profile of the velocity at each domain inlet was specified as a fully logarithmic boundary layer profile with a wind speed at a height of 10 m of 10 ms^{-1} ;

$$U10_n = \frac{u^*}{k_v} \ln \left(\frac{10}{z_0} \right) \quad (1)$$

where k_v is the von Karman constant (value 0.4), z_0 is the roughness length and u^* is the friction velocity calculated from the Smith (1980) drag coefficient relationship. The domain floor was allocated a small roughness length (order 10^{-4} m) in order to maintain the profile downwind of the inlet. All results presented in this report were obtained by comparing the wind speed at a particular anemometer position with the free stream wind speed profile well abeam (more than 190 m) of the anemometer position to arrive at a percentage wind speed bias for that position.

3. THE INSTRUMENT LOCATIONS

During WAGES the ship was instrumented with: an R3 sonic anemometer on the foremast platform; the ship's sonic mounted on the "bird table" at the top of the foremast; and a psychrometer and a Vaisala (temperature and humidity sensors) located on the port side of the monkey island. Details of the instruments are given in the WAGES metadata report (Moat et al., 2014). The instrument positions are indicated in Figure 1 and the co-ordinates are shown for the model with a flow directly over the bow. The instrument locations relative to the foremast and the bridge are shown schematically in Figures 2 and 3. Note that the ship model assumed a draught of 6.1 m which equates to a height above waterline of 16.0 m for the R3 (as shown in Figure 1 and throughout the rest of this report),

whereas the actual draught was 5.6 m on average (Moat et al., 2014) which equates to an R3 height of 16.5 m (as shown in Figure 2). In the VECTIS co-ordinates system, the instrument positions are;

Relative Wind Direction (degrees)	R3 sonic (x, y, z)	ship's sonic (x, y, z)	psychrometer (x, y, z)	Vaisala (x, y, z)
0 (bow-on)	(44.09,-1.24,16.02)	(43.80,0.61,21.51)	(11.52,6.7,18.03)	(11.52,6.7,17.83)
10 (starboard)	43.64,6.44,16.02	43.03,8.21,21.51	10.19,8.60,18.03	10.19,8.60,17.83
20 (starboard)	41.86,13.92,16.02	40.95,15.55,21.51	8.54,10.24,18.03	8.54,10.24,17.83
30 (starboard)	38.81,20.98,16.02	37.63,22.43,21.51	6.63,11.56,18.03	6.63,11.56,17.83
50 (starboard)	29.29,32.98,16.02	27.69,33.95,21.51	2.28,13.14,18.03	2.28,13.14,17.83
70 (starboard)	16.25,41.01,16.02	14.41,41.37,21.51	-2.35,13.12,18.03	-2.35,13.12,17.83
90 (beam-on starboard)	1.24,44.09,16.02	-0.61,43.8,21.51	-6.70,11.52,18.03	-6.70,11.52,17.83
110 (starboard side)	-13.91,41.86,16.02	-15.55,40.95,21.51	-10.24,8.54,18.03	-10.24,8.54,17.83

Table 1. Instrument positions in the VECTIS co-ordinate system for a bow-on flow and flows over the starboard side. The z value is the height of the anemometer above the sea surface. A schematic of the locations is shown in Figures 2 and 3.

Relative Wind Direction (degrees)	R3 sonic (x, y, z)	ship's sonic (x, y, z)	psychrometer (x, y, z)	Vaisala (x, y, z)
10 (port)	43.21,8.88,16.02	43.24,7.01,21.51	12.51,-4.60,18.03	12.51,-4.60,17.83
20 (port)	41.01,16.25,16.02	41.37,14.41,21.51	13.12,-2.35,18.03	13.12,-2.35,17.83
30 (port)	37.57,23.12,16.02	38.24,21.37,21.51	13.33,-0.04,18.03	13.33,-0.04,17.83
50 (port)	27.39,34.58,16.02	28.62,33.16,21.51	12.54,4.52,18.03	12.54,4.52,17.83
70 (port)	13.92,41.86,16.02	15.55,40.95,21.51	10.24,8.54,18.03	10.24,8.54,17.83
90 (beam-on port side)	-1.24,44.09,16.02	0.61,43.8,21.51	6.70,11.52,18.03	6.70,11.52,17.83
110 (port side)	-16.25,41.01,16.02	-14.41,41.37,21.51	2.35,13.12,18.03	2.35,13.12,17.83

Table 2. Instrument positions in the VECTIS co-ordinate system for effective port flows. The z value is the height of the anemometer above the sea surface. A schematic of the locations is shown in Figures 2 and 3.

4. CFD RESULTS

4.1 Introduction

This section summarises the results of all eight models. Each model had converged when the residuals of velocity (U, V, W), turbulent kinetic energy (K), rate of dissipation of K (E) and pressure (P) were less than 10^{-6} . As an example, Figure 4 shows the residuals for the bow-on model. Once the models had converged post-processing files were written for the extraction of data throughout the computational volumes. The flow at the sides and ends of the tunnel were examined to check that the flow was undisturbed by the presence of the ship and could therefore be used to estimate the free stream flow (Section 4.2). The vertical displacement of the flow at the instrument sites was quantified along with the angle of the deflection of the flow away from the horizontal ("tilt") and the angle of deflection on the horizontal plane ("twist") (Section 4.3). The absolute wind speed bias was calculated as well as the wind speed bias accounting for the vertical displacement of the air (Section 4.4).

4.2 The free stream flow

The flow in the computational volume was examined to check that free stream conditions existed at the sides and ends of the tunnel, i.e. that the presence of the ship did not cause a significant blockage of the flow to these regions. As an example, Figure 5a shows the variation in velocity along the tunnel for all simulations. The data were extracted on a plane 10 m in from the tunnel wall, i.e. towards one side of the tunnel, between $-330 \text{ m} < x < 330 \text{ m}$ and at heights z of 10 m, 30 m and 50 m. This shows a change in the free stream velocity for the bow-on run of 0.009 ms^{-1} at a height of 10 m and 0.006 ms^{-1} at a height of 30 m. These small changes indicate the ship caused a minimal blockage of the flow at the sides of the tunnel. However, since the changes are not zero, the free stream velocity for a particular instrument site is estimated from the vertical profile of the velocity directly abeam of the instrument site, rather than at the inlet or outlet of the tunnel. Examination of the free stream velocity close to the sides of the tunnel in the other models showed that the geometry likewise caused a minimal blockage of the flow.

Figure 5b shows the vertical profiles of wind speed at the tunnel inlet ($x=320 \text{ m}$) and outlet ($x=-320 \text{ m}$) for the bow-on simulation, and Figure 5c) shows the difference between the profiles for all simulations. Above a height of about 3 m the difference between the profiles is less than 0.3 m/s. These figures show that the shape of the wind speed profile changes slightly along the tunnel. Because of this change, the free stream velocities are estimated using the vertical profiles of velocity abeam of the anemometer site, rather than the profiles at the tunnel inlet or outlet.

4.3 The vertical displacement and angle of flow at the sensor locations

The vertical displacement of the flow reaching an instrument site is calculated by tracing a streamline from the instrument location upwind to the inlet (Table 5). The vertical displacement Δz for the R3 anemometer increases from around 1.7 m for bow-on flows to around 5 m for flows directly over the beam. The vertical displacement Δz for the ship's anemometer on top of the foremast extension is less than the R3 sonic, and increases from 1.37 m for bow-on flows to around 4 m for flows directly on the beam. The vertical displacement at the psychrometer and Vaisala temperature

sensor locations is far larger than at the well-exposed foremast sites. The airflow is raised about 6 m for bow-on flows, which increases to about 11 m for flows directly over the port side. The vertical displacement for these sensors has been included as a guide for future positioning of sensors in this area. However, for flows directly over the starboard side the vertical displacement at the temperature sensor sites is not reliable as the sensors are in a recirculation region with severe flow distortion (Figure A28).

The path of the streamlines to the R3 sonic and ship's sonic anemometer for each relative wind direction simulated is shown in Figure 6. The airflow is influenced by the ship to a far greater extent at the R3 anemometer site than at the ship's sonic site, e.g. at a distance of 20 m (2 seconds) upstream the vertical displacement is between 1.5 to 3 m at the R3 site, whilst at the ship's sonic site it is only about 1 to 2 m. This is due to the ship's sonic anemometer being located further away from the superstructure. The vertical displacement $\Delta z_{t=2}$ at a position two seconds upstream of the anemometer locations was also calculated for the R3 sonic and ship sonic anemometers (after Yelland et al. 2002). The co-ordinates of the streamlines were written to file and the vertical displacement using a position at 2 seconds upstream was calculated. The speed and deflection of the streamline was taken into account in the calculation. Compared to the full vertical displacements (Δz), the vertical displacement at 2 seconds upstream ($\Delta z_{t=2}$) was around 0.30 m less for bow-on flows (full displacement 1.67 m compared to 1.32 m for the two-second displacement) and around 2 m for beam on flows. The vertical displacements for each relative wind direction simulated are summarised in Tables 5 and B.1.

The angle of the flow from the horizontal ("tilt" of the flow) is greater at the R3 site than at the ship's sonic site, typically increasing from about 4 to 8 degrees for the R3 sonic to around 3 to 5 degrees for the ship's sonic. The horizontal deflection ("twist") of the streamlines is shown in Figure 7. A positive deflection of the flow indicates a rotation of the flow in a clockwise direction, e.g. for flows over the starboard side the substructure presents a large blockage to the flow and deflects the streamlines towards the bow. This means that the measured relative wind direction appear to come from further aft, i.e. the "twist" angle should be subtracted from the measured relative wind direction. The deflection increases with increases in relative wind direction, and the flow is deflected more at the R3 sonic site than the ship's sonic site. The twist at the psychrometer and Vaisala locations are larger than at the anemometer locations due to their close proximity to the superstructure. The flow angles are shown in Table B.1 and summarised in Tables 6 and 7.

4.4 Wind speed bias

The free stream velocity has small, predictable gradients and can be estimated accurately at any given point on the vertical profile. In contrast, the flow at an instrument site can suffer from severe flow distortion and from large gradients in the velocity field. In addition, it is not always possible to define the mesh so that the instruments are at the exact centres of the computational cells (see Moat et al., 1996). Therefore the velocity at an instrument site is estimated from lines of data extracted in all three directions. Figures 9 to 62 show the lines of data through the instrument sites for all wind directions, and the results are summarised in Tables 3, 4 and B.1. The wind speed error at an instrument site (height z) is expressed as a percentage of the free stream speed at height z and also as a

percentage of the free stream wind speed at which the airflow originated (at height $z - \Delta z$, where Δz is the full vertical displacement of the flow) with a positive error indicating an acceleration of the flow. In addition the wind speed error at an instrument site (height z) is expressed as a percentage of the free stream wind speed at a height two seconds upstream of the anemometer site (at height $z - \Delta z_{t=2}$). The change in the percentage wind speed bias (at height $(z - \Delta z)$, $(z - \Delta z_{t=2})$ and at the height z of the sensor) with relative wind direction for each sensor is summarised in Tables 3 and 4.

The airflow distortion at the well-exposed R3 sonic anemometer site varies from decelerations of 1 % for winds directly over the bow to accelerations of around 15% for winds directly over the port beam (Figure 8). These large accelerations are caused by the presence of the upwind foremast extension at this relative wind direction. For a flow at 110 degrees over the port beam the R3 sonic is in the downstream wake region of the foremast, where the airflow is severely decelerated. The ship's sonic anemometer is well-exposed with no upstream obstacles for all wind directions within ± 90 degrees of the bow. Nevertheless, the wind speed at the anemometer site is reduced by about 1-2% for bow-on flows and is accelerated by up to 9 % for flows over either beam. Vertical planes of velocity through the R3 sonic anemometer site are shown for all relative wind directions in Figures A1 to A8. Similarly, horizontal planes of velocity through the R3 sonic site are shown in Figures A9 to A16.

The wind speed bias and vertical displacement for all sensors is plotted in Figure 8. The rates of change of the wind speed bias with relative wind direction and vertical displacement for both the anemometers are relatively smooth. This suggests that the wind speed bias and vertical displacement may be parameterised for all relative wind directions between ± 110 degrees. The exception is a slight drop in the predicted wind speed bias at the R3 sonic site for a flow at 70 degrees over the starboard side. The wind speed at the anemometer location is slightly low due to the presence of a decelerated region directly upstream of the cylindrical foremast extension, which extends to the anemometer site at this wind direction.

Figure 8 also shows results for wind speed bias and vertical displacement at the ship anemometer site, obtained by Berry et al., (2001) at for model runs at 5 and 15 m/s (rather than 10 m/s as in this study). It can be seen that there is no significant difference in the results, i.e. that the effects of flow distortion do not vary significantly with wind speed, at least for winds speeds between 5 and 15 m/s.

The airflow distortion at the temperature and humidity instruments located on the port side of the monkey island are greater than those on the foremast. The wind speed bias was generally accelerated for flows over the port side when the instruments were well exposed. For flows over the starboard side the wind speed bias was generally accelerated at the psychrometer location, but to a lesser extent than for flows over the port side. The Vaisala was located closer to the deck of the monkey island and the wind speed bias was generally greater. For a flow at 10 degrees over the starboard side there is a noticeable reduction in the wind speed bias (Figure 8, Table 3 and Table 4). This is caused by the downstream wake of the foremast extension (Figure A10). For flows directly over the starboard side both instruments were in a region of re-circulation (see Figure A27 and A28) and experienced severe flow distortion and very large velocity gradients. The vertical displacement was

calculated for these instruments, but is only intended as a guide for any future anemometer deployments (Table 5).

Sensor locations above the bridge are examined for a potential position to locate a Picarro sensor to measure CO₂, CH₄ and H₂O. Figures A17 to A22 show horizontal cuts at height of 3 m and 5 m above the bridge top at 0, 50 and 90 degrees. To achieve a wind speed bias of less than 6 to 8 % increase in wind speed the sensor must be located at least 5 m above the bridge. At around 3 m the wind speed bias is closer to 9% with higher velocity gradients.

5. SUMMARY

During the WAGES campaign the AutoFlux system (Yelland et al., 2009) was installed on the RRS *James Clark Ross*. Even though the R3 sonic anemometer was situated in a well-exposed location on the ship's foremast it was subject to a bias caused by the presence of the ship distorting the flow of air to the anemometer. The acceleration and vertical displacement of the flow at the R3 sonic and the ship's foremast anemometer have been modelled in three dimensions at eight relative wind directions using the CFD package VECTIS. The acceleration and vertical displacement was also calculated for two temperature sensors above the bridge top.

The vertical displacement of the airflow was used to obtain the height at which the airflow originated a long way upstream and also from a point 2 seconds upstream (after Yelland et al., 2002). The free stream wind speed at these two heights was used to determine the wind speed bias at the anemometer locations. These measurements are required if data from the anemometer are to be used to calculate the wind stress via the dissipation method (Yelland et al., 1998). The results are summarised in Table 5.

The wind speed bias for all relative wind directions are summarised in Tables B1, 3 and 4. When the ship is head to wind (0 degrees) the airflow at both anemometer locations is decelerated by about 1% of the free stream wind speed. Over the full range of relative wind directions the flow to the R3 sonic is generally accelerated with the largest wind speed biases at flows directly over the beam. The ship's sonic is located on top on the foremast extension and is better exposed with generally smaller wind speed biases. Unfortunately this location can only be accessed by crane so routine maintenance of the anemometer and associated instrumentation would not be possible, so this site was not used for the WAGES instrumentation. The vertical displacement of the airflow increases from around 1 to 2 m for flows directly over the bow, to around 5 m for flows over the ship's beam as the blockage of the airflow by the ship becomes greater.

The airflow distortion at the temperature sensor locations was typically greater than the well-exposed foremast locations. These locations experienced wind speed biases from 6% increase for an airflow directly over the bow, to large decelerations of 55 % when the instruments were in the large recirculation region for flows directly over the starboard side.

	Relative wind direction (degrees)														
	-110	-90°	-70°	-50°	-30°	-20°	-10°	0°	10°	20°	30°	50°	70°	90°	110
R3 sonic	-17.60 (-21.74)	14.18 (11.76)	15.87 (14.15)	11.91 (11.01)	6.59 (6.10)	3.37 (2.98)	0.72 (0.41)	0.11 (-0.39)	-0.58 (-0.86)	1.07 (0.70)	3.35 (2.92)	5.91 (5.11)	6.24 (4.86)	10.50 (8.35)	11.07 (6.97)
ship's sonic	9.00 (7.11)	8.38 (7.11)	6.65 (5.78)	3.48 (2.98)	1.16 (0.86)	-0.08 (-0.33)	-0.62 (-0.83)	-1.03 (-1.24)	-0.45 (-0.66)	0.21 (-0.04)	1.64 (1.32)	4.31 (3.77)	7.89 (7.01)	9.35 (8.00)	10.53 (6.95)
psychrometer	-	6.84	16.73	20.47	17.96	14.21	13.89	12.28	3.64	11.95	12.84	12.26	-0.92	-48.22	-
Vaisala	-	-1.31	14.92	22.08	20.53	13.88	11.45	6.41	-6.17	5.21	7.72	7.77	-2.58	-51.29	-

Table 3. The percentage wind speed bias at the sensor location accounting for the height the airflow was raised (i.e. at height $z - \Delta z$). The values in brackets indicate the wind speed error using a free stream velocity from a location 2 seconds upstream of the anemometer site, i.e. $z - \Delta z t = 2$ (after Yelland et al., 2002). A negative relative wind direction indicates a flow over the port side.

	Relative wind direction (degrees)														
	-110	-90°	-70°	-50°	-30°	-20°	-10°	0°	10°	20°	30°	50°	70°	90°	110
R3 sonic	-23.46	8.91	11.63	9.07	4.75	1.85	-0.63	-1.38	-1.94	-0.49	1.53	3.26	2.59	5.77	4.83
ship's sonic	5.84	5.94	4.75	2.19	0.29	-0.83	-1.32	-1.67	-1.13	-0.55	0.74	2.98	5.95	6.79	7.15
psychrometer	-	-5.59	5.92	11.61	10.05	6.88	6.64	6.94	-1.33	3.56	0.53	0.33	-11.73	-55.15	-
Vaisala	-	-12.63	3.49	12.30	11.81	6.06	3.77	1.05	-10.92	-3.31	-5.54	-4.34	-13.90	-57.53	-

Table 4. The percentage wind speed bias at the sensor location z . A negative relative wind direction indicates a flow over the port side.

	Relative wind direction (degrees)														
	-110	-90°	-70°	-50°	-30°	-20°	-10°	0°	10°	20°	30°	50°	70°	90°	110
R3 sonic	6.92 (3.15)	5.11 (3.11)	4.18 (2.79)	3.12 (2.25)	2.20 (1.66)	1.89 (1.44)	1.73 (1.35)	1.67 (1.32)	1.76 (1.41)	1.98 (1.54)	2.23 (1.76)	3.09 (2.27)	3.95 (2.73)	4.78 (2.96)	6.92 (3.15)
ship's sonic	5.95 (2.58)	4.18 (2.18)	3.43 (1.98)	2.49 (1.57)	1.75 (1.18)	1.54 (1.05)	1.43 (1.00)	1.37 (0.95)	1.39 (0.99)	1.52 (1.03)	1.77 (1.16)	2.56 (1.56)	3.46 (2.00)	4.34 (2.22)	5.95 (2.58)
psychrometer	-	11.21	0.12	8.52	7.84	7.57	7.54	5.98	7.26	8.54	11.24	11.17	11.42	4.98	-
Vaisala	-	11.60	10.51	9.00	8.19	7.87	7.89	6.17	7.69	8.99	12.05	11.49	11.77	5.28	-

Table 5. The variation of the vertical displacement (Δz , meters) with changes in relative wind direction. The values in brackets indicate the vertical displacement at a location 2 seconds upstream of the anemometer site, i.e. $\Delta z_{t=2}$ (after Yelland et al., 2002). A negative relative wind direction indicates a flow over the port side.

	Relative wind direction (degrees)														
	-110	-90°	-70°	-50°	-30°	-20°	-10°	0°	10°	20°	30°	50°	70°	90°	110
R3 sonic	6.1	4.9	4.2	4.2	3.3	3.5	4.2	4.3	5.2	5.4	5.8	7.0	7.5	7.7	8.3
ship's sonic	6.6	5.4	5.5	4.4	3.6	3.6	3.7	3.5	3.6	3.4	3.4	3.9	4.9	5.0	6.5
psychrometer	-	22.5	25.4	23.6	16.4	14.1	11.7	13.0	15.8	12.6	13.4	10.0	1.8	-2.1	-
Vaisala	-	27.3	28.1	26.1	17.4	14.6	11.4	13.1	16.4	12.8	13.9	9.5	1.2	-2.2	-

Table 6. The variation of the angle of the flow to the horizontal (tilt) at the sensor site (degrees). A negative relative wind direction indicates a flow over the port side.

	Relative wind direction (degrees)														
	-110	-90°	-70°	-50°	-30°	-20°	-10°	0°	10°	20°	30°	50°	70°	90°	110
R3 sonic	-3.0	-3.8	-6.5	-5.6	-5.8	-4.9	-4.3	-1.4	0.7	3.1	4.7	6.6	7.7	6.0	8.0
ship's sonic	-4.8	-4.1	-4.8	-4.5	-3.2	-2.3	-1.1	0.1	1.4	2.5	3.4	4.6	4.7	3.9	4.4
psychrometer	-	-19.3	-17.1	-12.9	-8.4	-4.7	0.0	2.6	4.4	5.5	3.9	-1.0	7.3	34.9	-
Vaisala	-	-21.9	-17.7	-13.7	-10.5	-7.3	-2.5	0.2	2.5	4.5	2.8	-1.5	8.0	36.7	-

Table 7. The variation in the horizontal twist ($\tan^{-1}(v/u)$) of the flow at the sensor site (degrees). A negative twist indicates a flow, which has moved anti-clockwise due to the presence of the ship. A negative relative wind direction indicates a flow over the port side.

6. ACKNOWLEDGEMENTS.

This work was supported by the Natural Environment Research Council (grants NE/G003696/1 and NE/G00353X/1) and by the UK National Capability programme.

7. REFERENCES

- Berry, D. I., B. I. Moat, M. J. Yelland, 2001: Airflow distortion at instrument sites on the RRS James Clark Ross, SOC Internal Document No. 75, Southampton Oceanography Centre, UK. 83 pp. [available from: <http://eprints.soton.ac.uk/150025/>]
- TNO Diana, 2010: Femgv user's manual Pre and post processing release 7.2, TNO DIANA BV Schoemakerstraat 97, 2628 VK Delft, The Netherlands.
- Lauder, B. E., and D. B. Spalding, 1974: The numerical computation of turbulent flows, *Computer Methods in Applied Mechanics and Engineering*, **3**, 269 - 289pp.
- Moat, B. I., M. J. Yelland, and J. Hutchings, 1996: Airflow over the R.R.S. Discovery using the Computational Fluid Dynamics package VECTIS, Southampton Oceanography Centre, Southampton, UK. SOC Internal Report No. 2, 41 pp.
- Moat, B. I. and M. J. Yelland, 2006: Validation of the VECTIS steady state solver, NOC internal document No. 4, National Oceanography Centre, UK., 15 pp [available from: <http://eprints.soton.ac.uk/41394/>]
- Moat, B. I. and M. J. Yelland, 2008: Going with the flow: state of the art marine meteorological measurements on the new NERC research vessel, *Weather*, 63(6), 158-159.
- Moat, B. I., M. J. Yelland, R. W. Pascal and J. Prytherch, 2014: Metadata for the WAGES instrumentation deployed on the RRS James Clark Ross between May 2010 and August 2013. NOC internal document No. 13, National Oceanography Centre, UK., 146 pp.
- Ricardo, 2013, VECTIS 2013.3 user guide, Ricardo software, Shoreham-by-sea, Sussex, UK, 1129pp.
- Yelland, M. J., B. I. Moat, P. K. Taylor, R. W. Pascal, J. Hutchings and V. C. Cornell, 1998: Wind stress measurements from the open ocean corrected for air flow distortion by the ship. *Journal of Physical Oceanography*, 28, 1511 – 1526.
- Yelland, M. J., B. I. Moat, R. W. Pascal and D. I. Berry, 2002: CFD model estimates of the airflow over research ships and the impact on momentum flux measurements, *Journal of Atmospheric and Oceanic Technology*, 19, 1477-1499.
- Yelland, M. J., R. W. Pascal, P. K. Taylor and B. I. Moat, 2009: AutoFlux: an autonomous system for the direct measurement of the air-sea fluxes of CO₂, heat and momentum, *Journal of Operational Oceanography*, 2(1), 15-23.

8. FIGURES

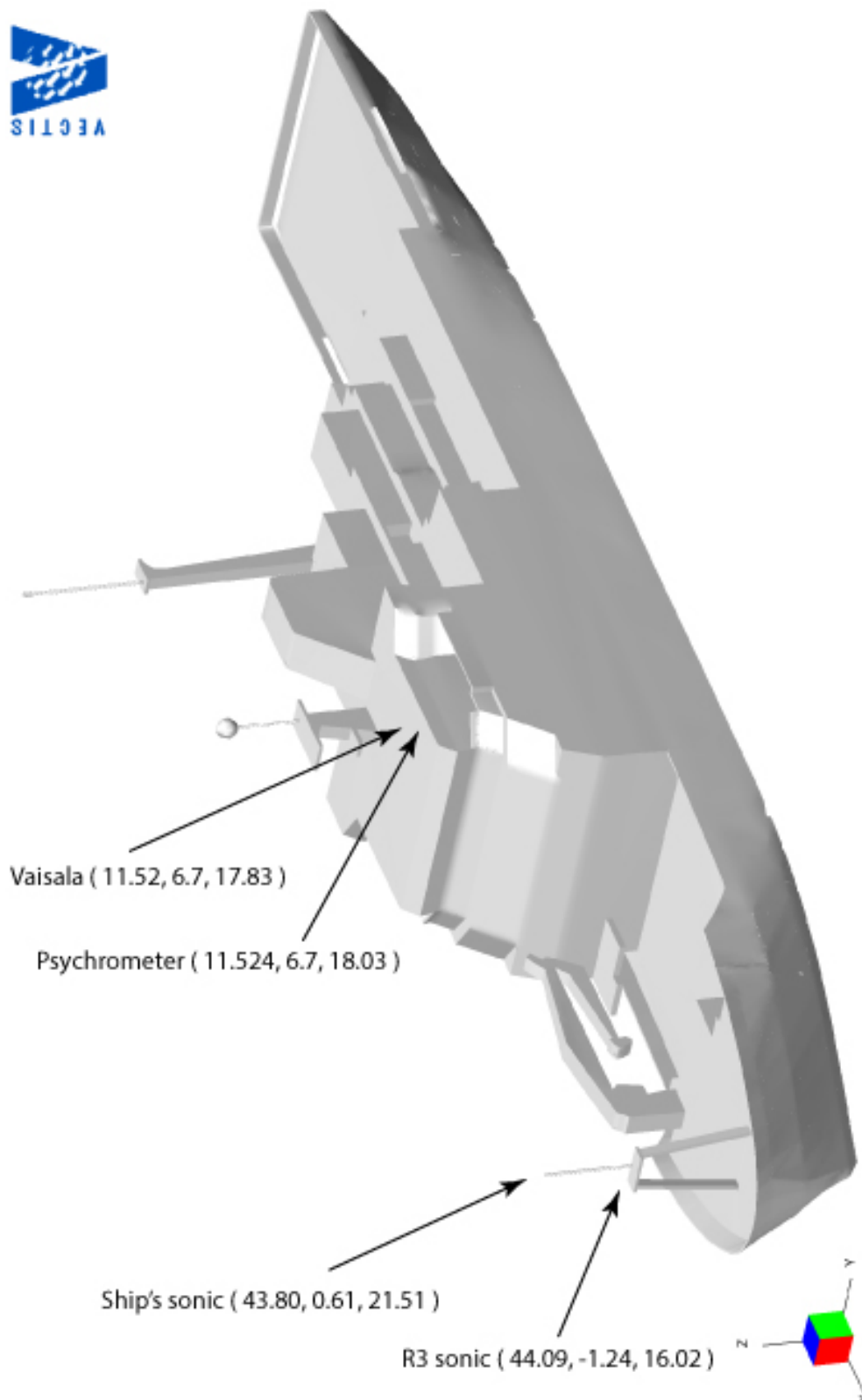


Figure 1. The *R.R.S. James Clark Ross* geometry. The x, y and z co-ordinates of the instruments are shown.

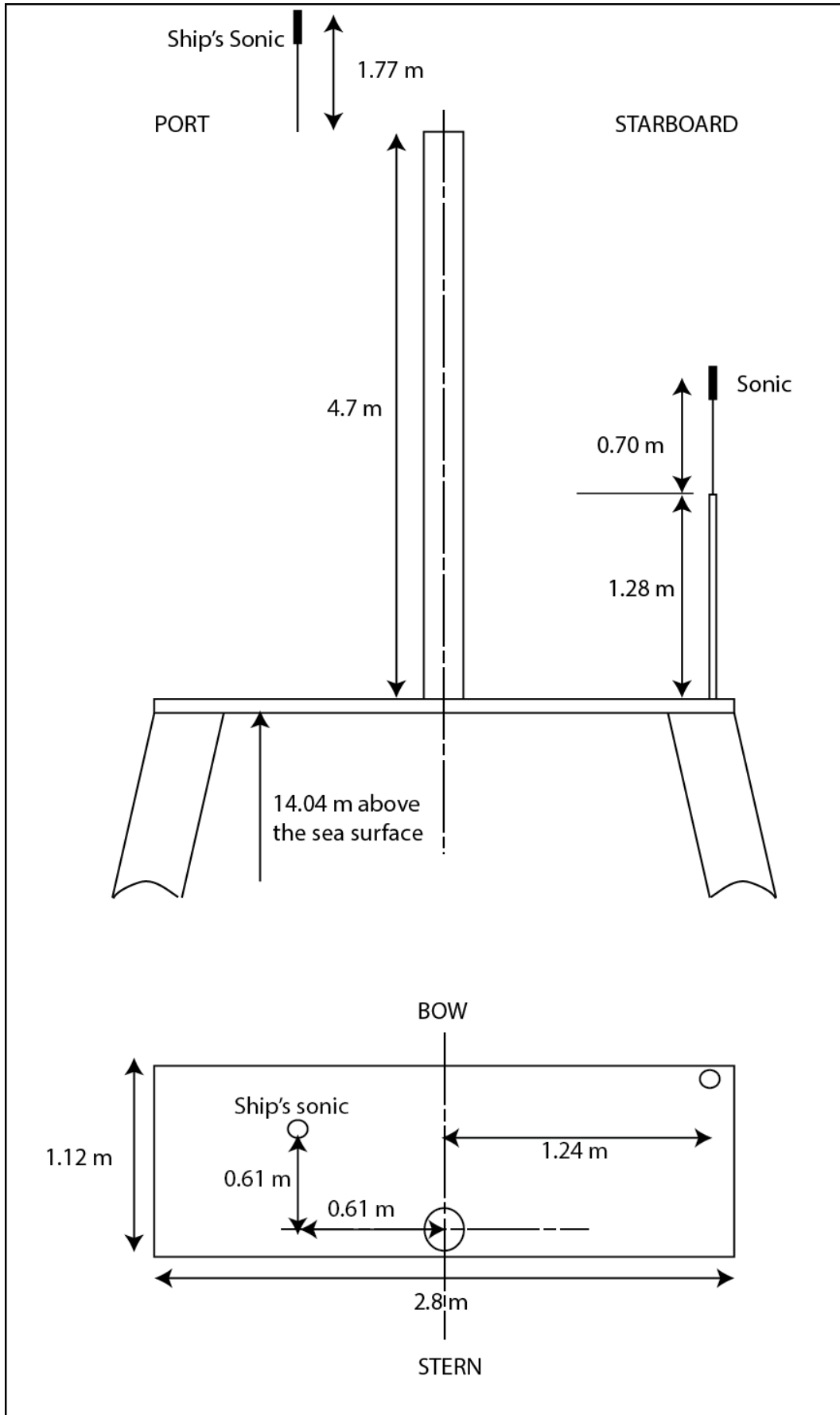


Figure 2. Schematic of the instrument positions relative to the foremast platform and bird table.

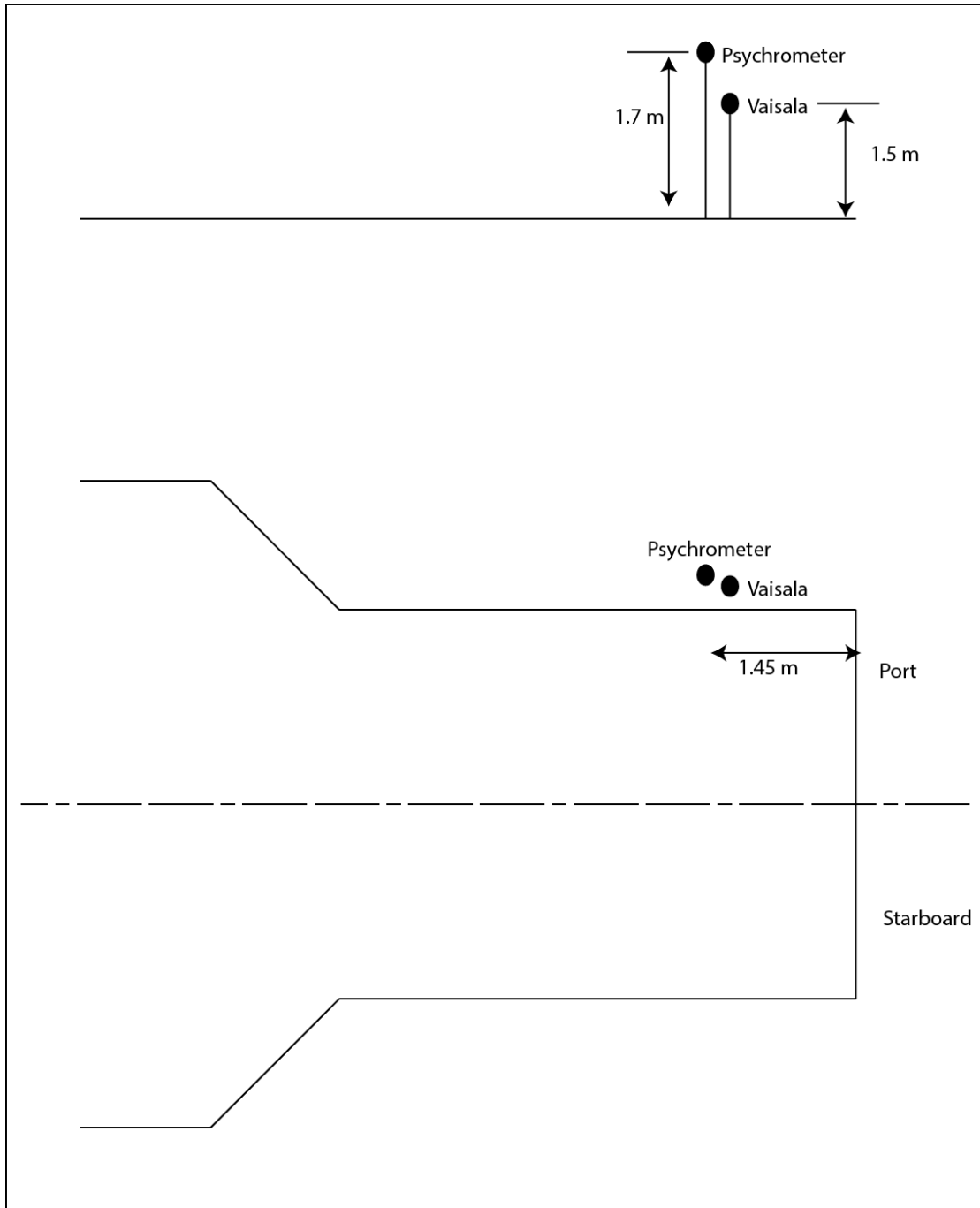


Figure 3. Schematic of the instrument positions of the psychrometer and Vaisala temperature sensors above the bridge. Top: side view. Bottom: plan view.

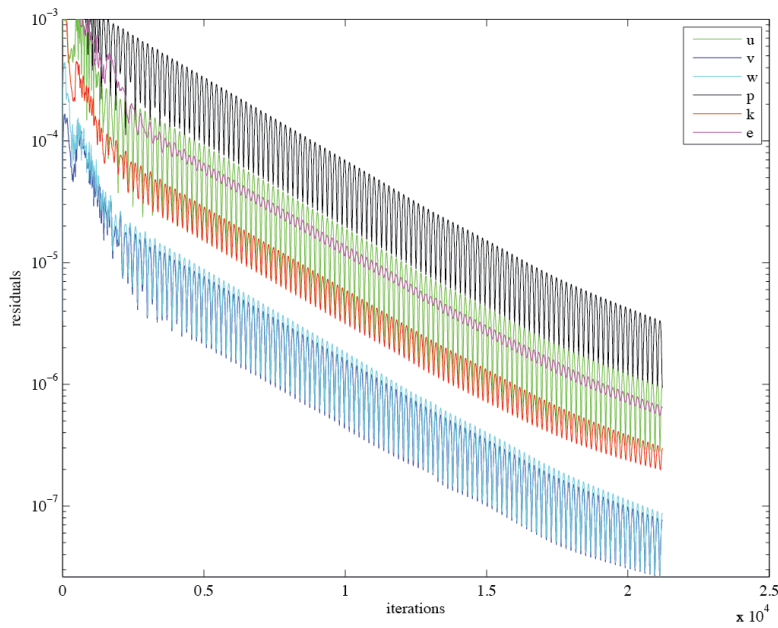


Figure 4. The CFD model convergence for the bow-on simulation (0 degrees). The residuals of velocity u (along stream), v (across stream), w (vertical), and p (pressure), k (turbulent kinetic energy) and e (rate of dissipation of k) are shown.

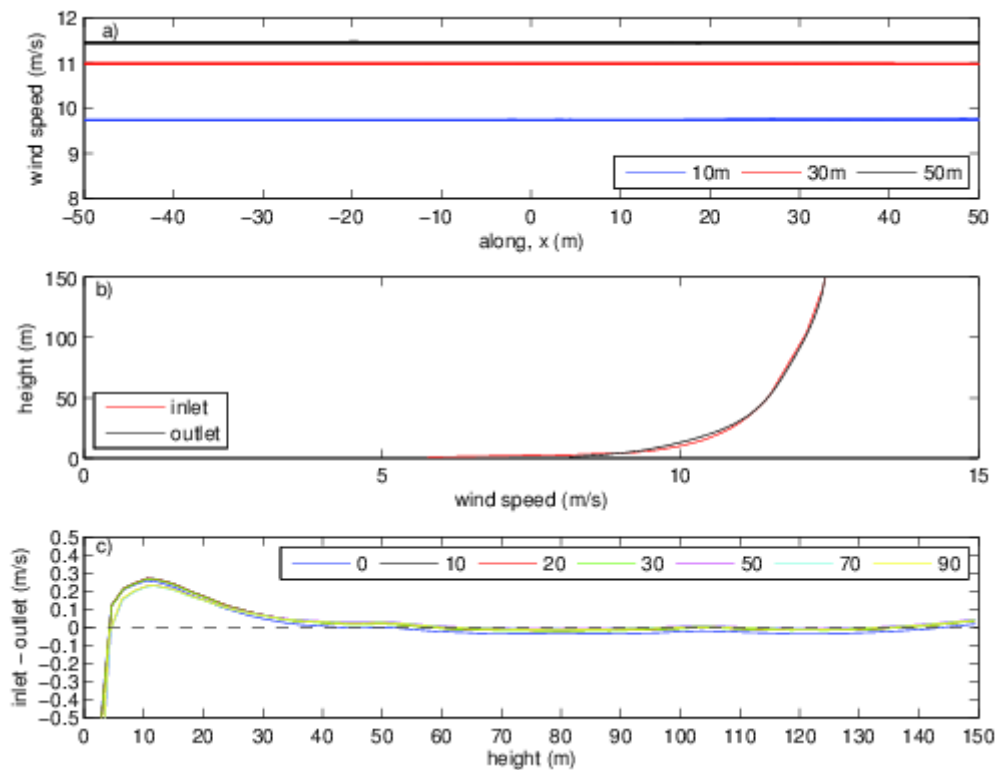


Figure 5. a) Lines of velocity data along the length of the tunnel for all CFD simulations. The data were obtained at heights of 10, 30 and 50 m, in the free stream region on the port side of the models. b) The inlet and outlet velocity profile for the bow-on flow. c) The difference between the inlet and outlet velocity for all wind direction runs as shown in the key.

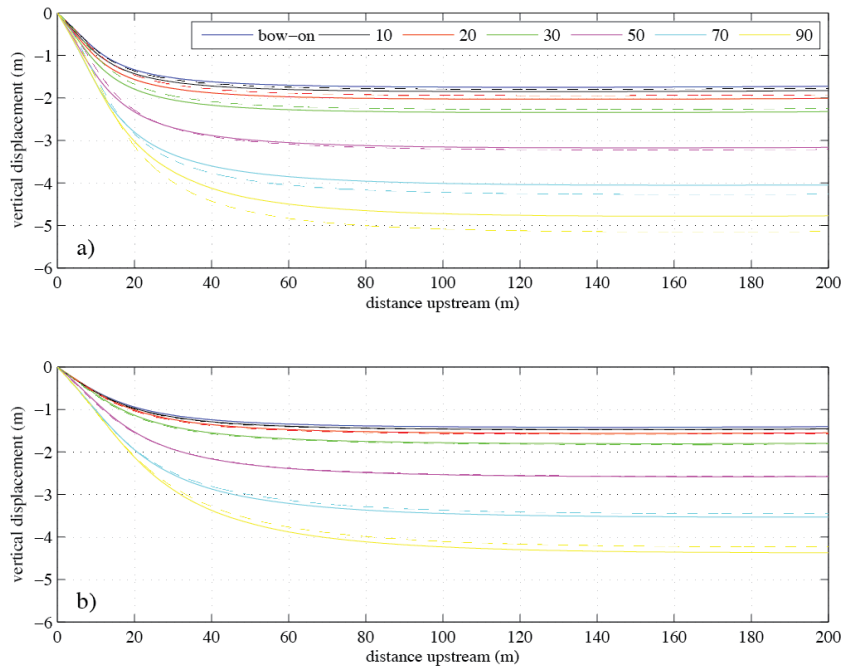


Figure 6. The variation in the vertical displacement of the flow with distance upwind of the a) R3 sonic anemometer and b) ship's sonic site. Dashed lines indicate the streamlines for effective anemometer positions for flows over the port side.

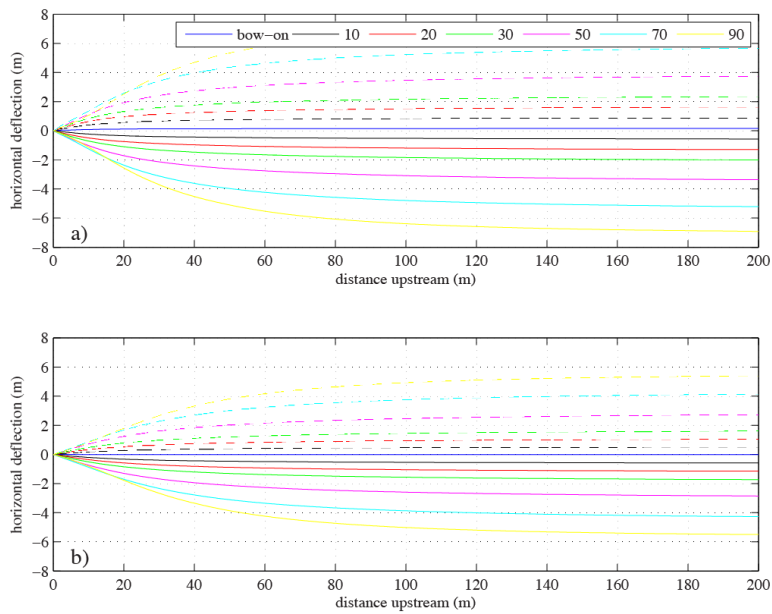


Figure 7. The variation in the horizontal deflection of the flow with distance upwind of the a) R3 sonic anemometer and b) ship's sonic site. Dashed lines indicate the streamlines for effective anemometer positions for flows over the port side.

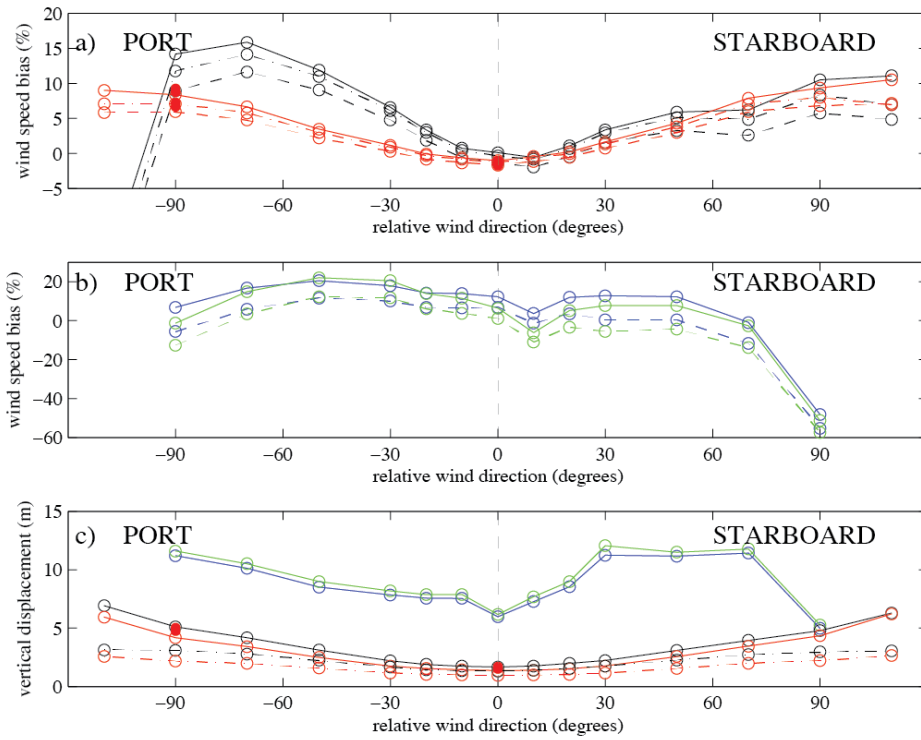


Figure 8. The wind speed bias and vertical displacement at the sonic anemometer (black), ship's anemometer (red), psychrometer (blue) and Vaisala (green). The solid lines indicate the wind speed bias using the free stream velocity from the height it originated (i.e. includes the full vertical displacement Δz_i) and the chain lines indicate the wind speed bias using the free stream velocity from the height 2 seconds upstream of the anemometer location. (i.e. includes $\Delta z_{t=2}$) The dashed lines indicate a wind speed bias at the height of the instrument. The solid symbols indicate the previous ship sonic results of (Berry et al., 2001) at 5 and 15 m/s.

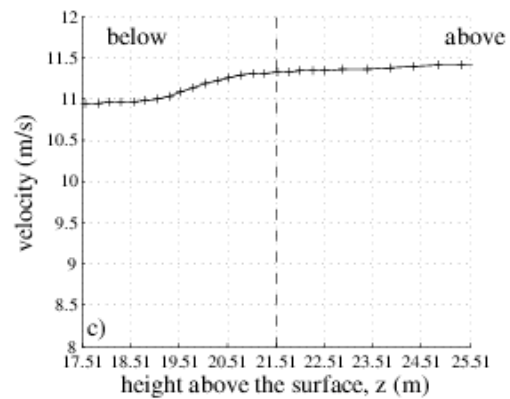
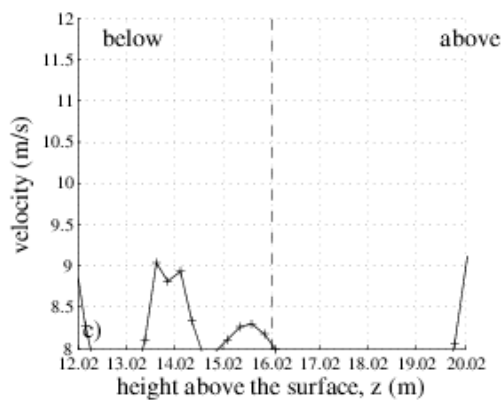
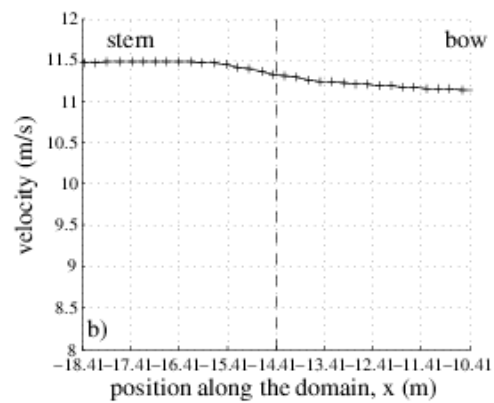
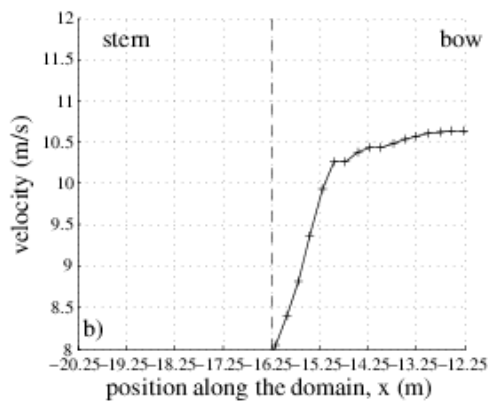
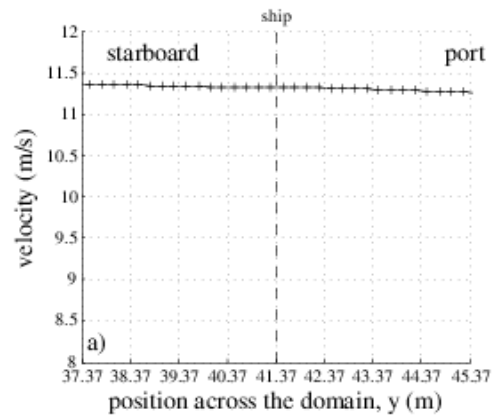
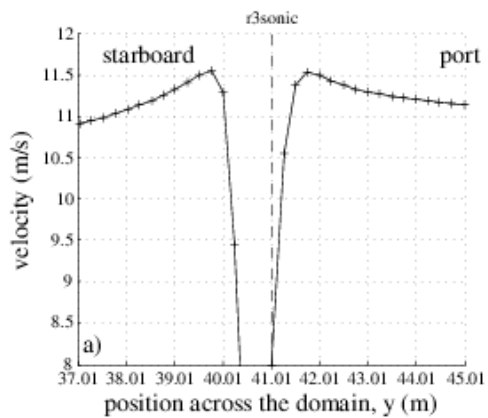


Figure 9. Lines of velocity data through the instrument position (indicated by the dashed line) in all three directions: top – across the domain; middle – along the domain, and bottom – vertically. The results are for a flow to the **R3 sonic at 110 degrees** over the port side.

Figure 10. The ship's sonic sensor at **110 degrees** over the port side.

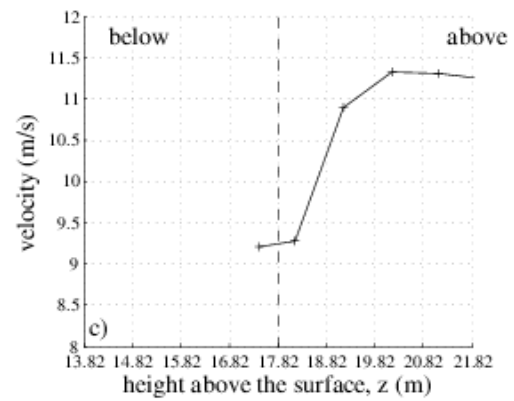
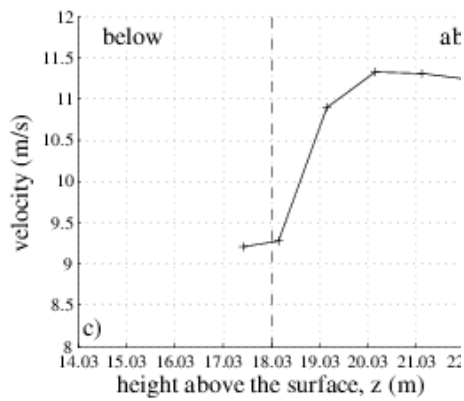
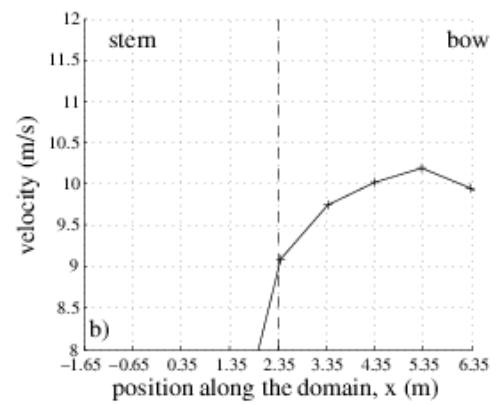
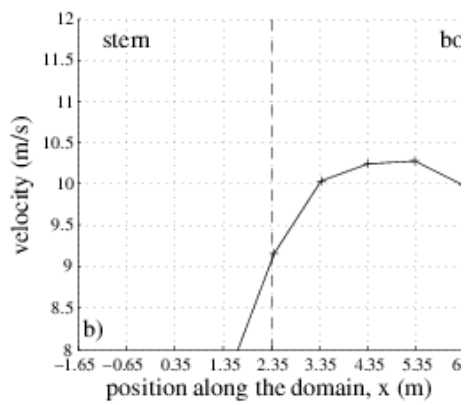
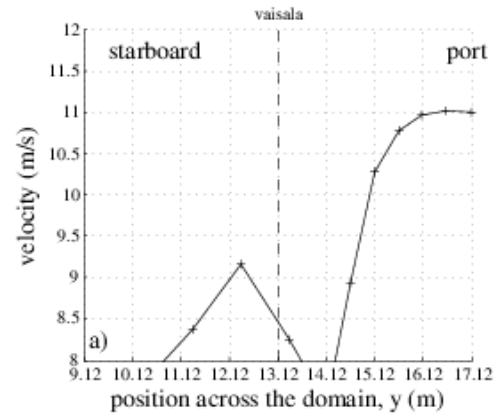
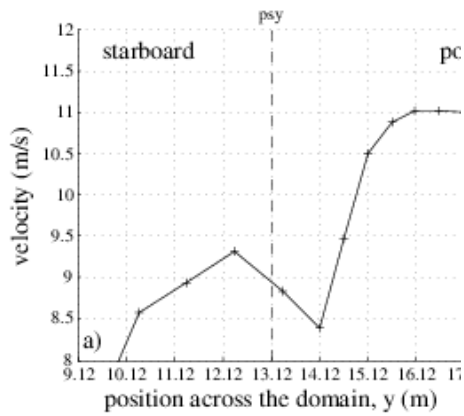


Figure 11. The psychrometer sensor site at 110 degrees over the port side.

Figure 12. The Vaisala sensor site at 110 degrees over the port side.

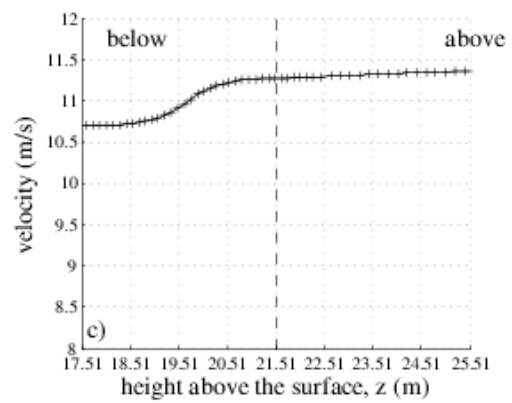
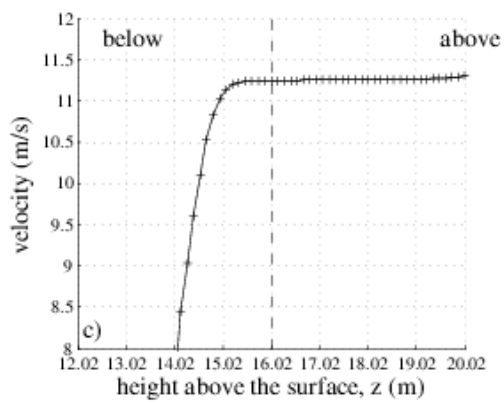
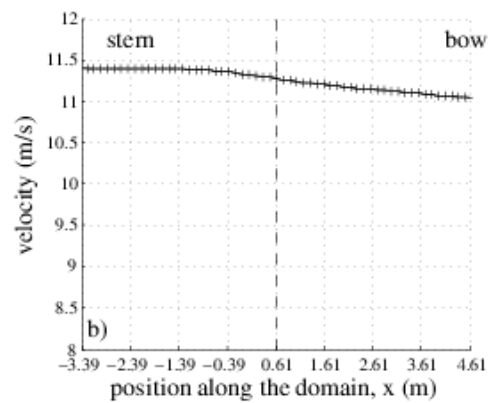
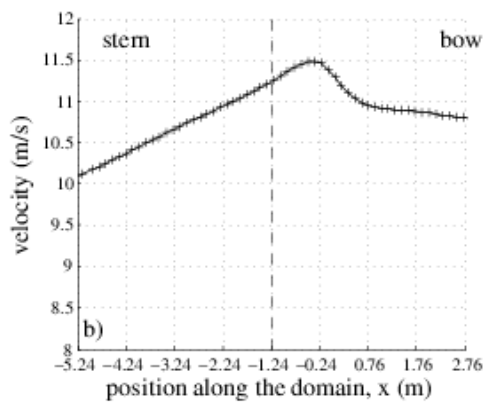
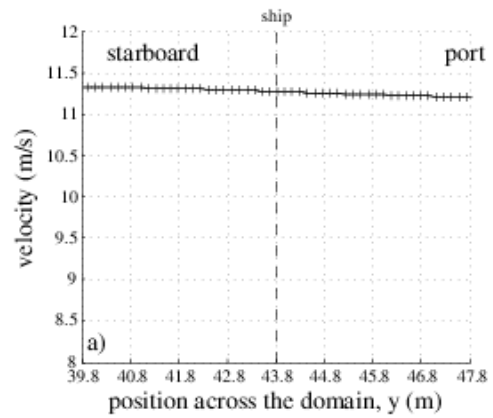
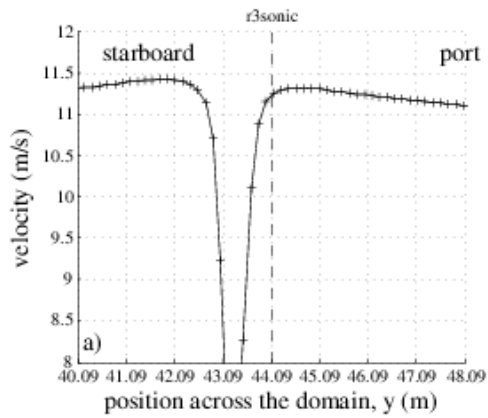


Figure 13. Lines of velocity data through the instrument position (indicated by the dashed line) in all three directions: top – across the domain; middle – along the domain, and bottom – vertically. The results are for a flow to the **R3 sonic at 90 degrees** over the port side.

Figure 14. The **ship's sonic** sensor site at **90 degrees** over the port side.

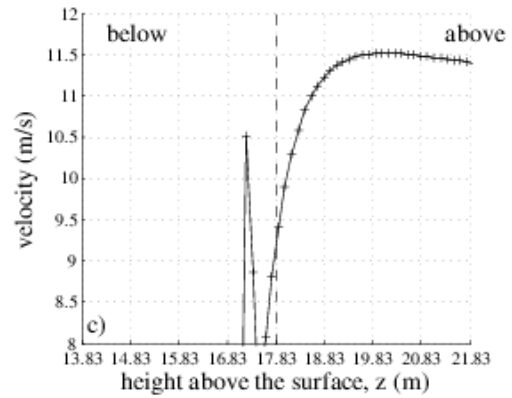
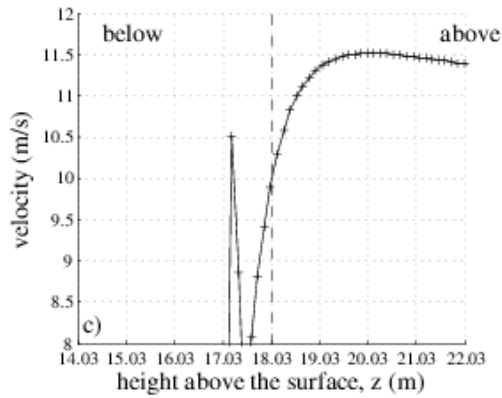
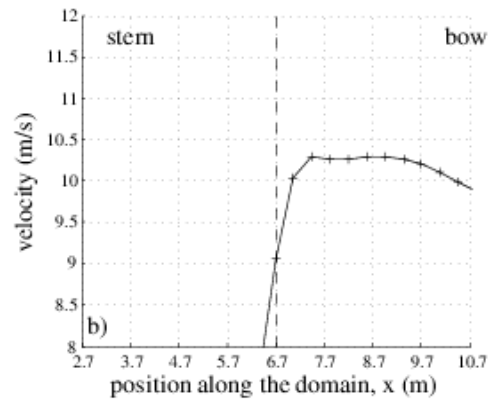
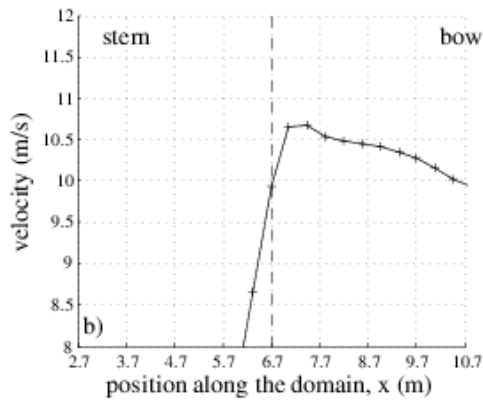
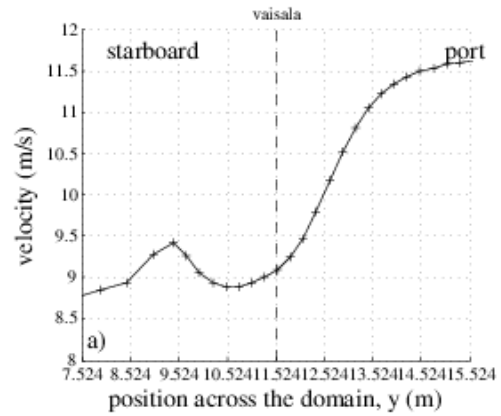
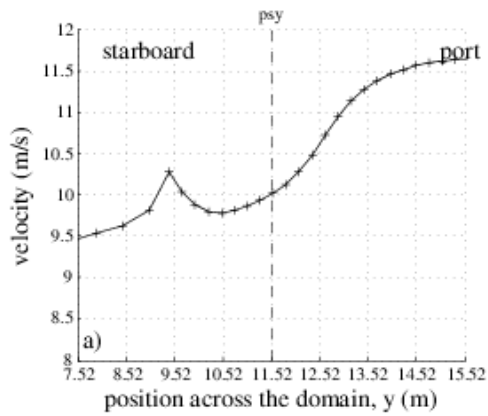


Figure 15. The psychrometer sensor site at 90 degrees over the port side.

Figure 16. The Vaisala site at 90 degrees over the port side.

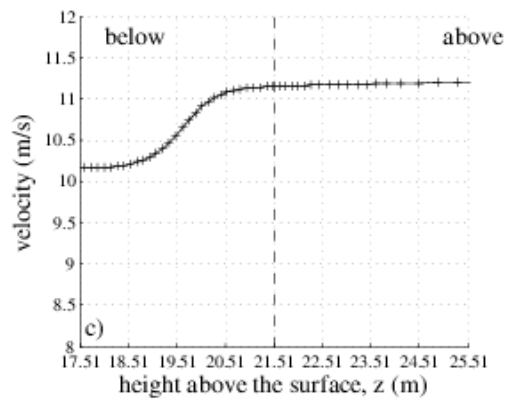
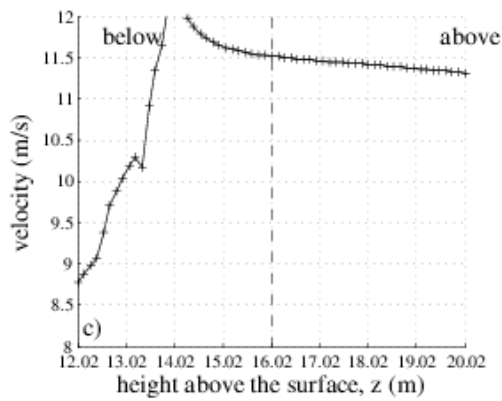
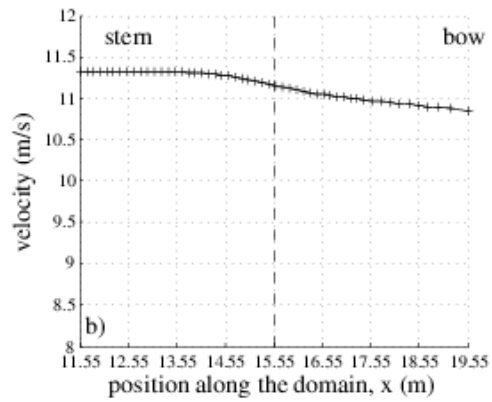
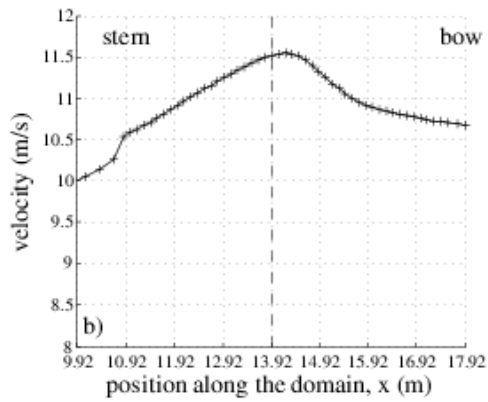
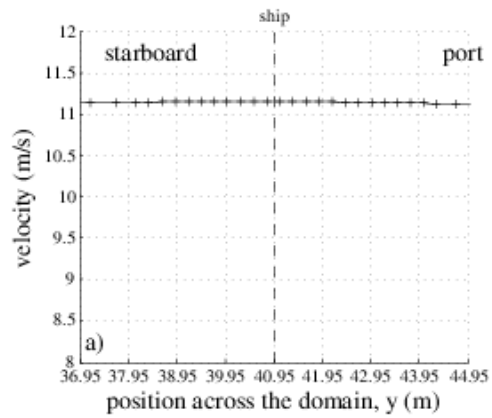
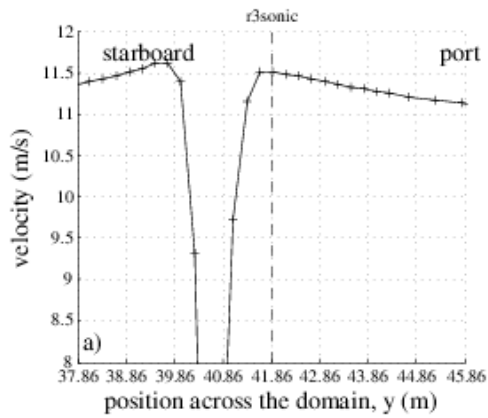


Figure 17. Lines of velocity data through the instrument position (indicated by the dashed line) in all three directions: top – across the domain; middle – along the domain, and bottom – vertically. The results are for a flow to the **R3 sonic at 70 degrees** over the port side.

Figure 18. The **ship's sonic site at 70 degrees** over the port side.

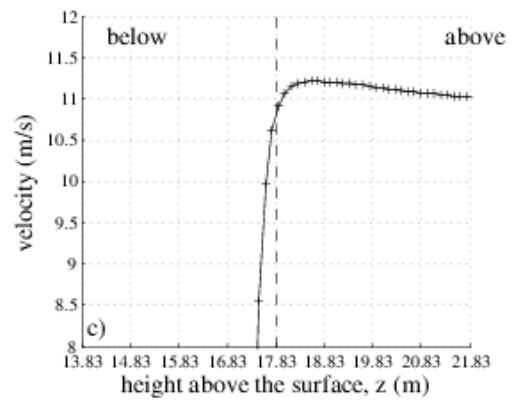
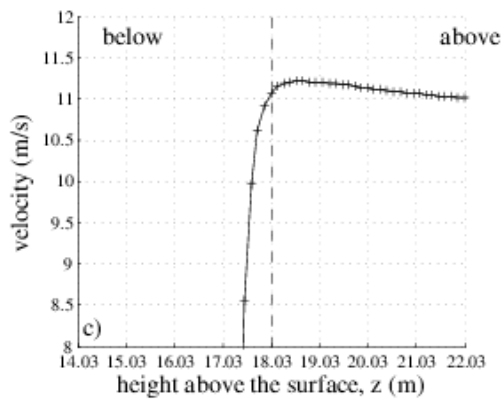
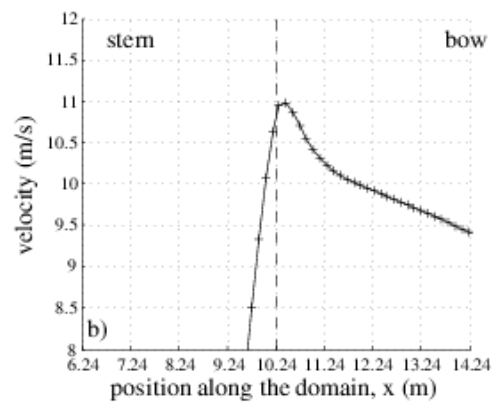
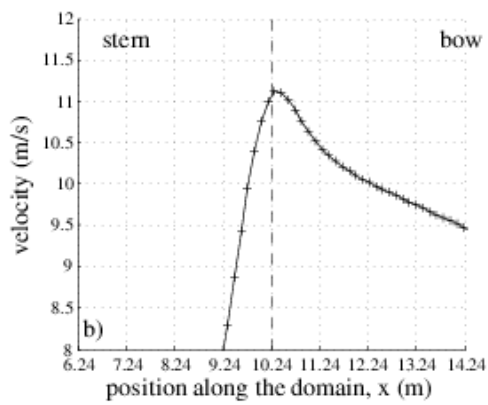
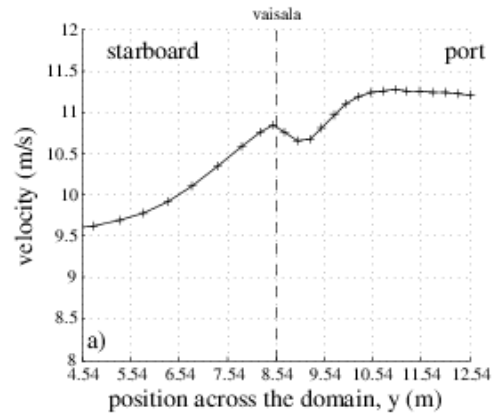
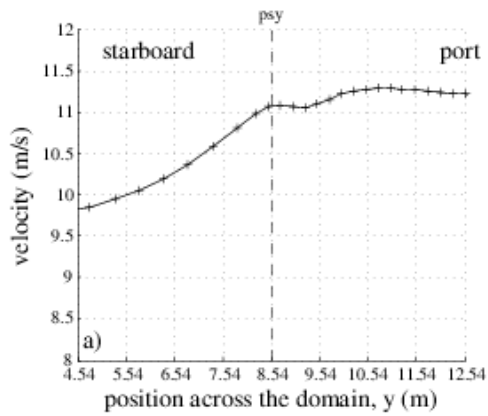


Figure 19. The psychrometer site at 70 degrees over the port side.

Figure 20. The Vaisala site at 70 degrees over the port side.

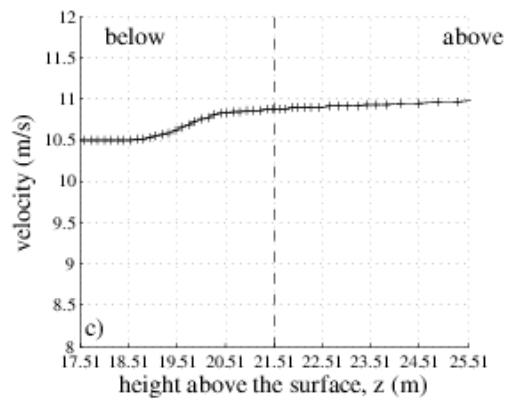
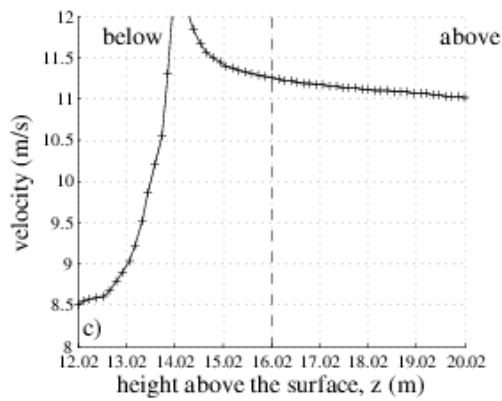
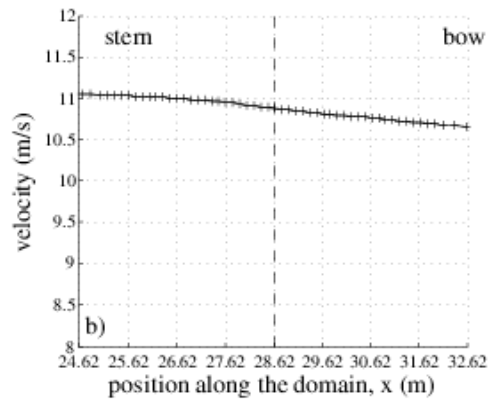
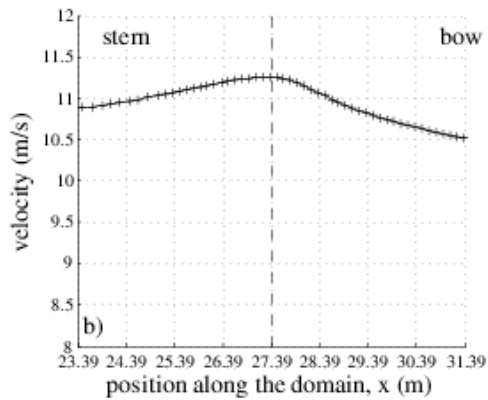
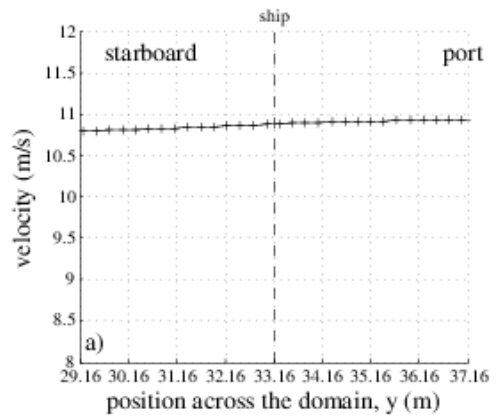
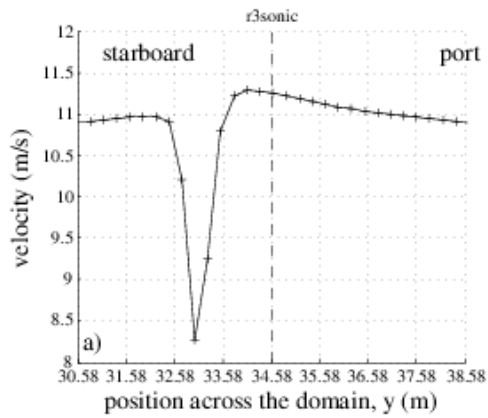


Figure 21. Lines of velocity data through the instrument position (indicated by the dashed line) in all three directions: top – across the domain; middle – along the domain, and bottom – vertically. The results are for a flow to the **R3 sonic at 50 degrees** over the port side.

Figure 22. The **ship's sonic site at 50 degrees** over the port side.

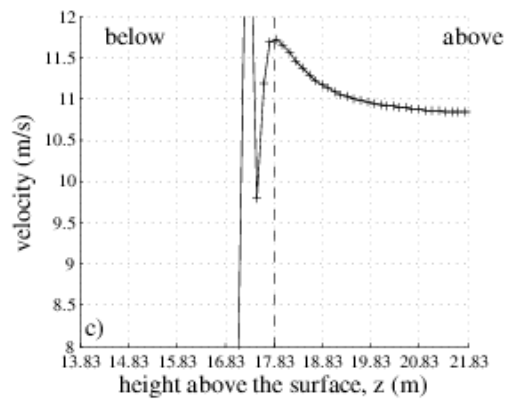
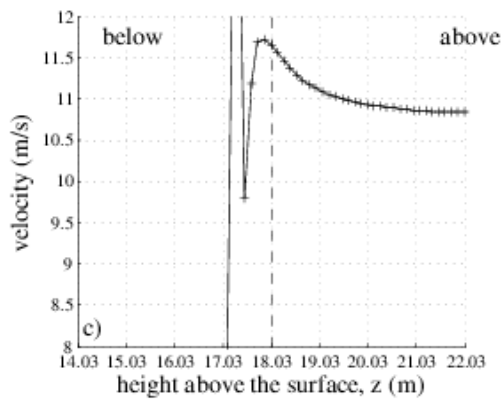
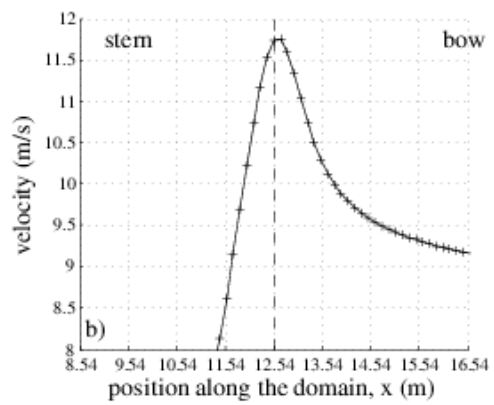
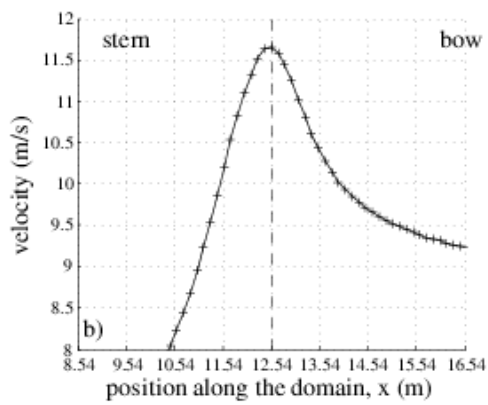
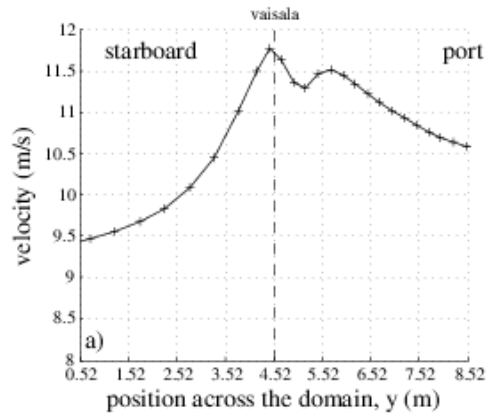
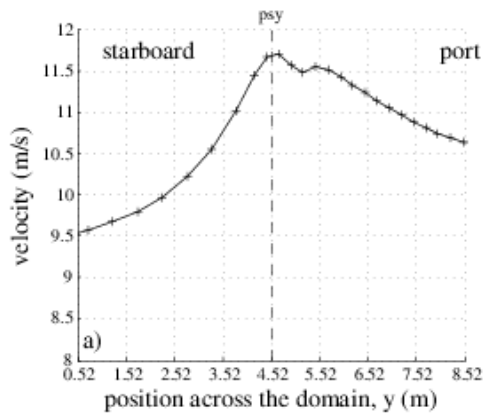


Figure 23. The psychrometer site at 50 degrees over the port side.

Figure 24. The Vaisala site at 50 degrees over the port side.

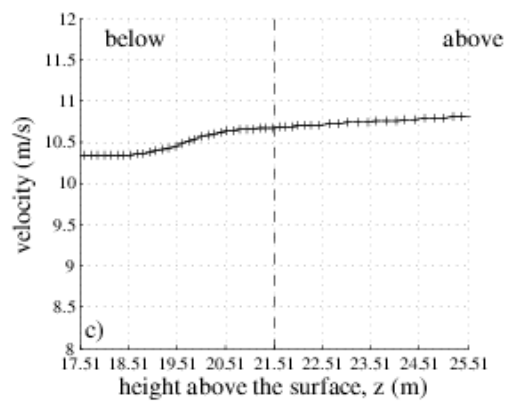
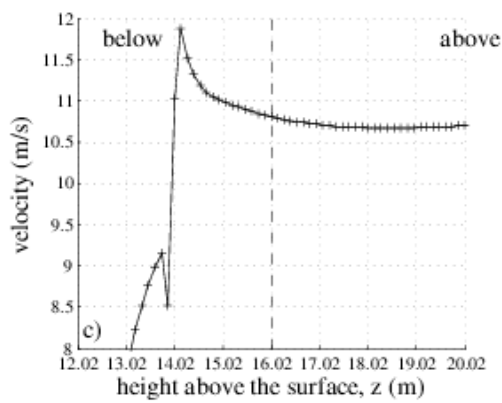
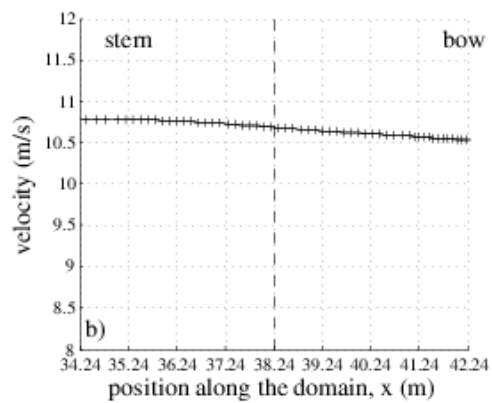
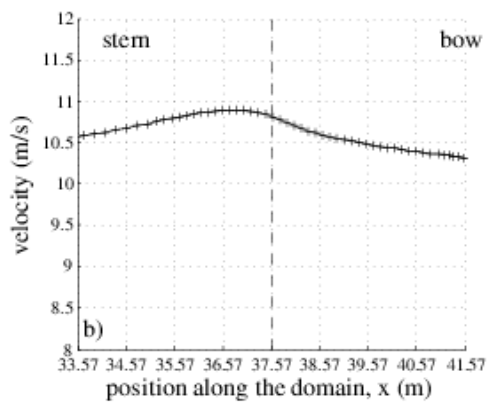
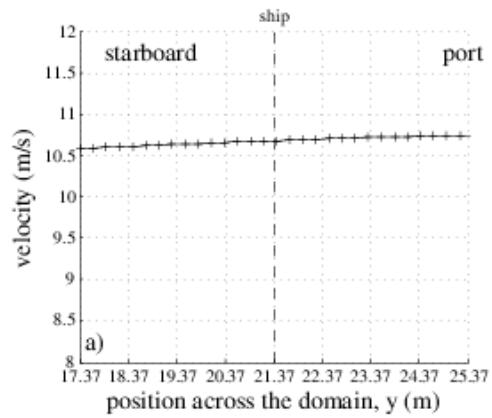
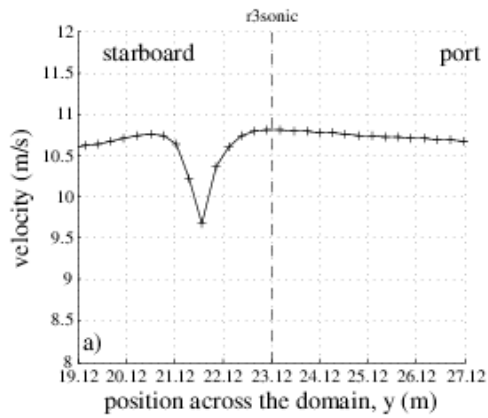


Figure 25. Lines of velocity data through the instrument position (indicated by the dashed line) in all three directions: top – across the domain; middle – along the domain, and bottom – vertically. The results are for a flow to the **R3 sonic at 30 degrees** over the port side.

Figure 26. The **ship's sonic site at 30 degrees** over the port side.

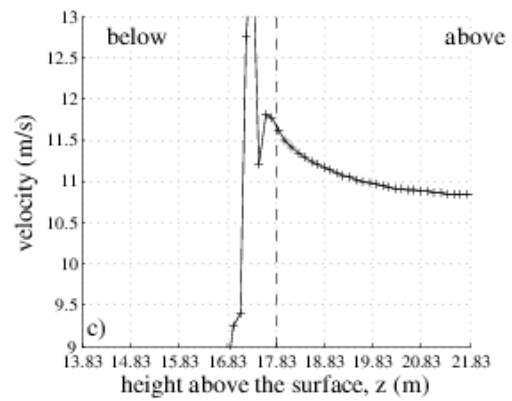
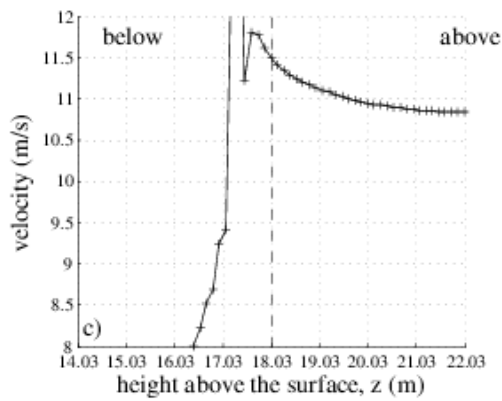
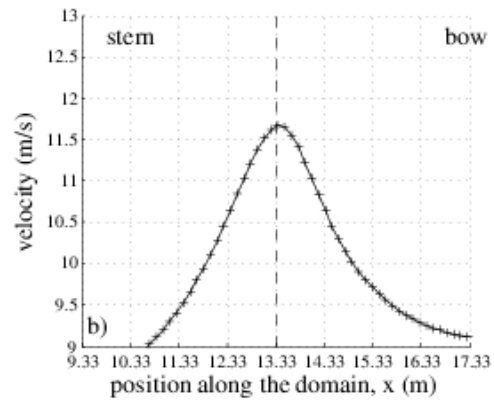
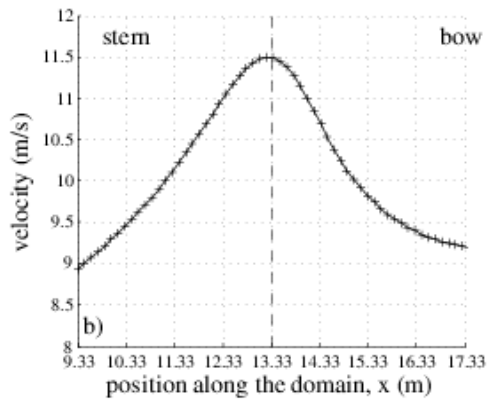
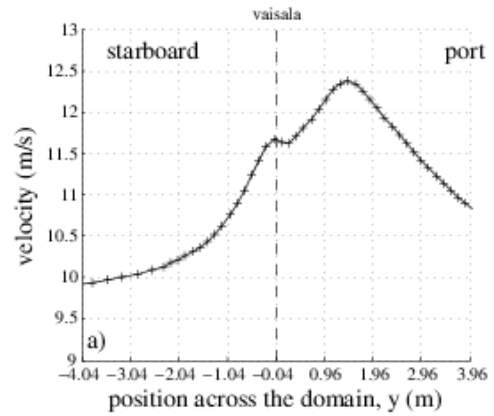
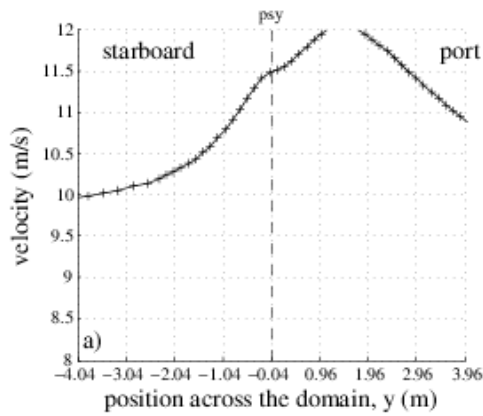


Figure 27. The psychrometer site at 30 degrees over the port side.

Figure 28. The Vaisala site at 30 degrees over the port side.

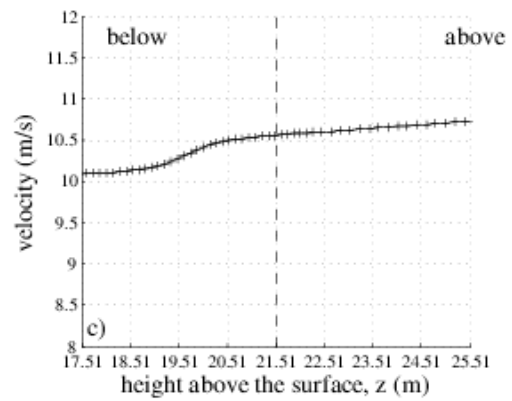
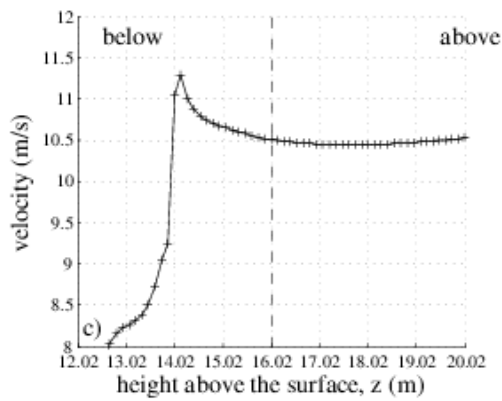
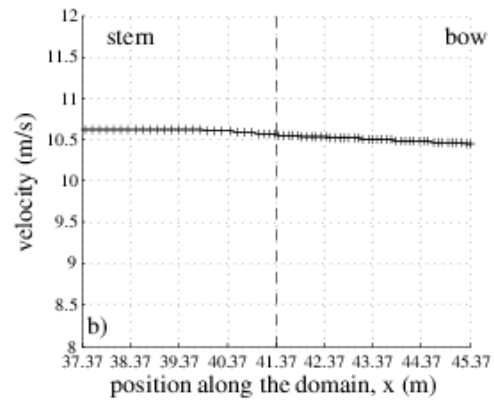
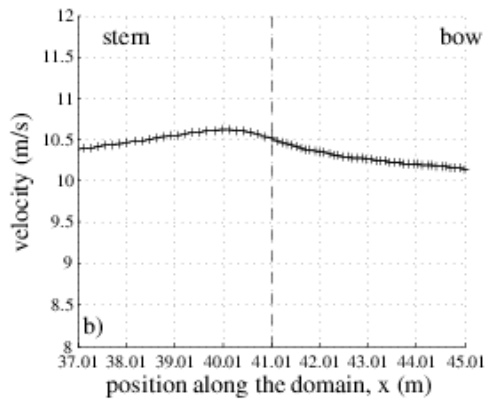
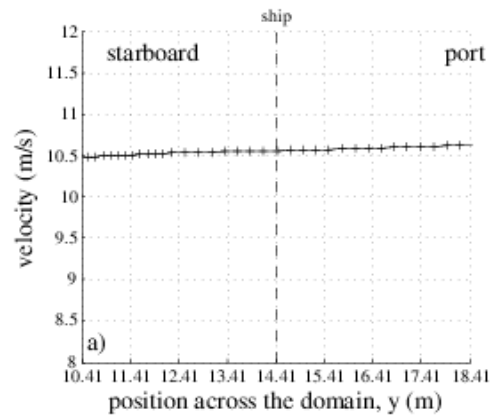
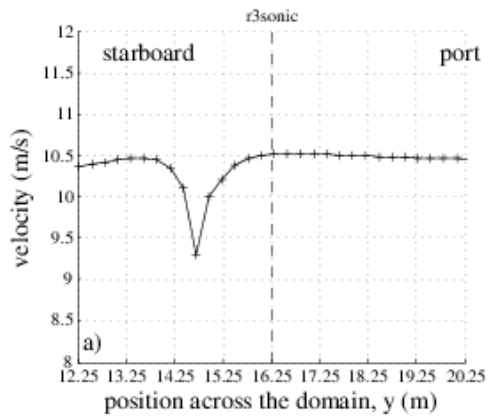


Figure 29. Lines of velocity data through the instrument position (indicated by the dashed line) in all three directions: top – across the domain; middle – along the domain, and bottom – vertically. The results are for a flow to the **R3 sonic at 20 degrees** over the port side.

Figure 30. The ship's sonic site at 20 degrees over the port side.

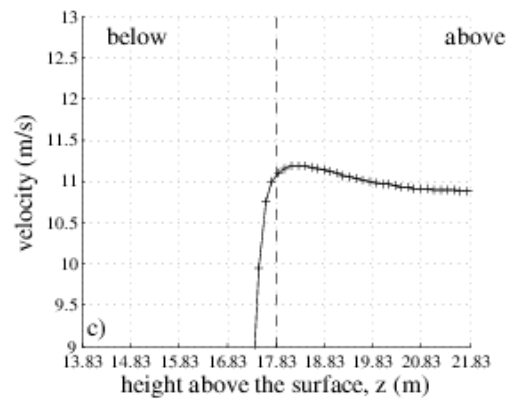
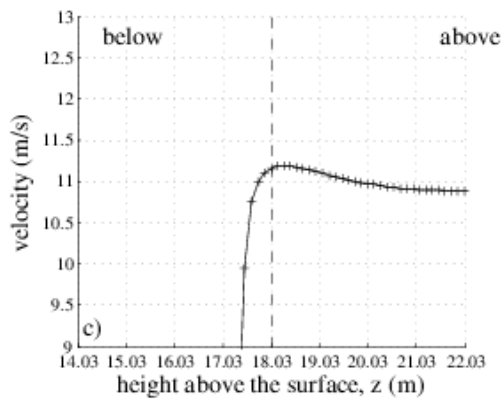
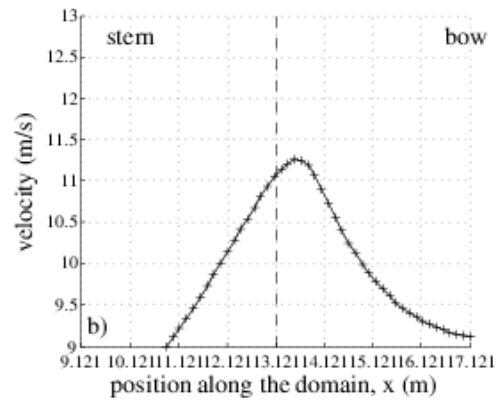
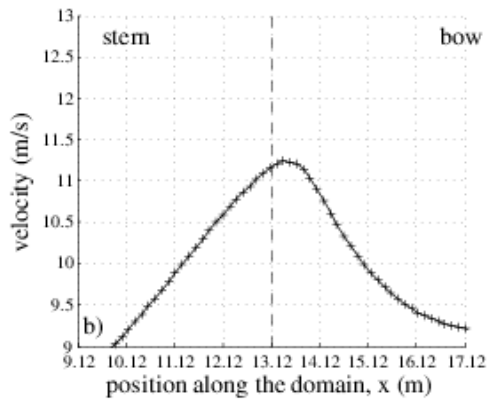
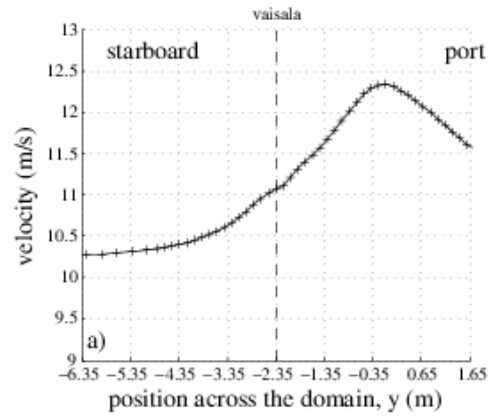
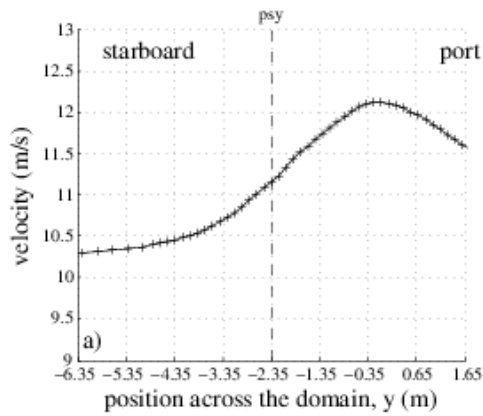


Figure 31. The psychrometer site at 20 degrees over the port side.

Figure 32. The Vaisala site at 20 degrees over the port side.

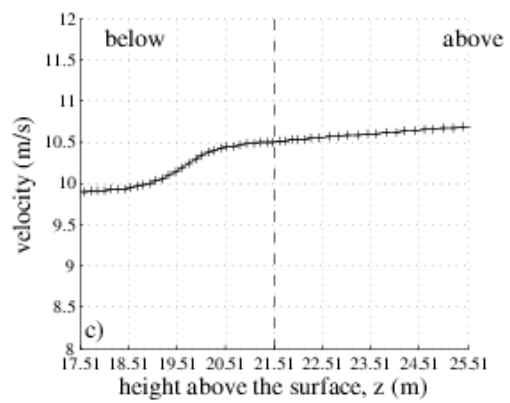
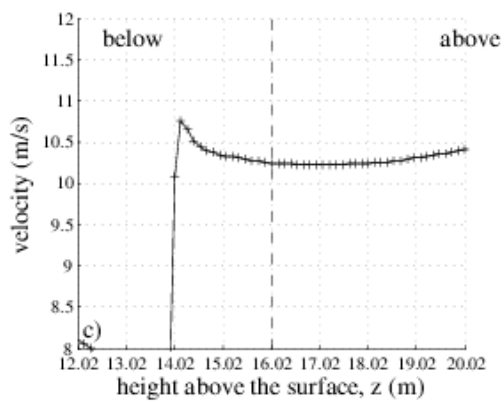
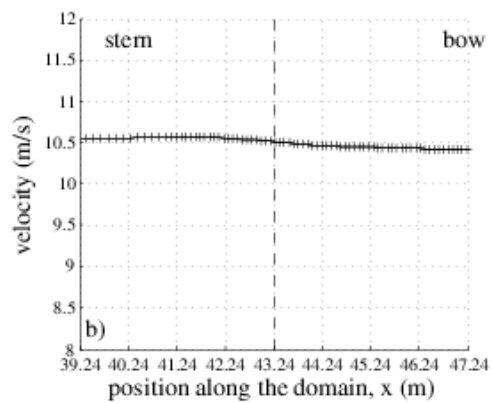
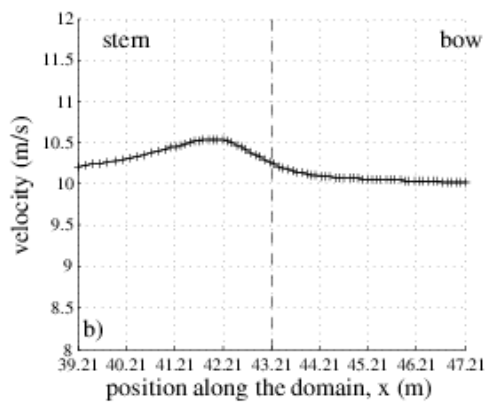
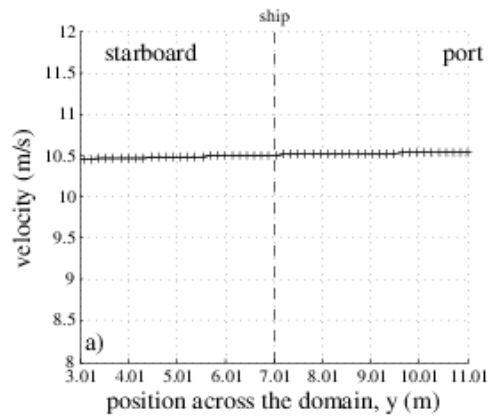
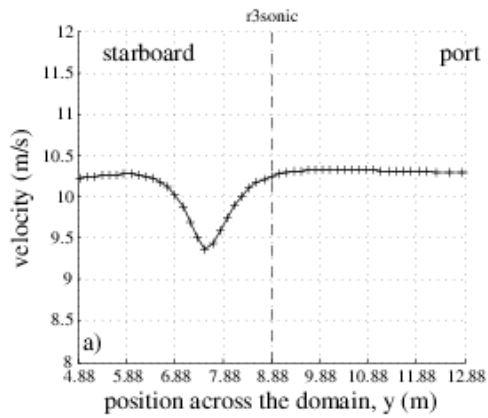


Figure 33. Lines of velocity data through the instrument position (indicated by the dashed line) in all three directions: top – across the domain; middle – along the domain, and bottom – vertically. The results are for a flow to the **R3 sonic at 10 degrees** over the port side.

Figure 34. The **ship's sonic site at 10 degrees** over the port side.

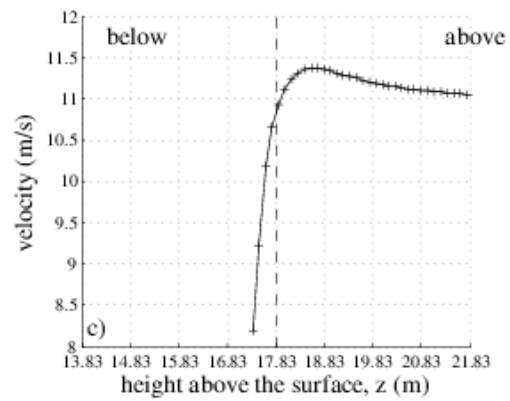
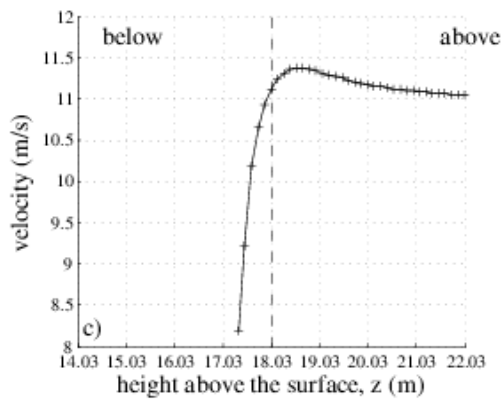
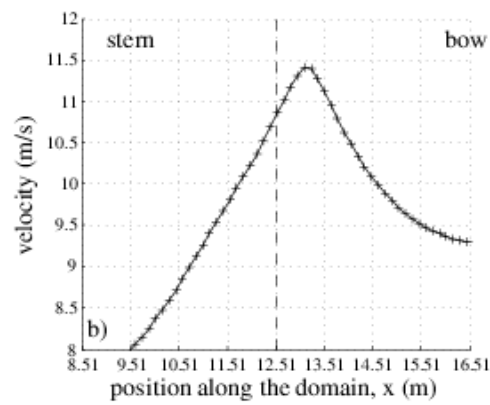
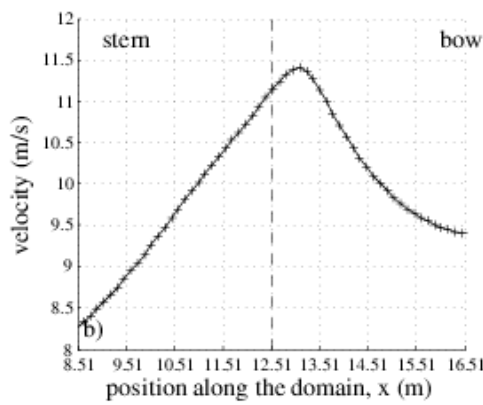
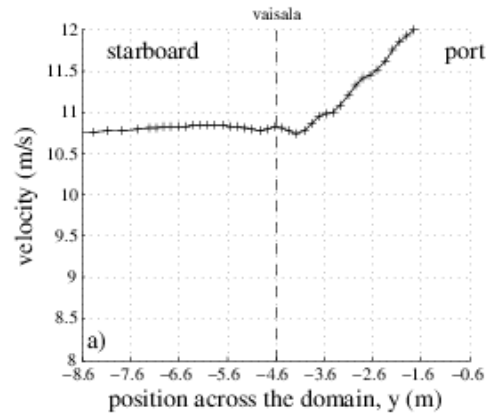
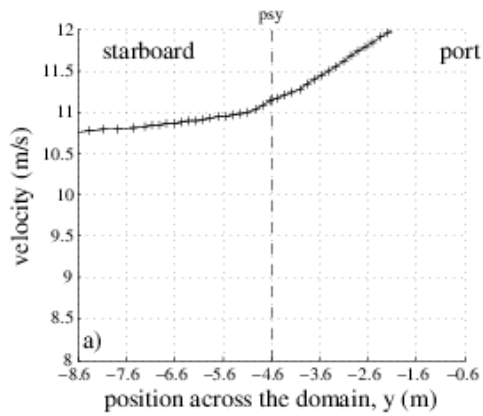


Figure 35. The psychrometer site at 10 degrees over the port side.

Figure 36. The Vaisala site at 10 degrees over the port side.

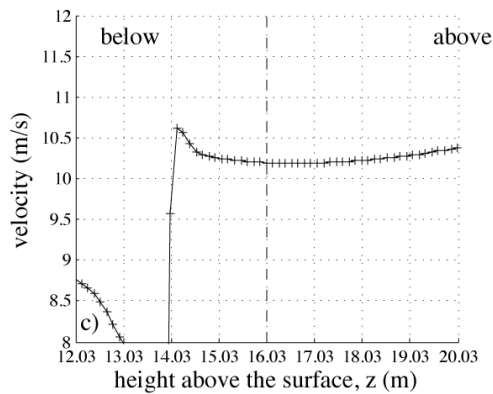
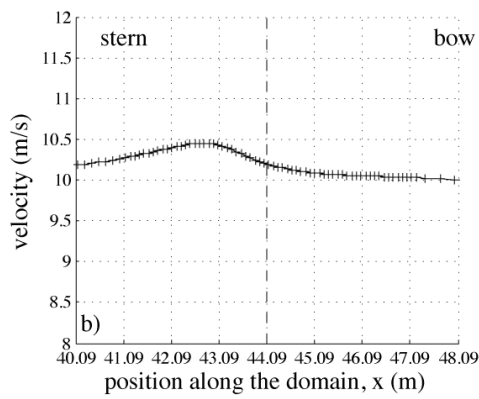
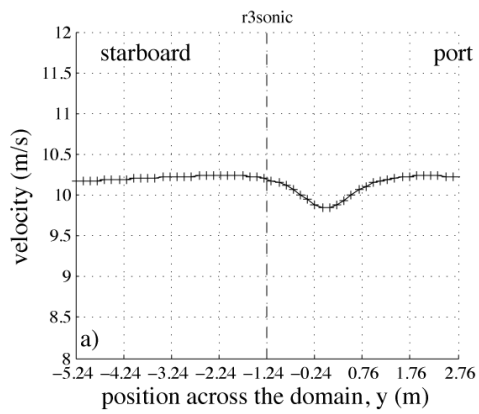


Figure 37. Lines of velocity data through the instrument position (indicated by the dashed line) in all three directions: top – across the domain; middle – along the domain, and bottom – vertically. The results are for a flow to the R3 sonic at 0 degrees (bow-on).

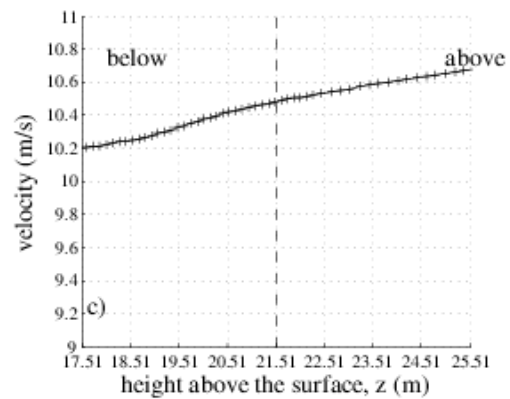
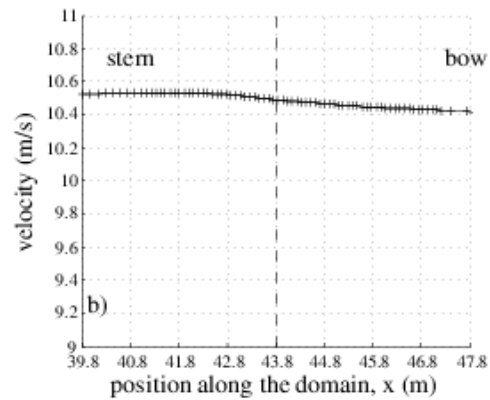
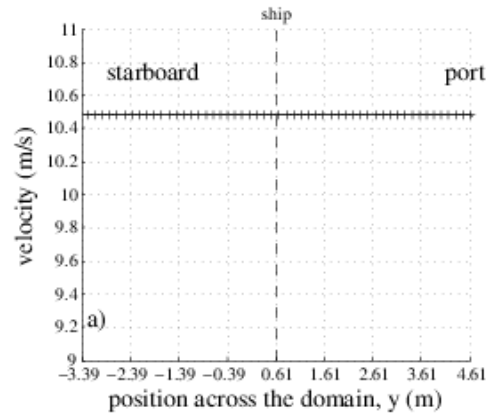


Figure 38. The ship's sonic site at 0 degrees (bow-on).

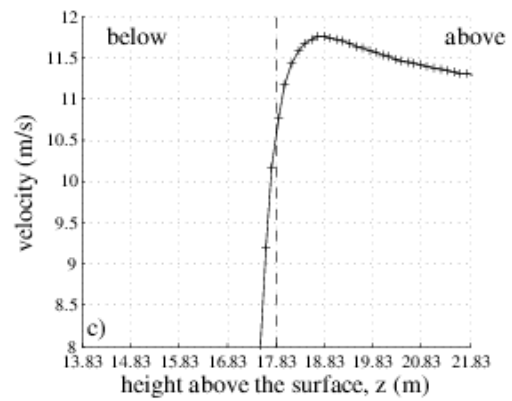
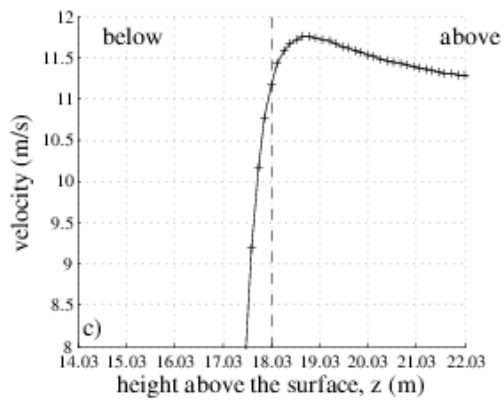
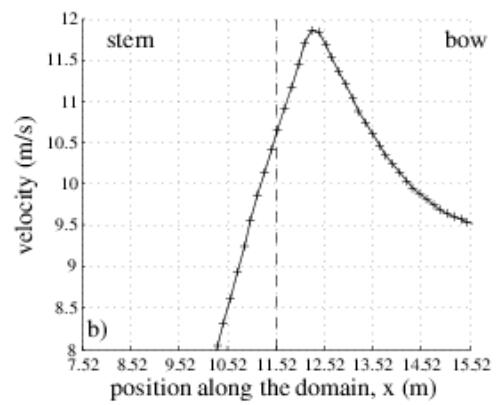
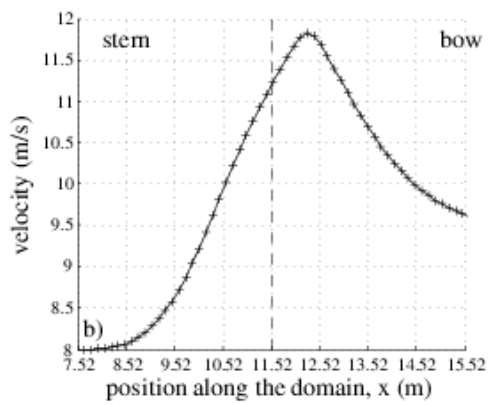
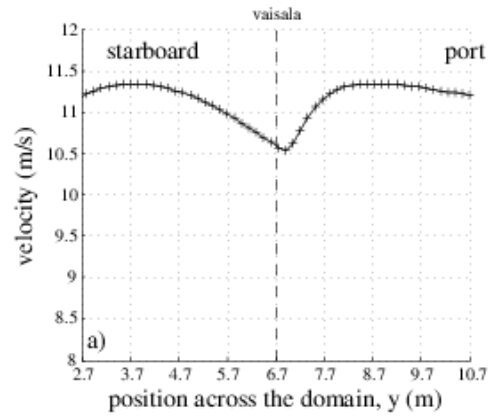
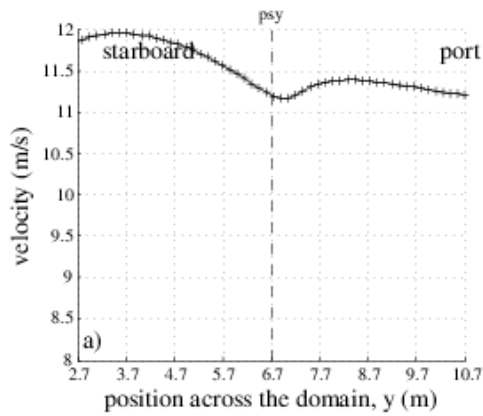


Figure 39. The psychrometer site at 0 degrees (bow-on).

Figure 40. The Vaisala site at 0 degrees (bow-on).

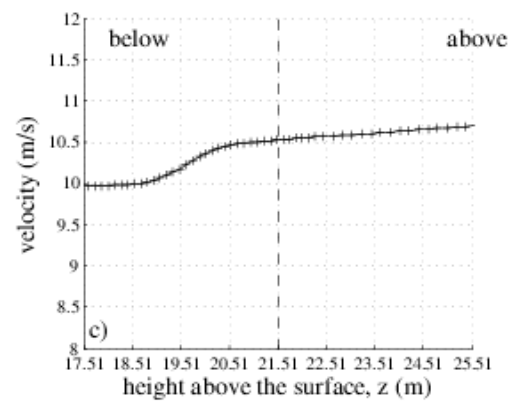
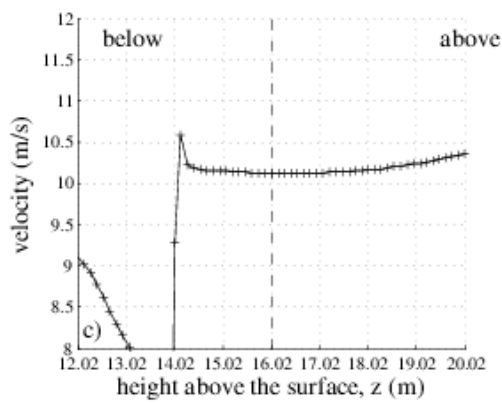
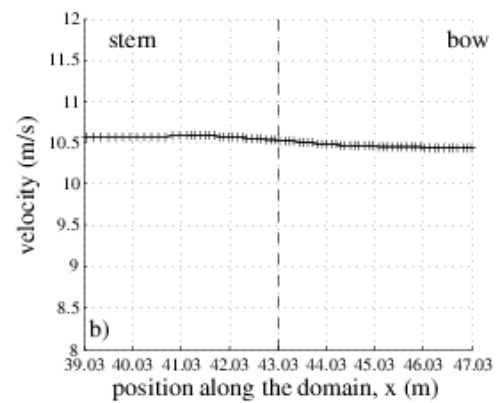
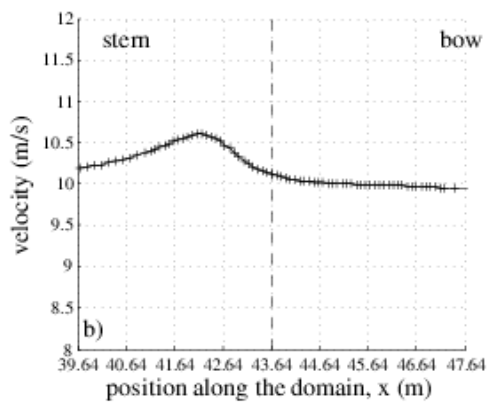
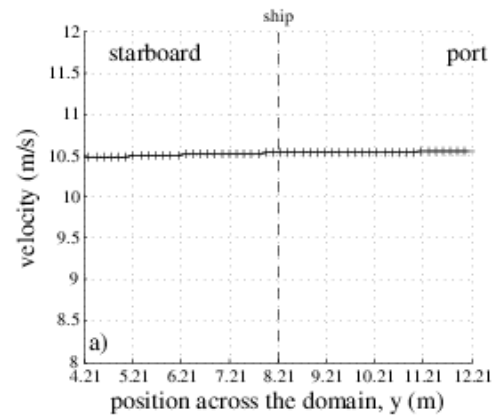
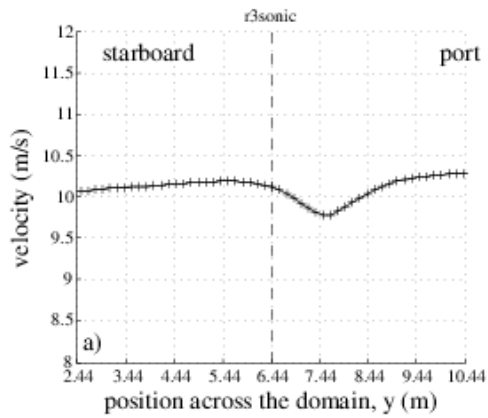


Figure 41. Lines of velocity data through the instrument position (indicated by the dashed line) in all three directions: top – across the domain; middle – along the domain, and bottom – vertically. The results are for a flow to the **R3 sonic** at 10 degrees over the starboard side.

Figure 42. The ship's sonic site at 10 degrees over the starboard side.

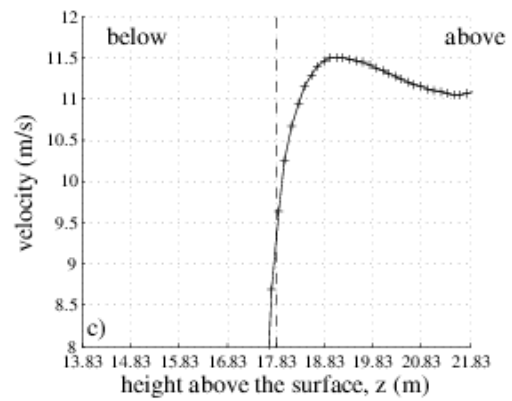
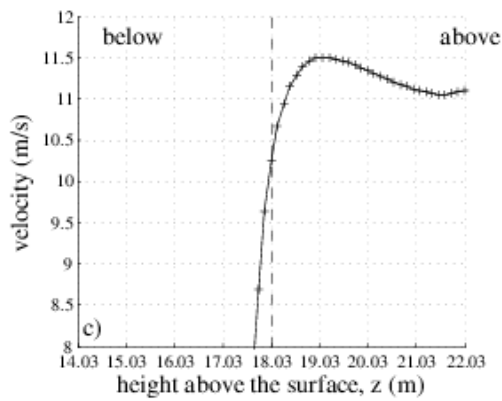
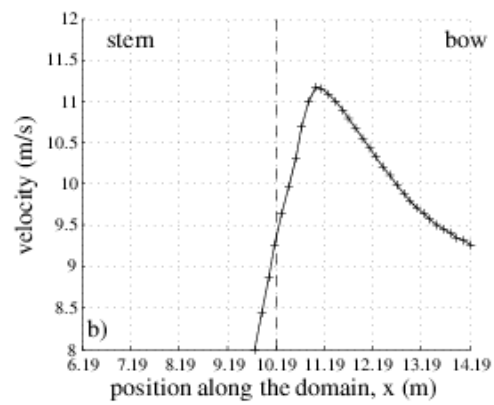
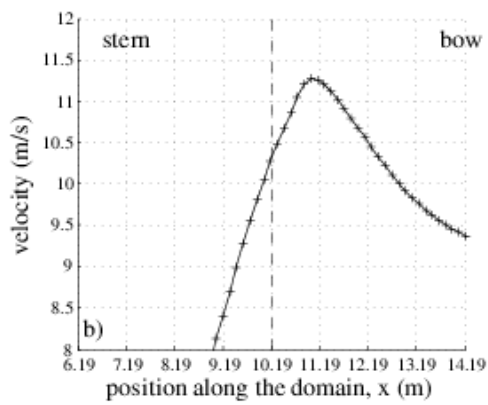
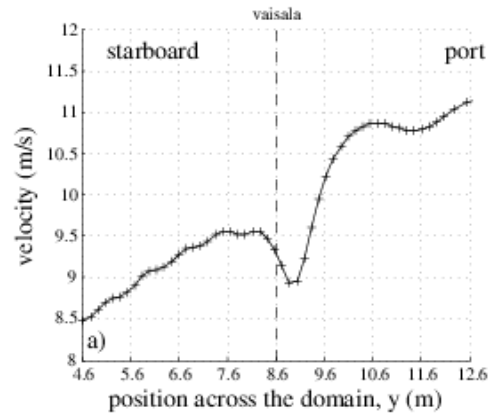
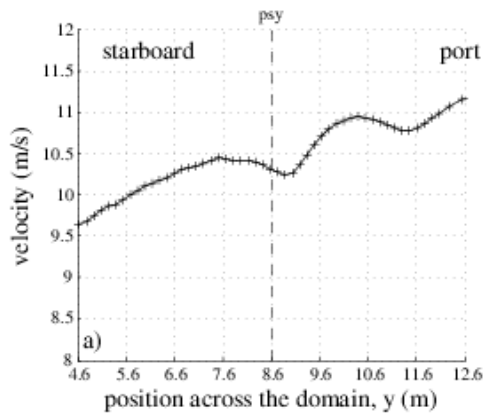


Figure 43. The psychrometer site at 10 degrees over the starboard side.

Figure 44. The Vaisala site at 10 degrees over the starboard side.

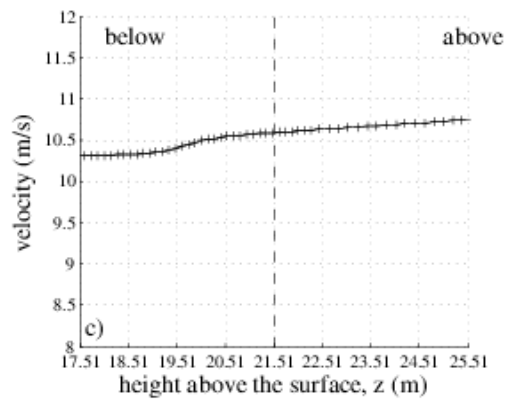
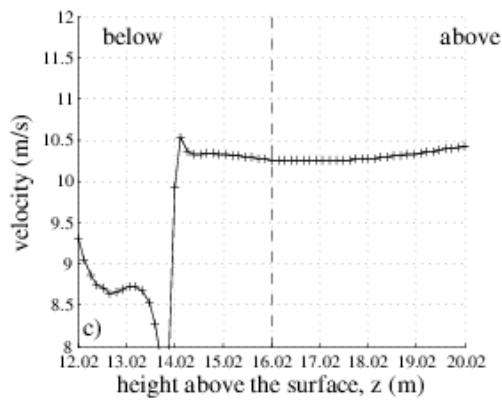
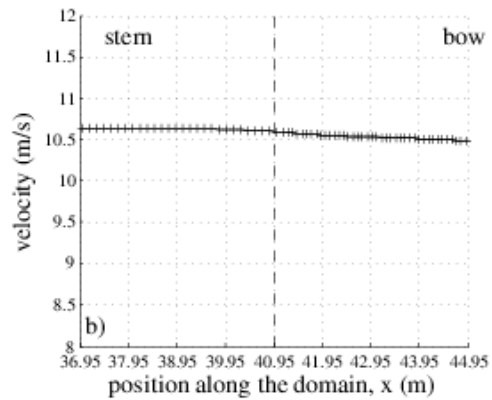
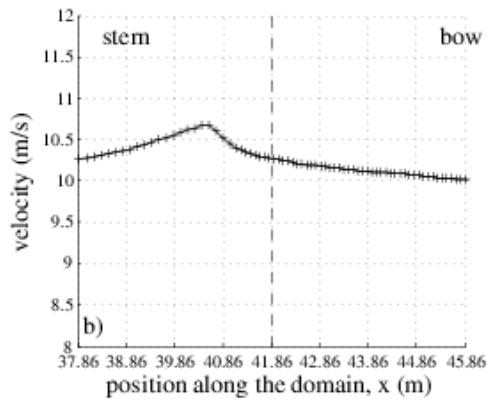
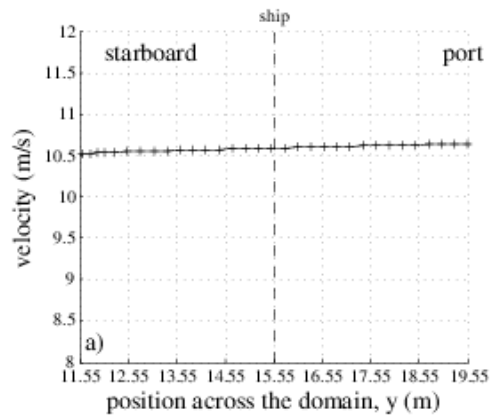
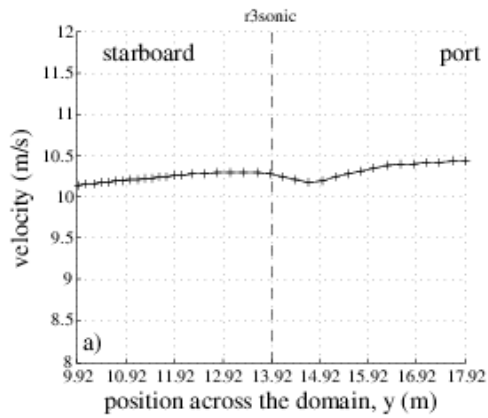


Figure 45. Lines of velocity data through the instrument position (indicated by the dashed line) in all three directions: top – across the domain; middle – along the domain, and bottom – vertically. The results are for a flow to the **R3 sonic at 20 degrees** over the starboard side.

Figure 46. The **ship's sonic site at 20 degrees** over the starboard side.

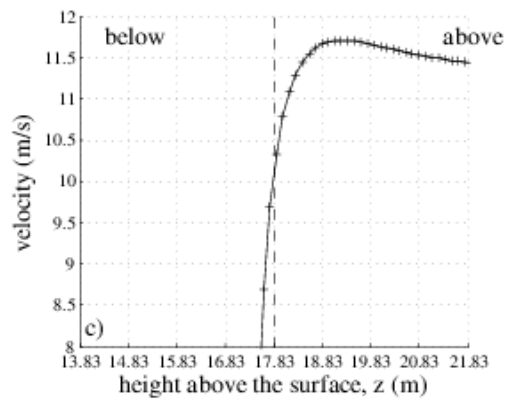
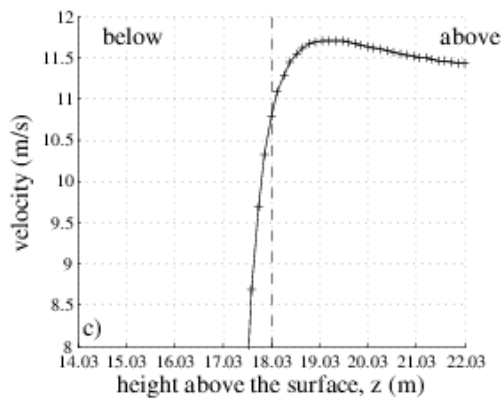
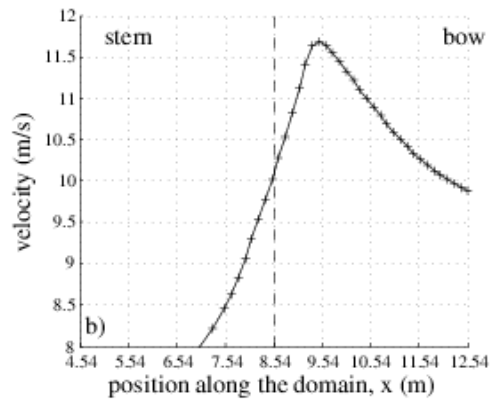
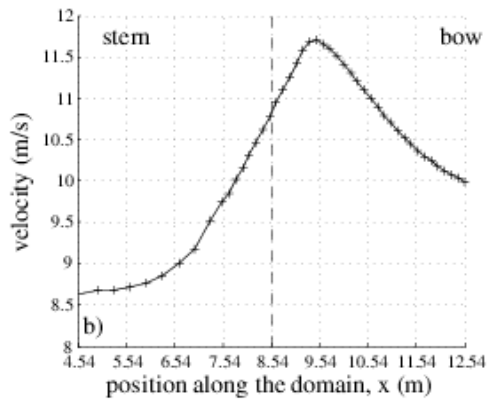
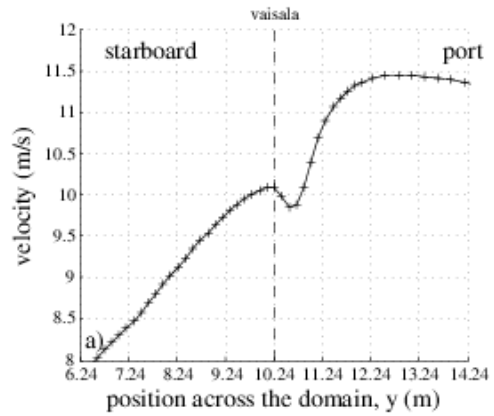
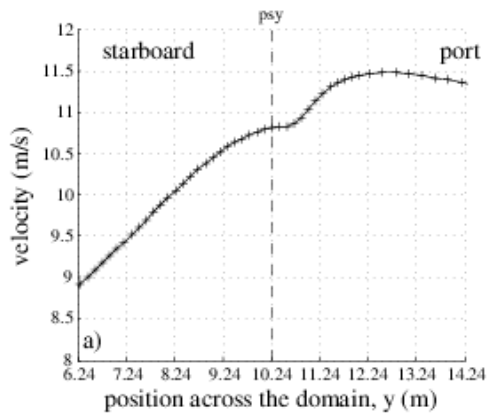


Figure 47. The psychrometer site at 20 degrees over the starboard side.

Figure 48. The Vaisala site at 20 degrees over the starboard side.

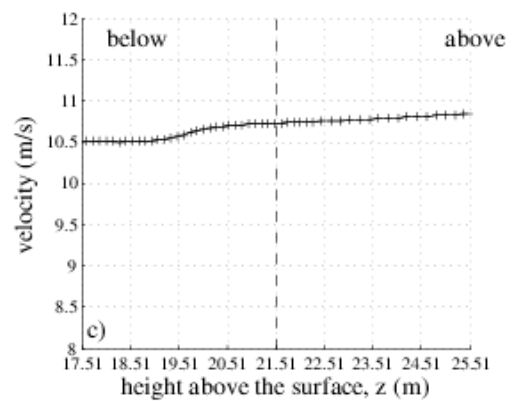
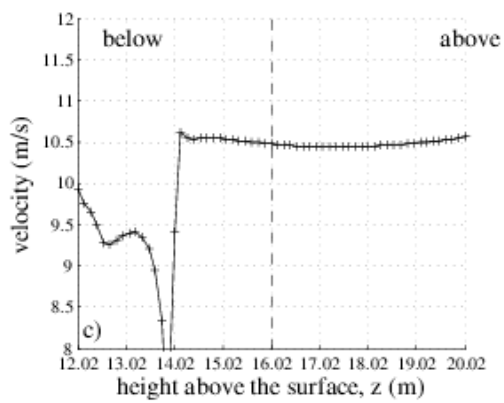
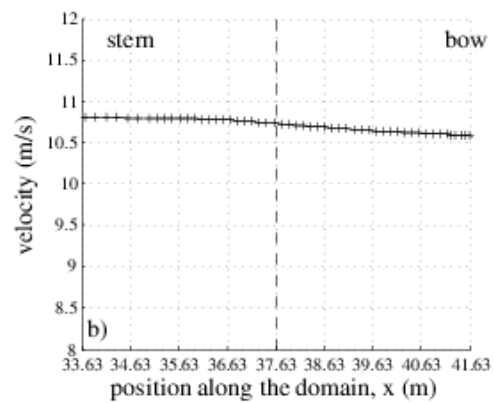
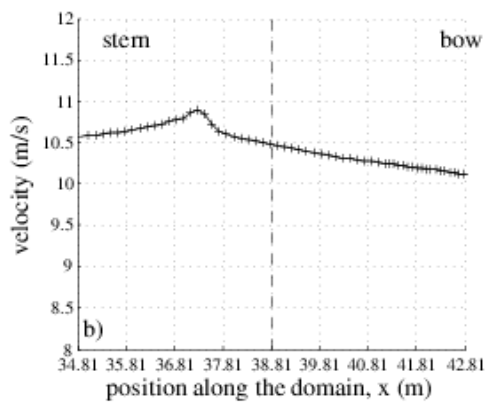
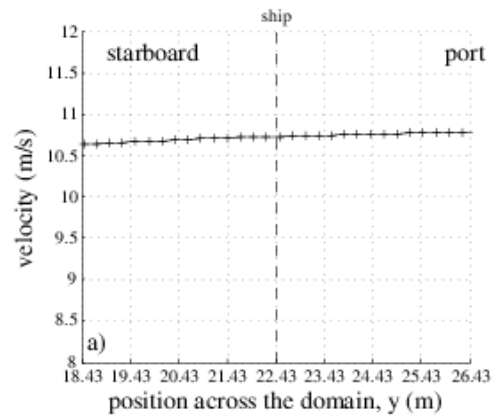
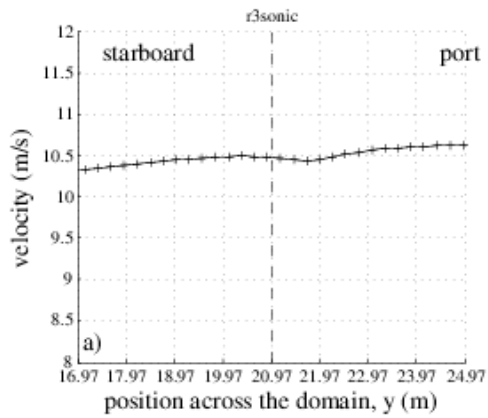


Figure 49. Lines of velocity data through the instrument position (indicated by the dashed line) in all three directions: top – across the domain; middle – along the domain, and bottom – vertically. The results are for a flow to the **R3 sonic at 30 degrees** over the starboard side.

Figure 50. The ship's sonic site at 30 degrees over the starboard side.

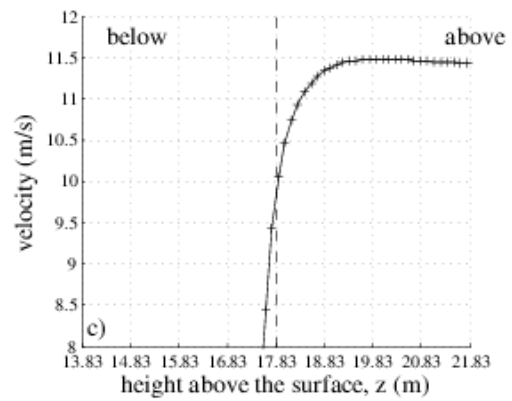
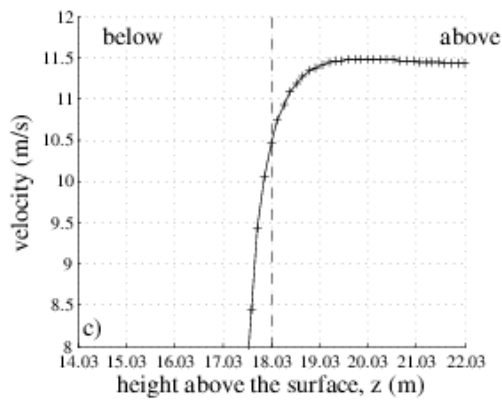
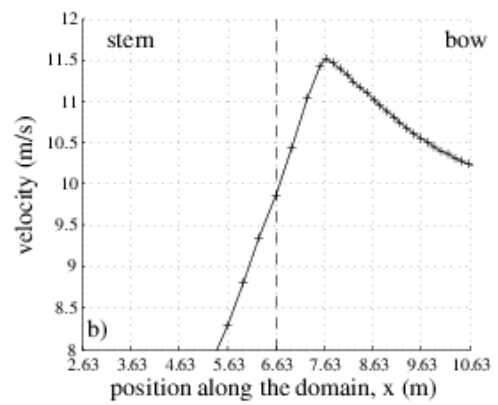
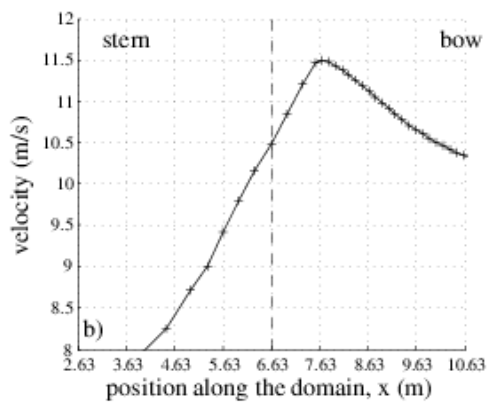
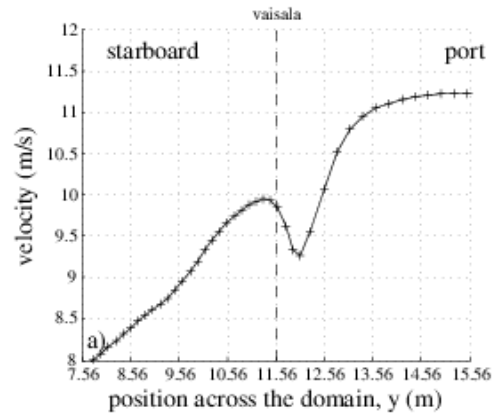
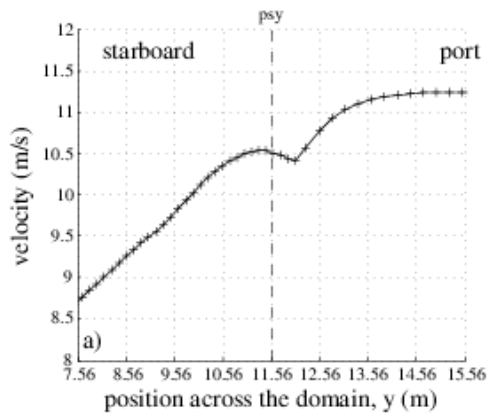


Figure 51. The psychrometer site at 30 degrees over the starboard side.

Figure 52. The Vaisala site at 30 degrees over the starboard side.

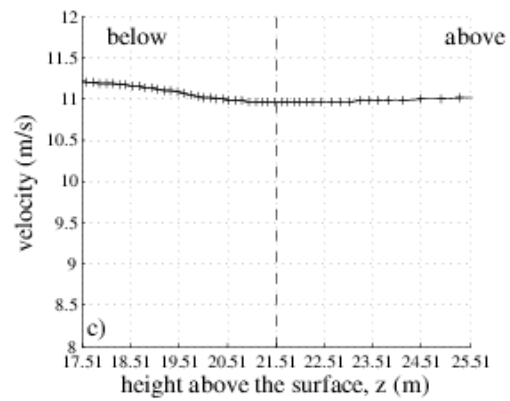
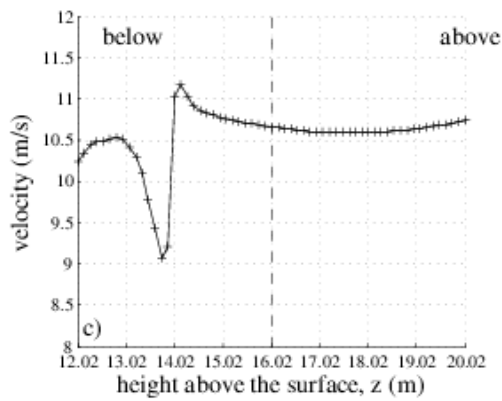
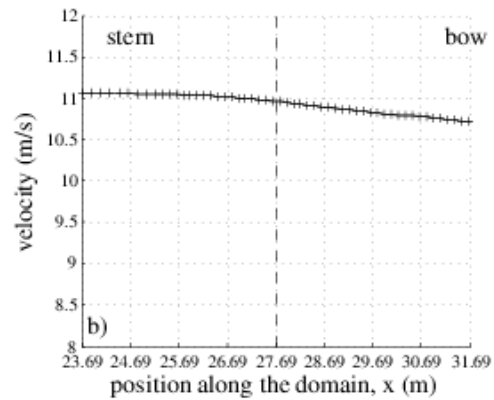
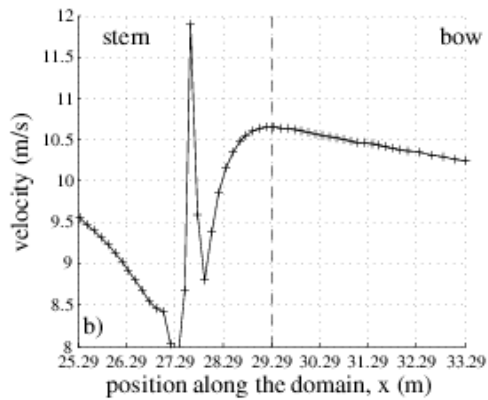
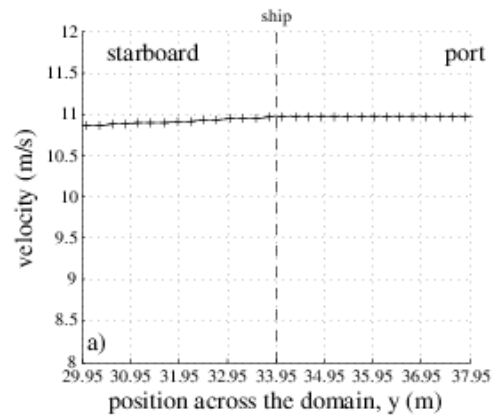
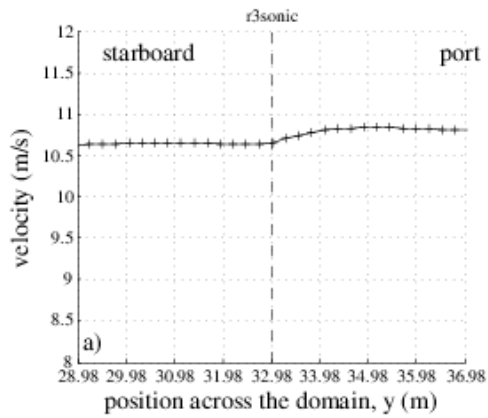


Figure 53. Lines of velocity data through the instrument position (indicated by the dashed line) in all three directions: top – across the domain; middle – along the domain, and bottom – vertically. The results are for a flow to the **R3 sonic at 50 degrees** over the starboard side.

Figure 54. The ship's sonic site at 50 degrees over the starboard side.

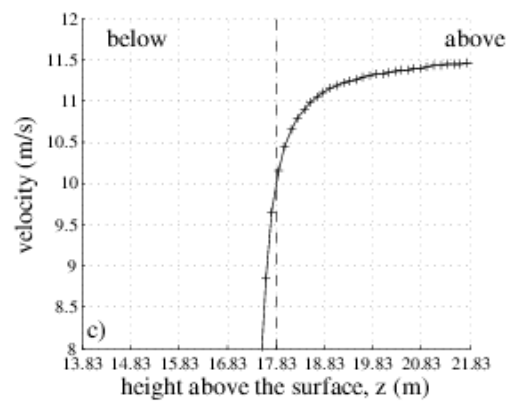
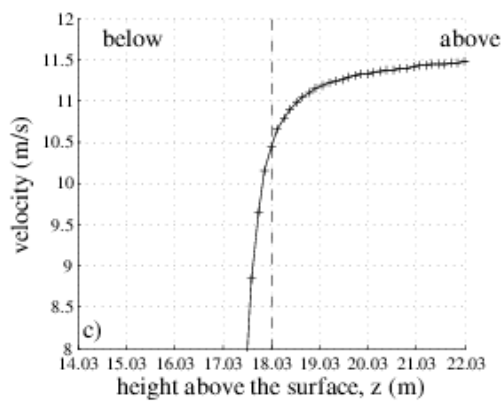
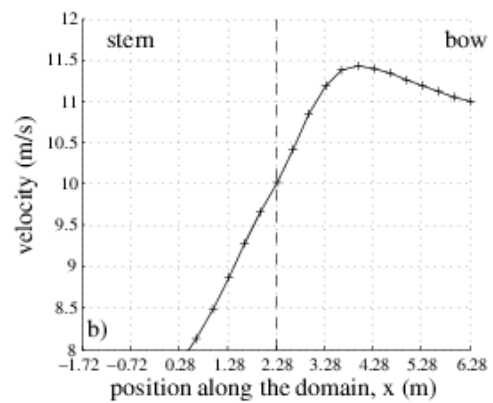
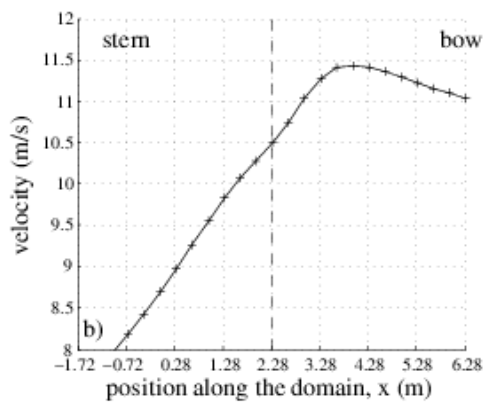
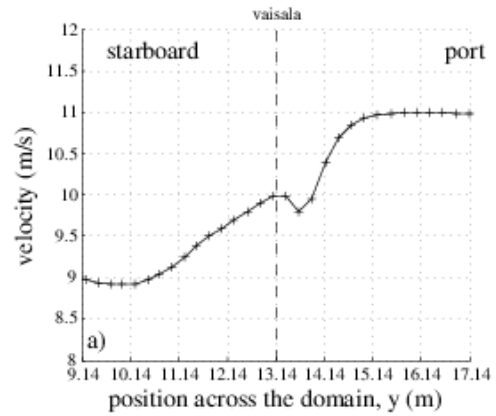
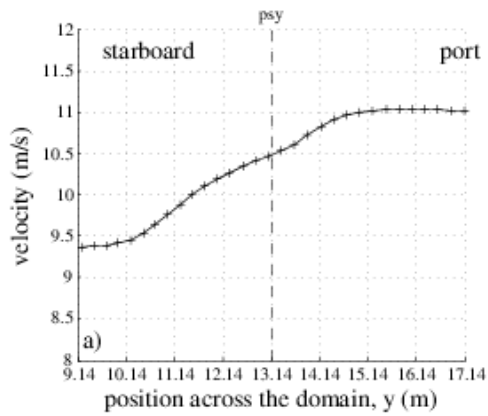


Figure 55. The psychrometer site at 50 degrees over the starboard side.

Figure 56. The Vaisala site at 50 degrees over the starboard side.

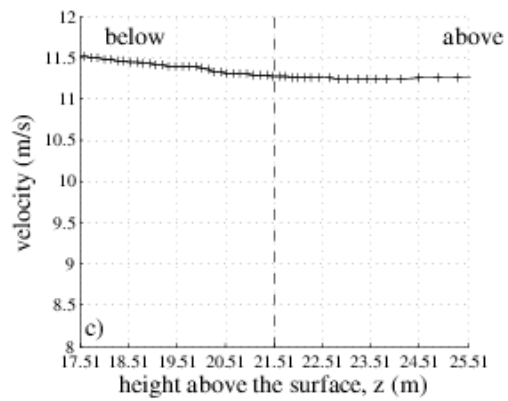
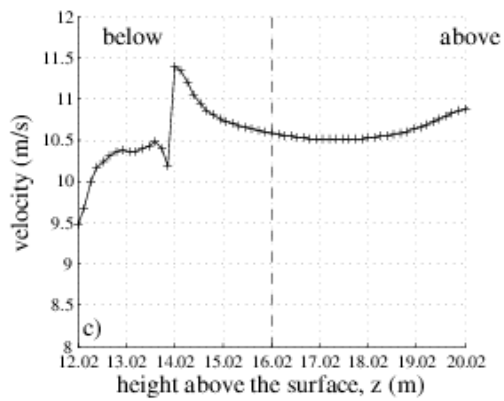
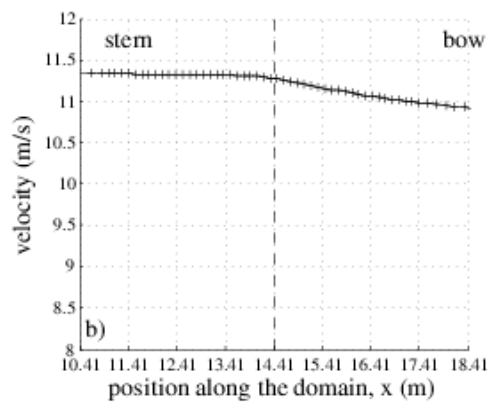
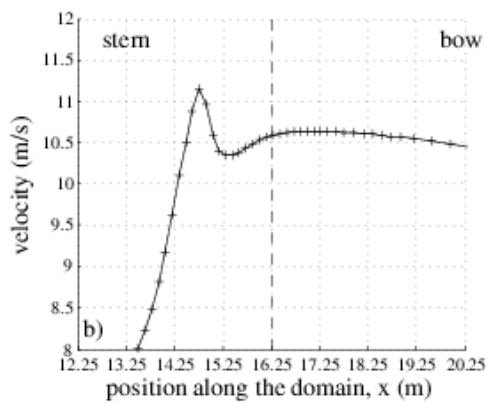
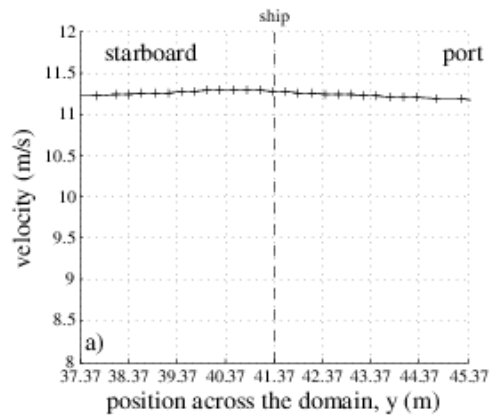
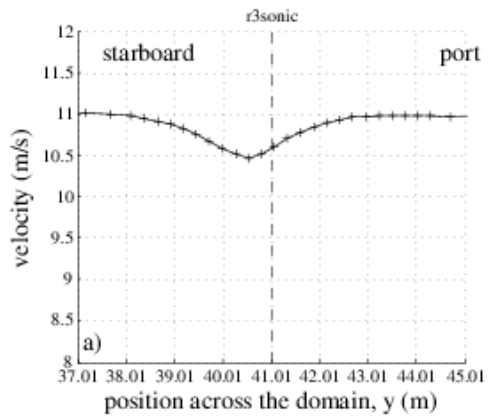


Figure 57. Lines of velocity data through the instrument position (indicated by the dashed line) in all three directions: top – across the domain; middle – along the domain, and bottom – vertically. The results are for a flow to the **R3 sonic at 70 degrees** over the starboard side.

Figure 58. The ship's sonic site at 70 degrees over the starboard side.

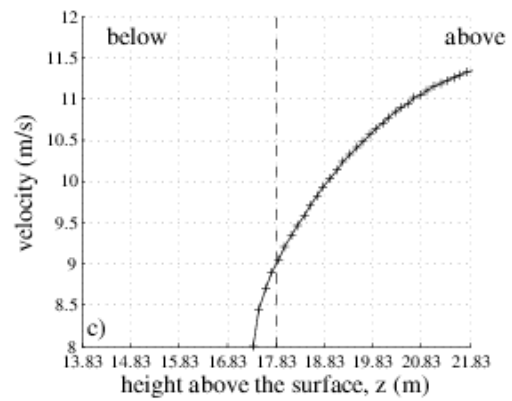
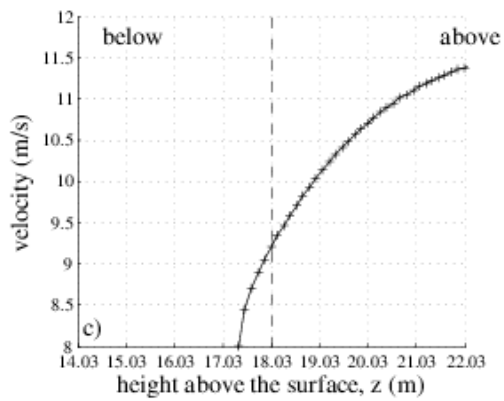
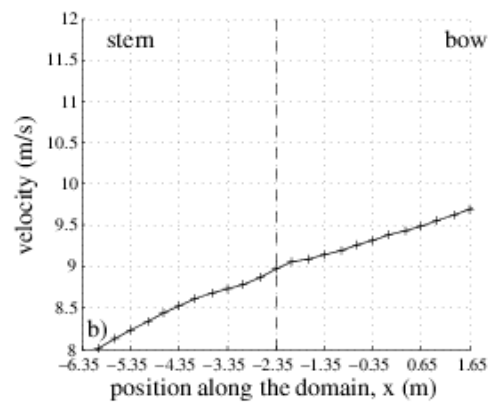
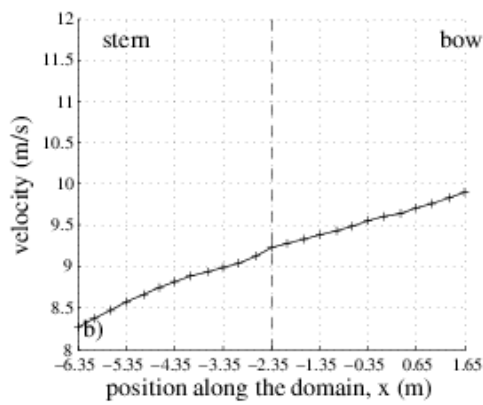
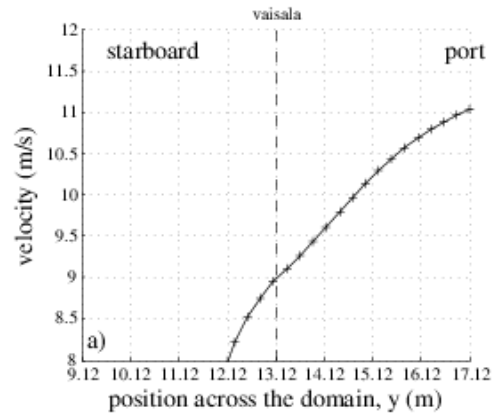
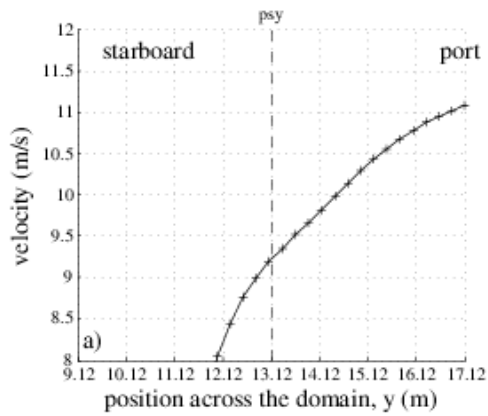


Figure 59. The psychrometer site at 70 degrees over the starboard side.

Figure 60. The Vaisala site at 70 degrees over the starboard side.

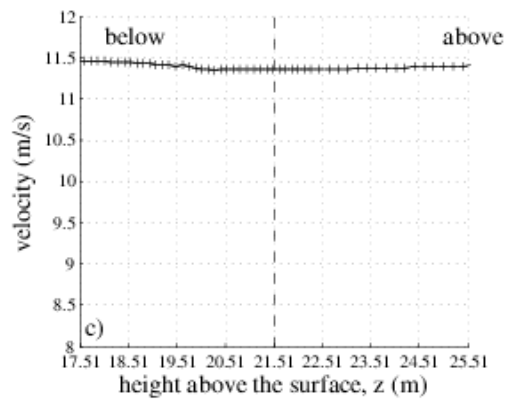
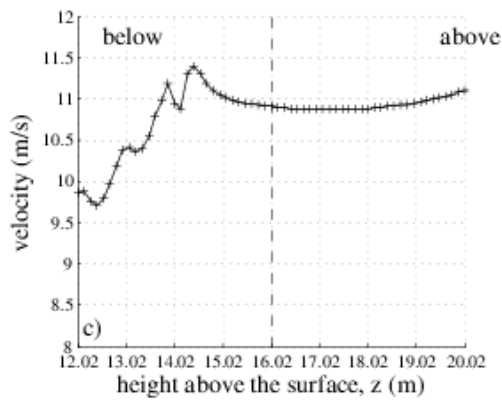
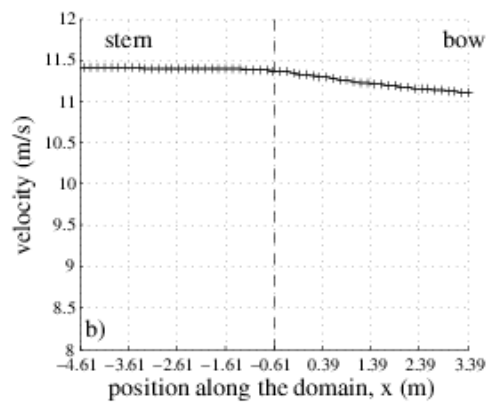
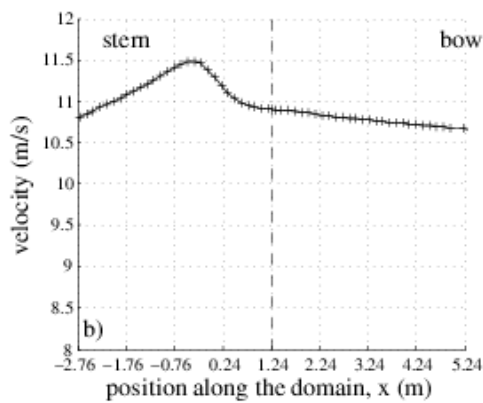
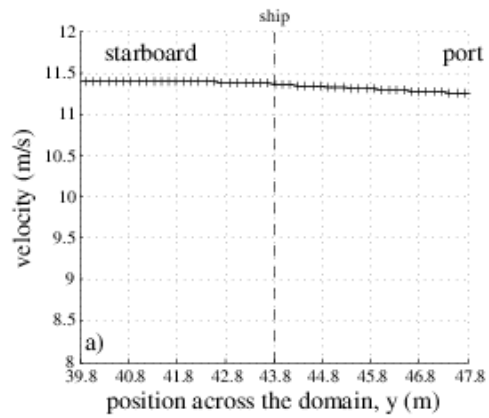
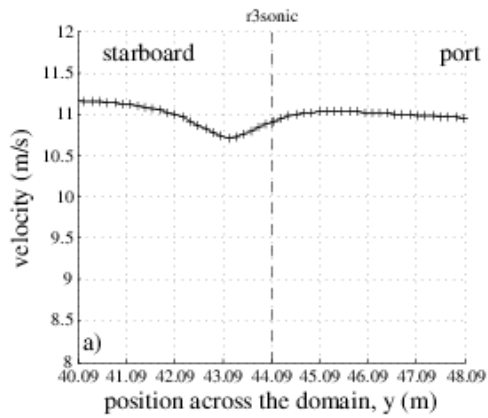


Figure 61. Lines of velocity data through the instrument position (indicated by the dashed line) in all three directions: top – across the domain; middle – along the domain, and bottom – vertically. The results are for a flow to the **R3 sonic at 90 degrees** over the starboard side.

Figure 62. The ship's sonic site at 90 degrees over the starboard side.

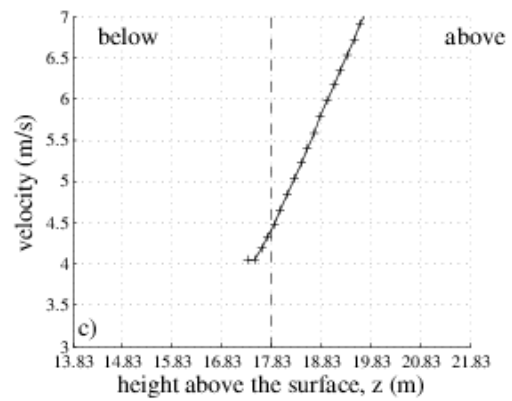
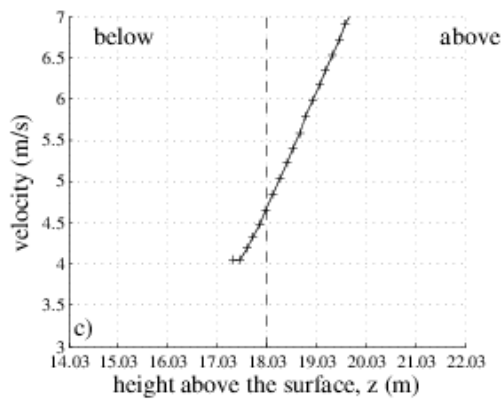
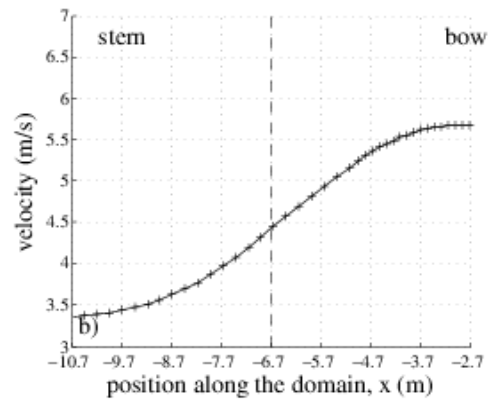
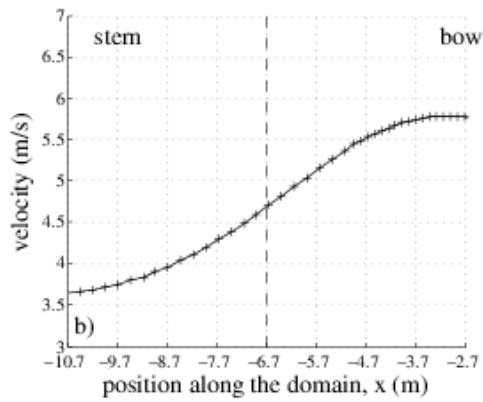
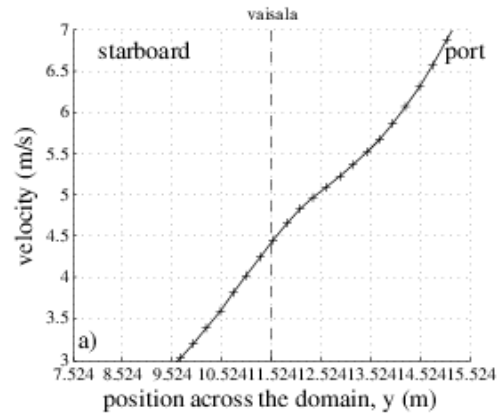
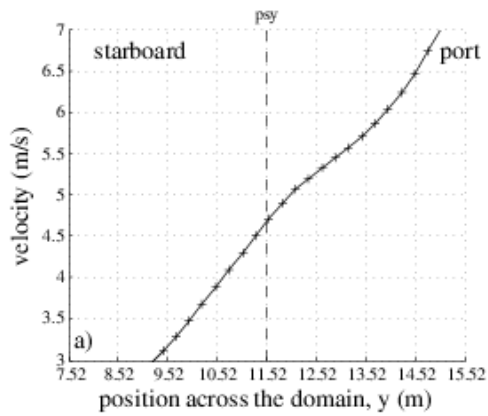


Figure 63. The psychrometer site at 90 degrees over the starboard side.

Figure 64. The Vaisala site at 90 degrees over the starboard side.

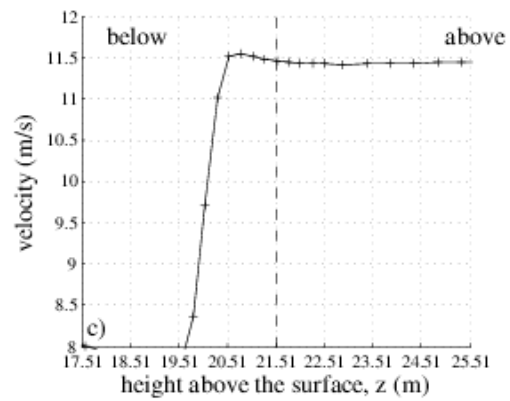
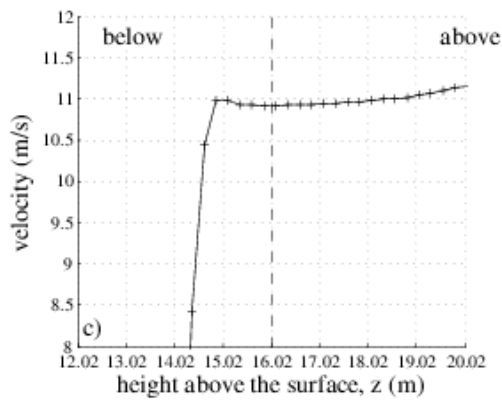
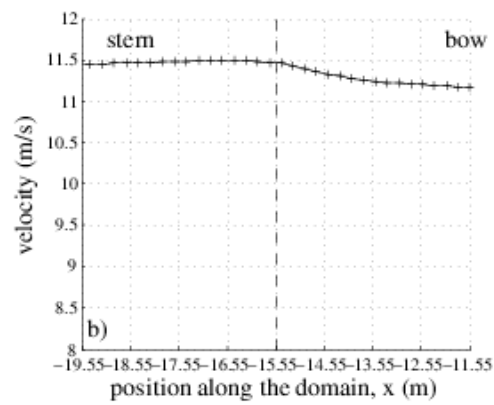
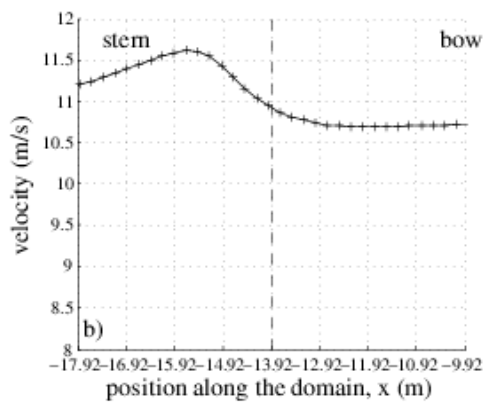
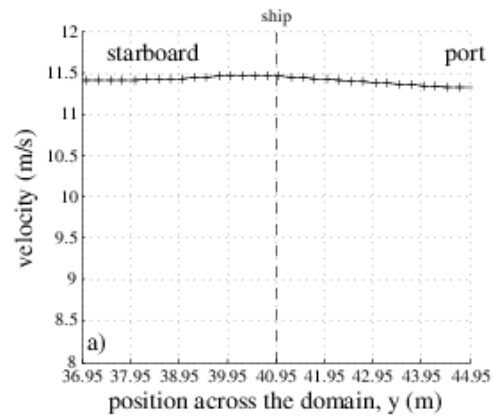
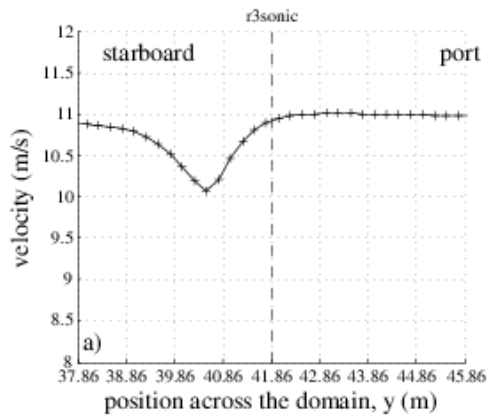


Figure 65. Lines of velocity data through the instrument position (indicated by the dashed line) in all three directions: top – across the domain; middle – along the domain, and bottom – vertically. The results are for a flow to the **R3 sonic at 110 degrees** over the starboard side.

Figure 66. The ship's sonic site at **110 degrees** over the starboard side.

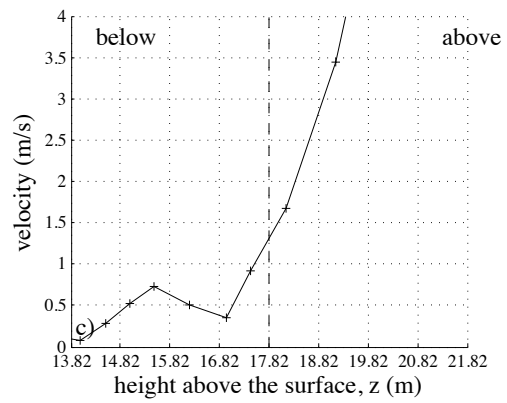
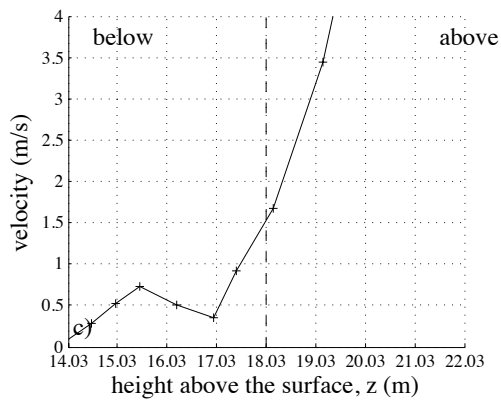
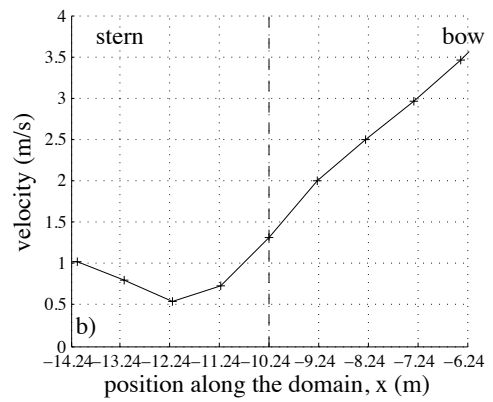
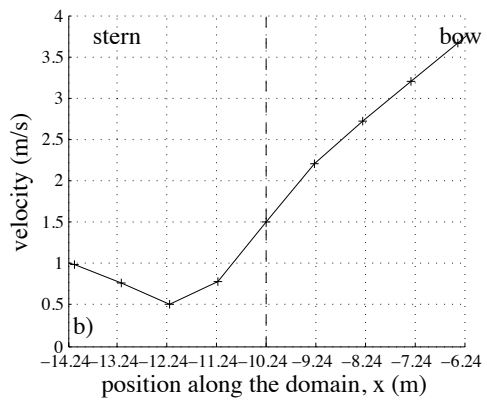
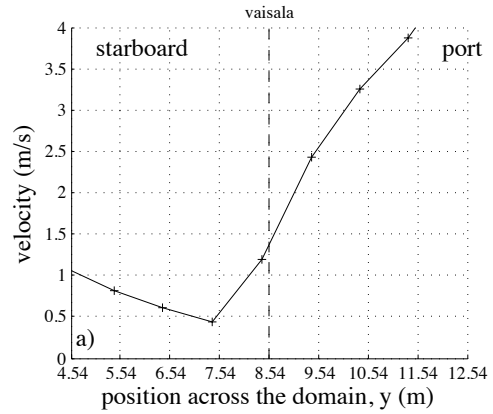
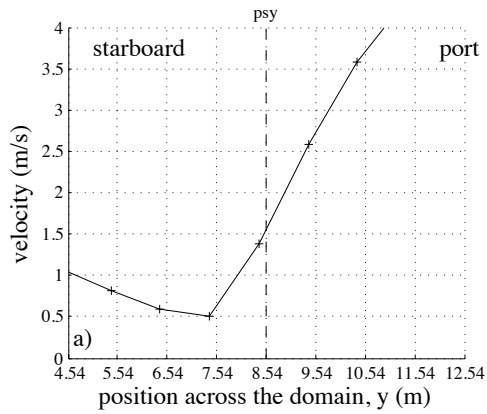


Figure 67. The psychrometer site at 110 degrees over the starboard side.

Figure 68. The Vaisala site at 110 degrees over the starboard side.

9. APPENDIX A: Figures showing sections of data on 2-D planes.

The Figures in this Appendix were generated using the VECTIS post-processing software.

FIGURE A1. Velocity vectors on a vertical plane through the R3 sonic anemometer site for a flow directly over the bow. The magnitude of the velocity is indicated by the colour of the arrows. The length and direction of the arrows represent the magnitude and component of the velocity in the plane of view. Each arrow represents the results from one computational cell. The position of the anemometer is indicated by a cross and the velocity scale corresponds to 8 ms^{-1} to 12 ms^{-1} .

FIGURE A2. As Figure A1 for a flow 10 degrees to starboard.

FIGURE A3. As Figure A1 for a flow 20 degrees to starboard.

FIGURE A4. As Figure A1 for a flow 30 degrees to starboard.

FIGURE A5. As Figure A1 for a flow 50 degrees to starboard.

FIGURE A6. As Figure A1 for a flow 70 degrees to starboard.

FIGURE A7. As Figure A1 for a flow 90 degrees to starboard.

FIGURE A8. As Figure A1 for a flow 110 degrees to starboard.

FIGURE A9. Velocity vectors on a horizontal plane through the R3 sonic anemometer site for a flow directly over the bow. The magnitude of the velocity is indicated by the colour of the arrows. The length and direction of the arrows represent the magnitude and component of the velocity in the plane of view. Each arrow represents the results from one computational cell. The position of the anemometer is indicated by a cross and the velocity scale corresponds to 8 ms^{-1} to 12 ms^{-1} .

FIGURE A10. As Figure A9 for a flow 10 degrees to starboard.

FIGURE A11. As Figure A9 for a flow 20 degrees to starboard.

FIGURE A12. As Figure A9 for a flow 30 degrees to starboard.

FIGURE A13. As Figure A9 for a flow 50 degrees to starboard.

FIGURE A14. As Figure A9 for a flow 70 degrees to starboard.

FIGURE A15. As Figure A9 for a flow 90 degrees to starboard (beam on).

FIGURE A16. As Figure A9 for a flow 110 degrees to starboard.

FIGURE A17. Total velocity on a horizontal plane at a height of 3 m above the monkey island for a flow directly over the bow. The dashed lines indicate the wind speed bias (difference between the wind speed and the free stream wind speed at that height).

FIGURE A18. Total velocity on a horizontal plane at a height of 5 m above the monkey island for a flow directly over the bow. The dashed lines indicate the wind speed bias (difference between the wind speed and the free stream wind speed at that height).

FIGURE A19. As Figure A17 for a flow 50 degrees to starboard.

FIGURE A20. As Figure A18 for a flow 50 degrees to starboard.

FIGURE A21. As Figure A17 for a flow 90 degrees to starboard (beam on).

FIGURE A22. As Figure A18 for a flow 90 degrees to starboard (beam on).

FIGURE A23. Vertical plane of total velocity at the front edge of the bridge for a flow directly over the bow (0 degrees). The velocity scale corresponds to 8 ms^{-1} to 12 ms^{-1} .

FIGURE A24. As figure 23, but for a vertical plane 1 m back from the front edge.

FIGURE A25. As figure 24, but for a vertical plane 2 m back from the front edge.

FIGURE A26 Vertical plane of total velocity at the front edge of the bridge for a flow directly over the starboard beam (90 degrees). The velocity scale corresponds to 8 ms^{-1} to 12 ms^{-1} .

FIGURE A27. As Figure A26, but for a vertical plane 2 m back from the front edge.

Figure A1 - 0 degree bow-on flow

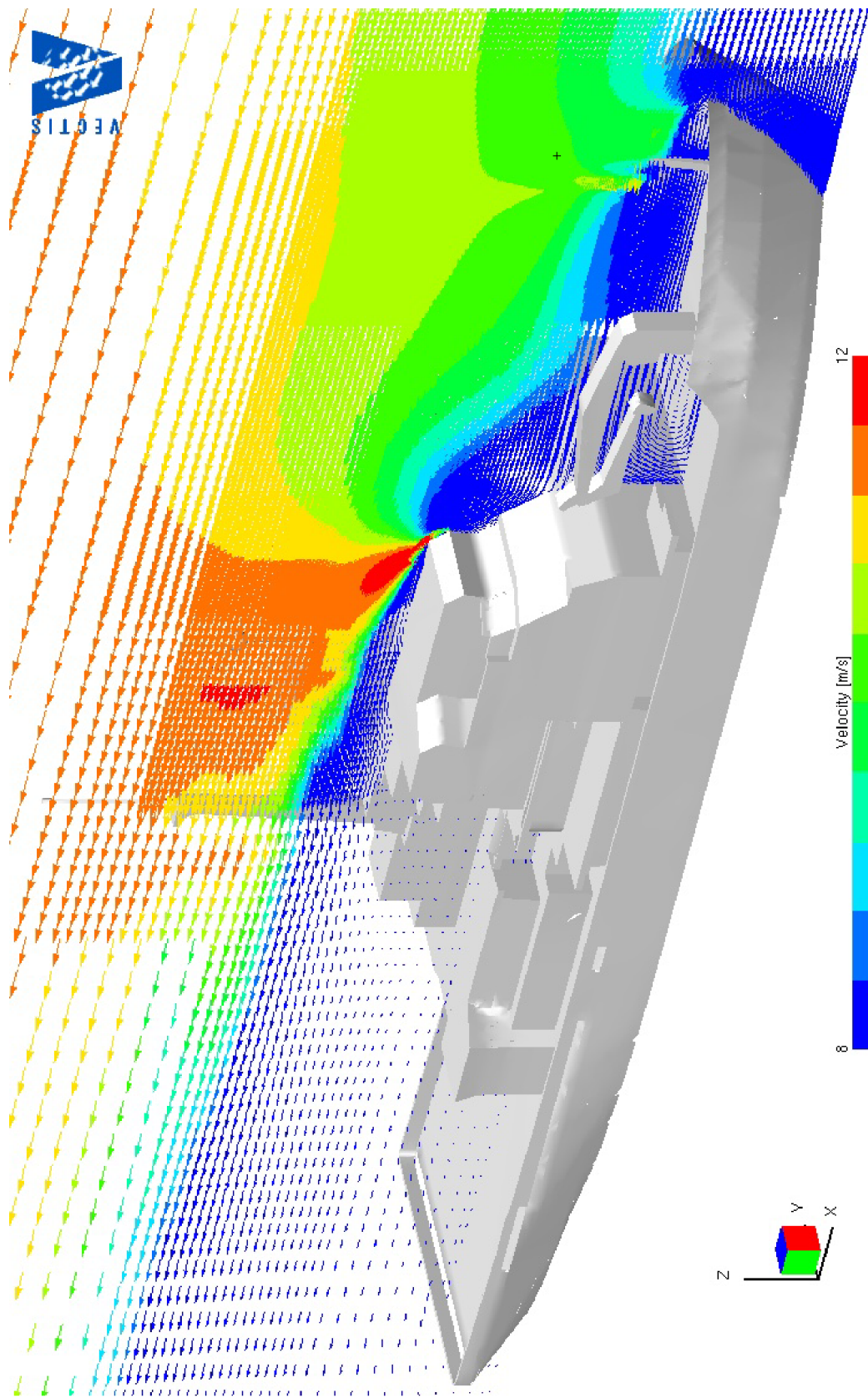


Figure A2 - 10 degree starboard flow

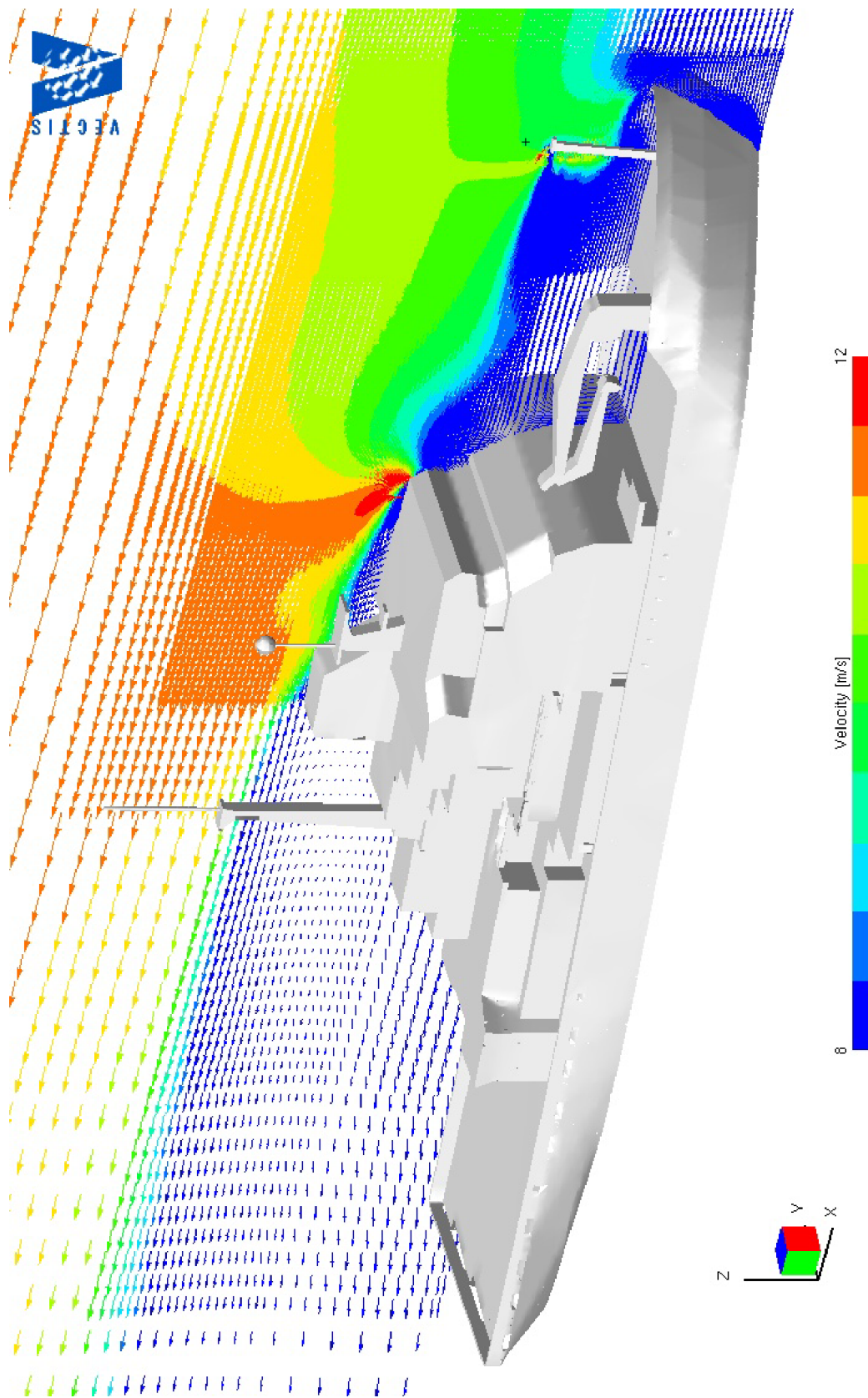


Figure A4 - 30 degree starboard flow

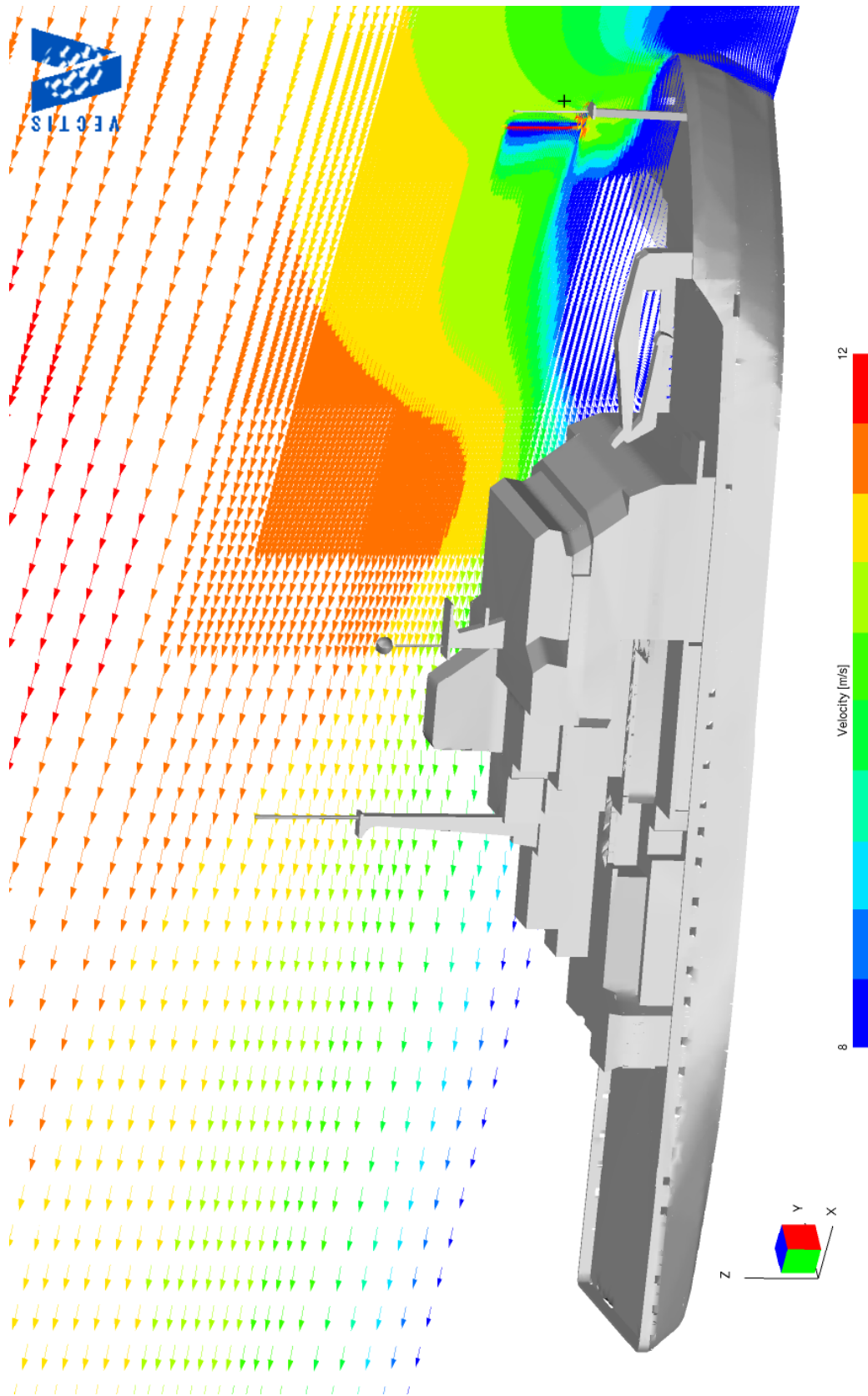


Figure A5 - 50 degree starboard flow

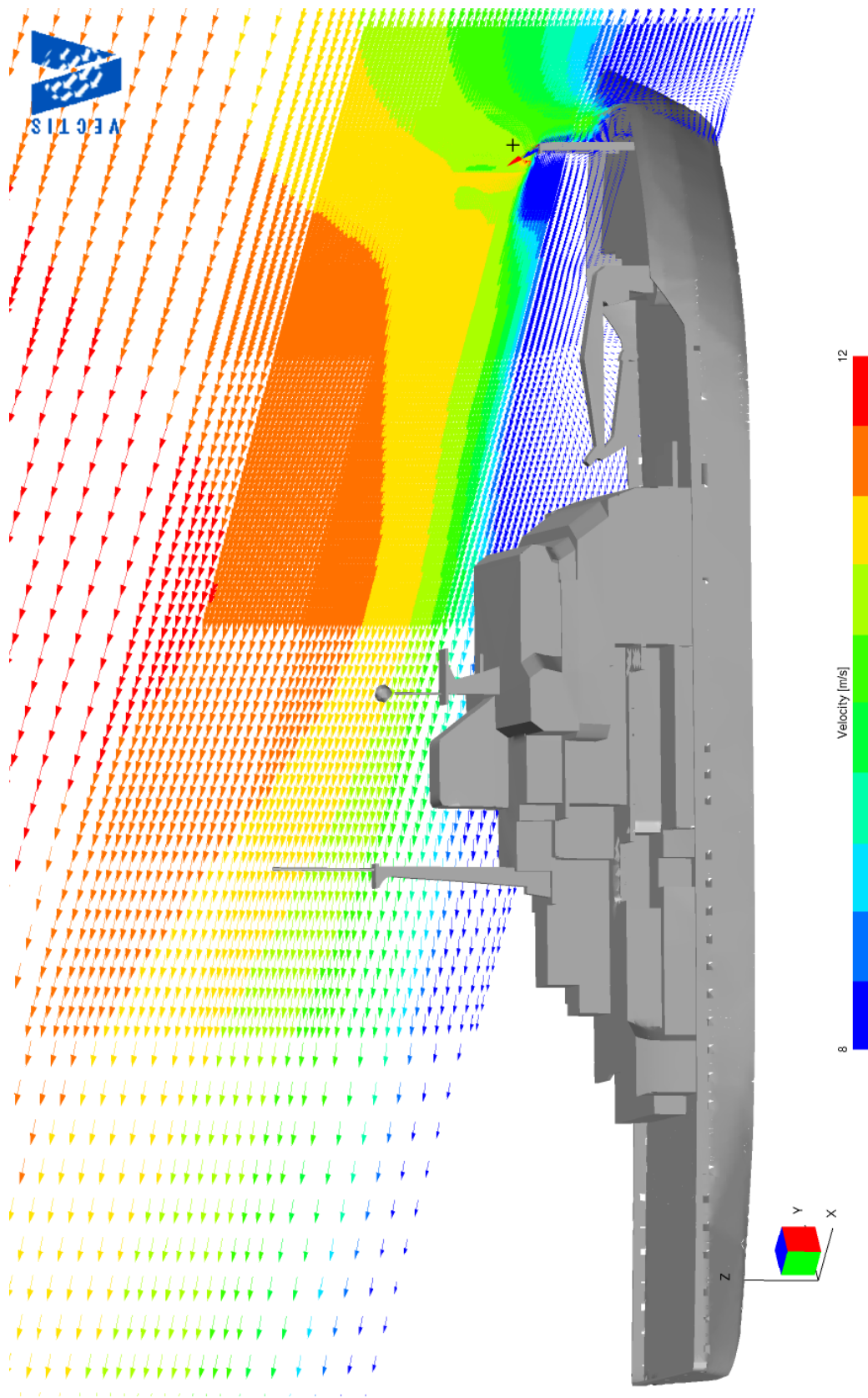


Figure A6 - 70 degree starboard flow

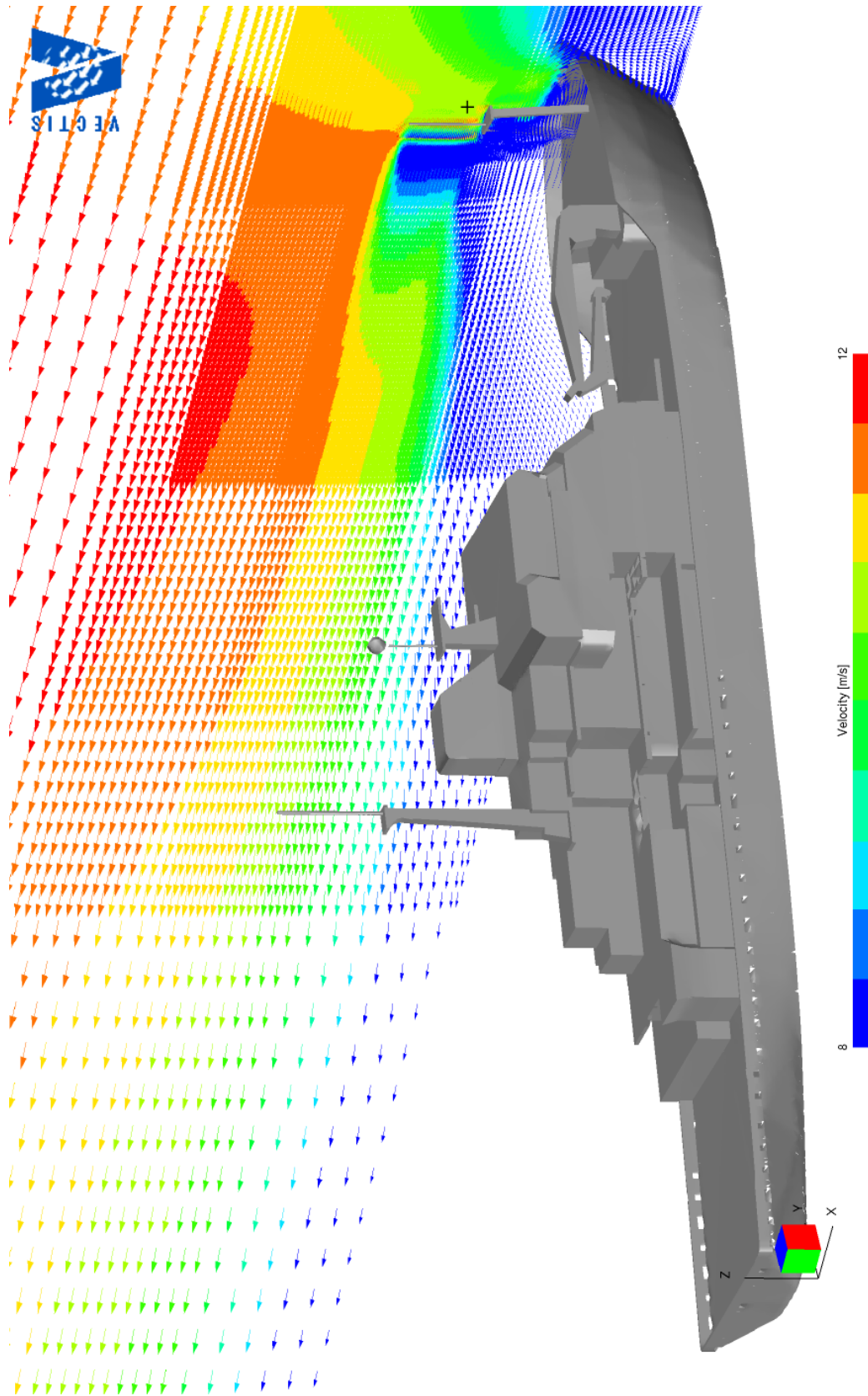


Figure A7 – 90 degree starboard flow

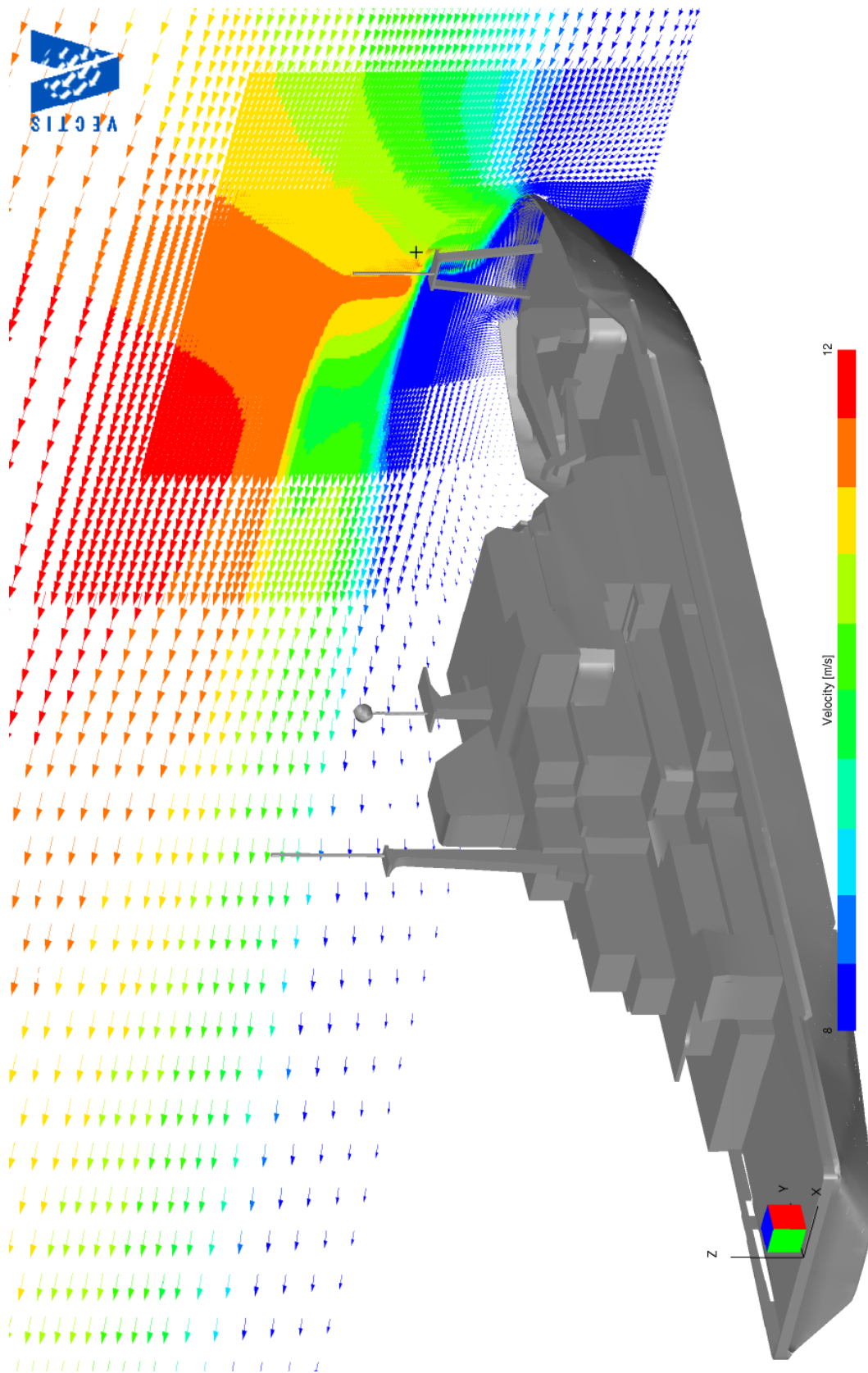


Figure A8 – 110 degree starboard flow

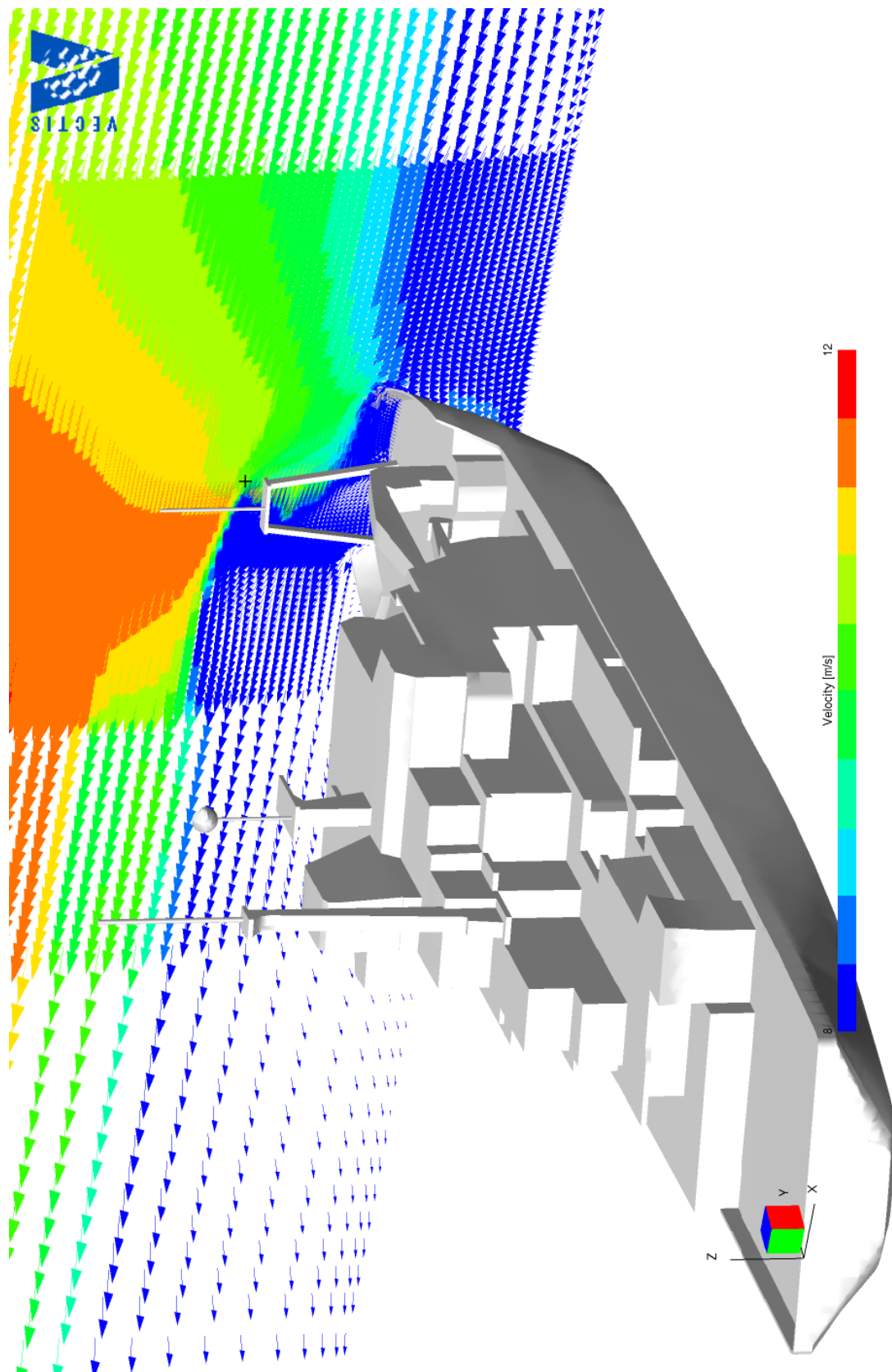


Figure A9 – 0 degree bow-on flow

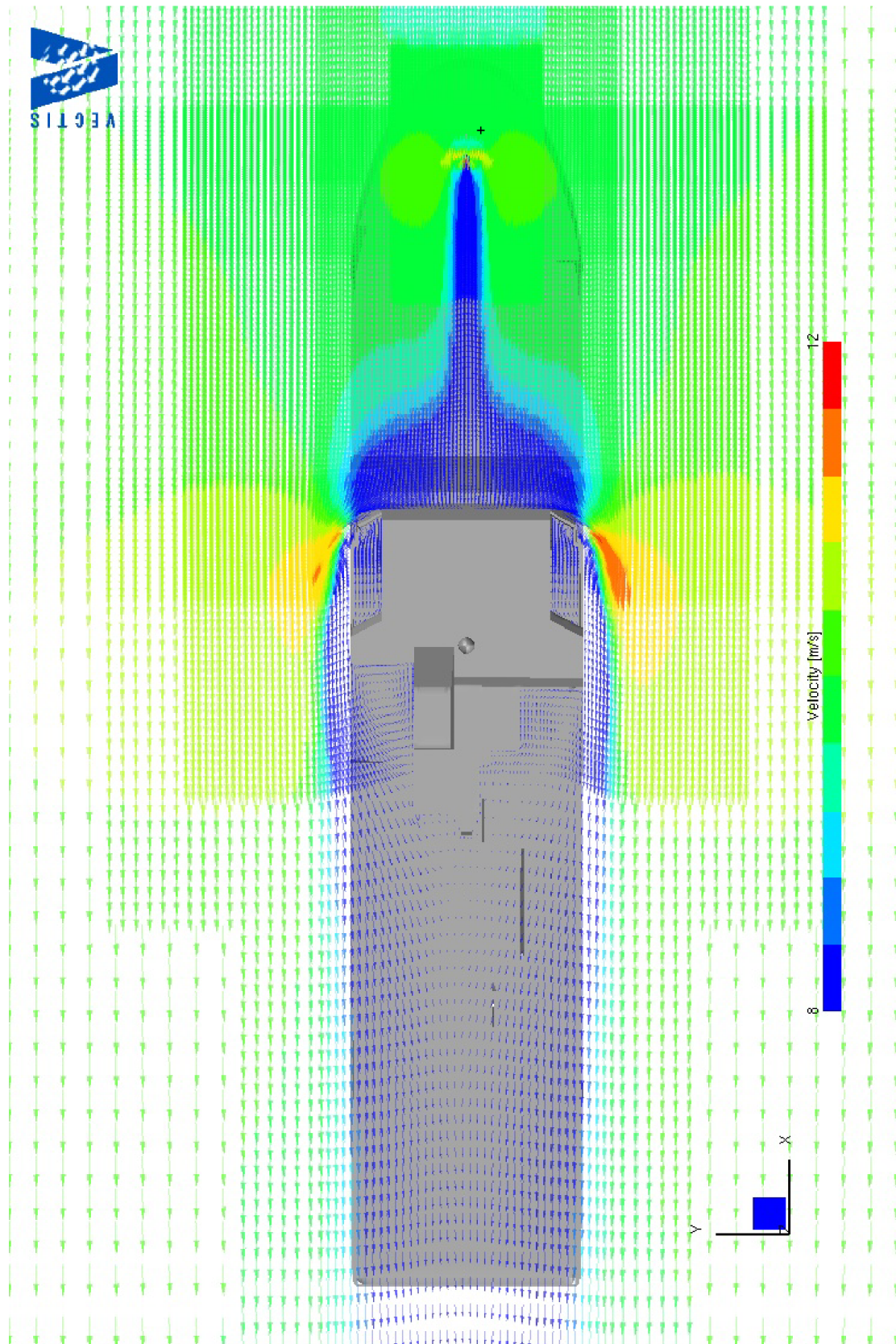


Figure A10 - 10 degree starboard flow

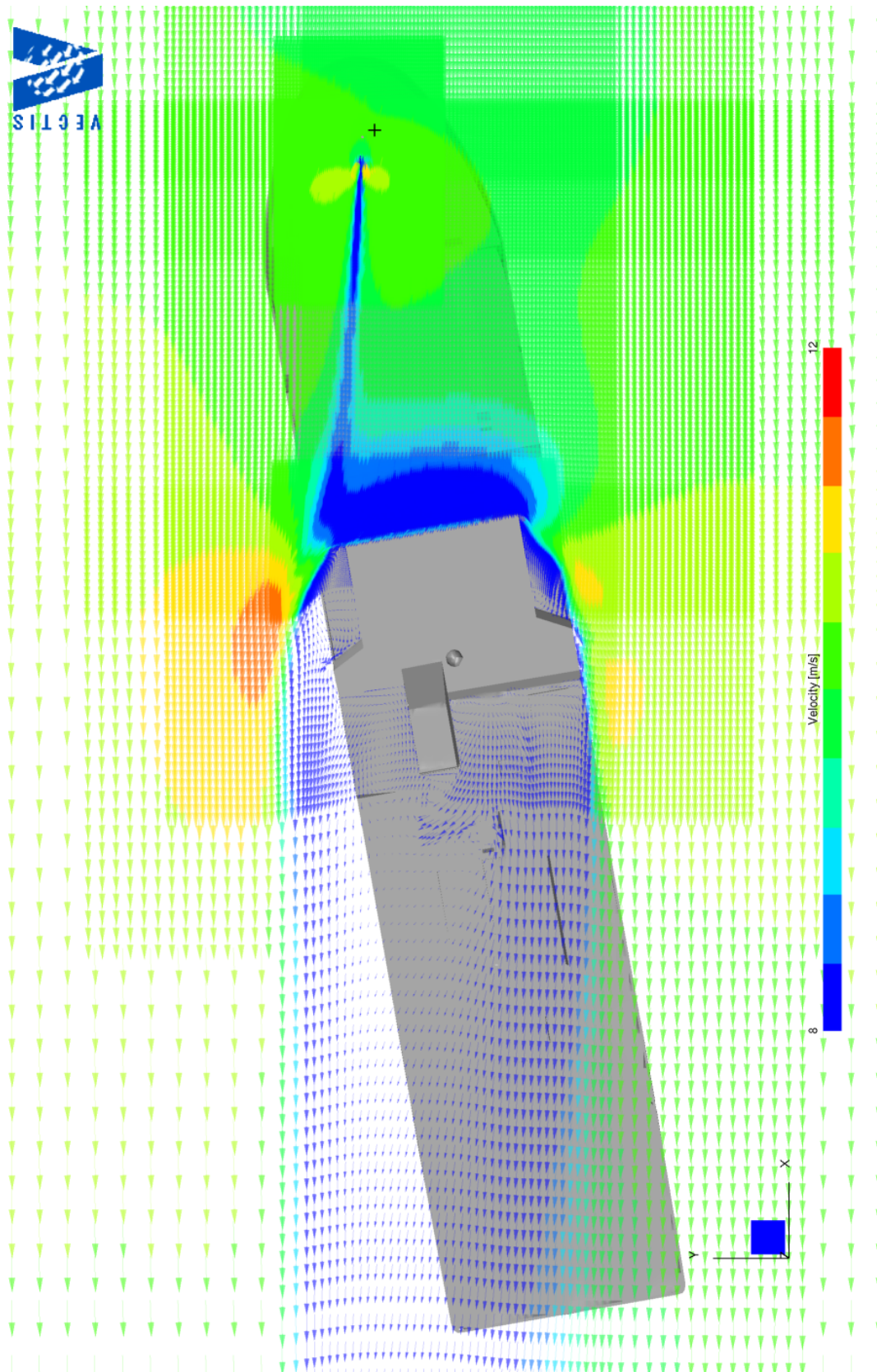


Figure A11 - 20 degree starboard flow

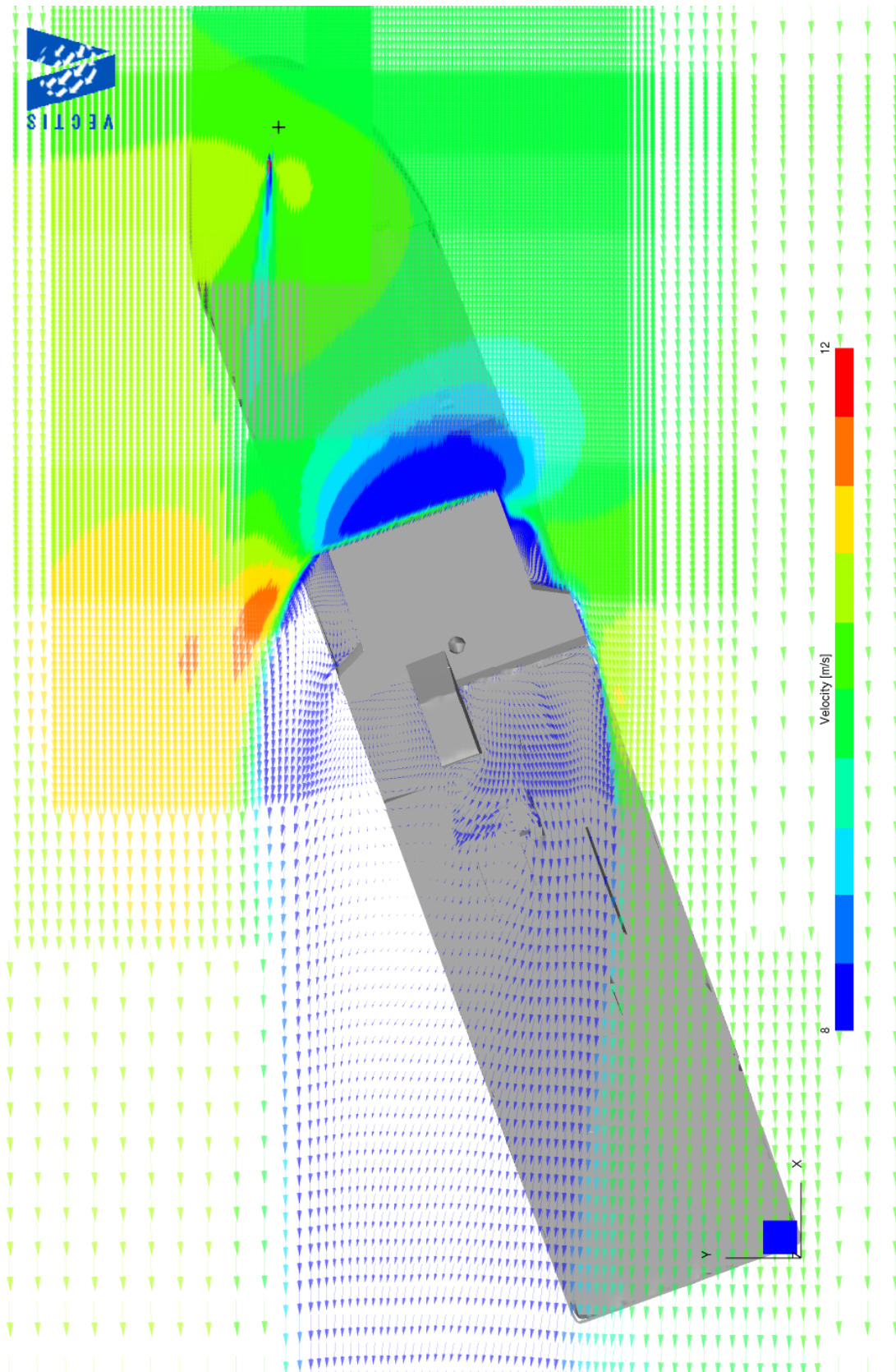


Figure A12 - 30 degree starboard flow

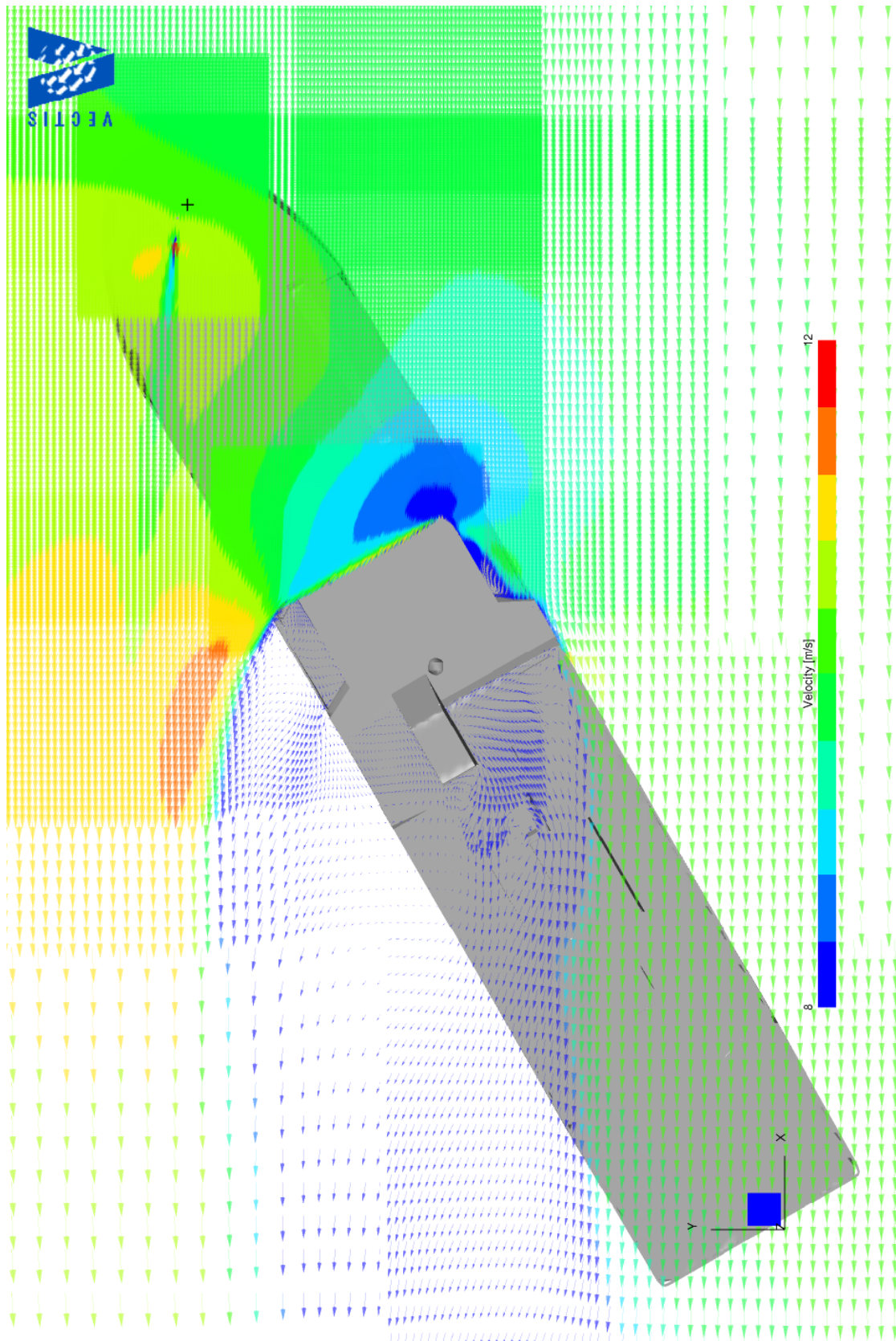


Figure A13 - 50 degree starboard flow

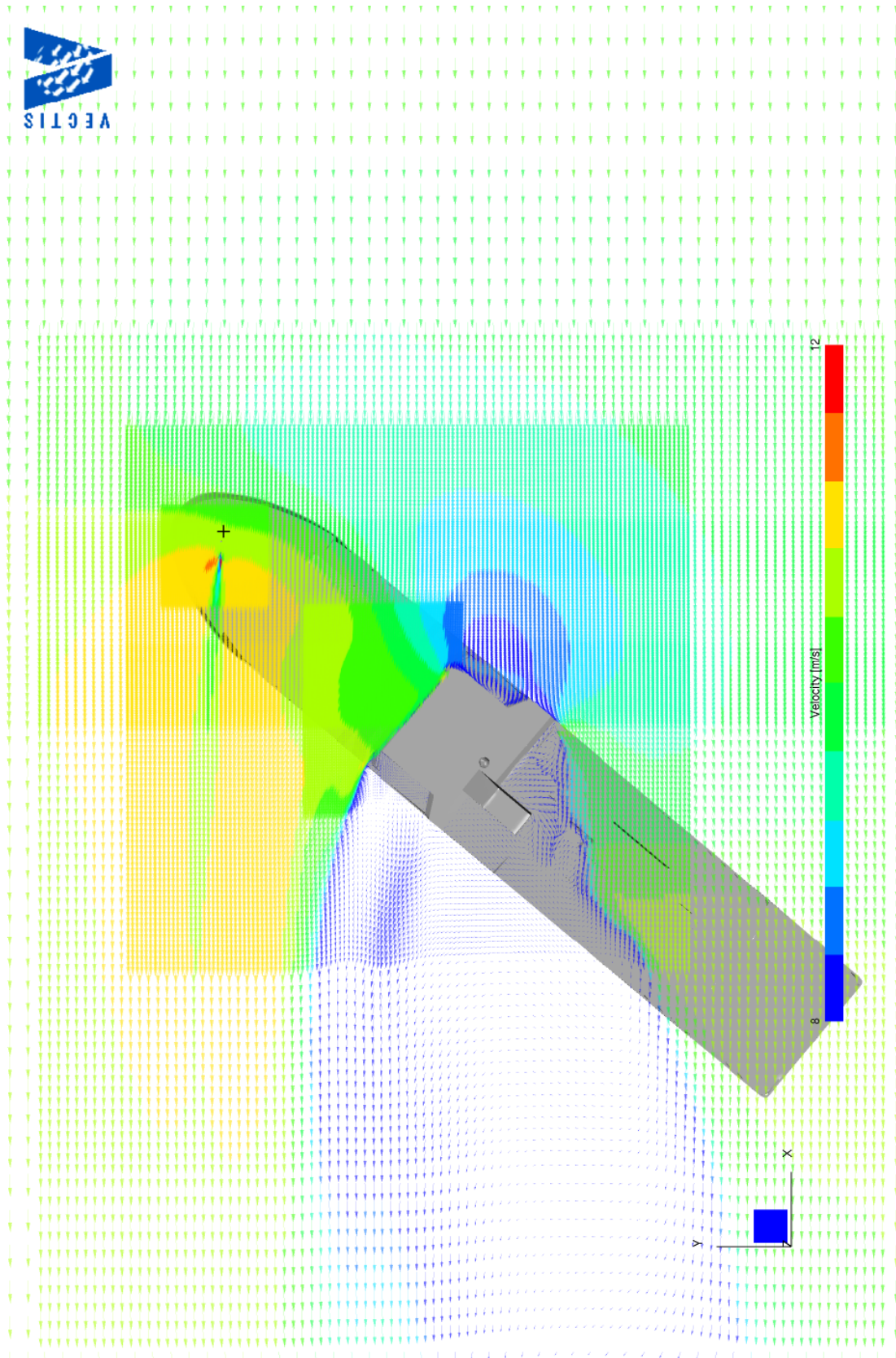


Figure A14 - 70 degree starboard flow

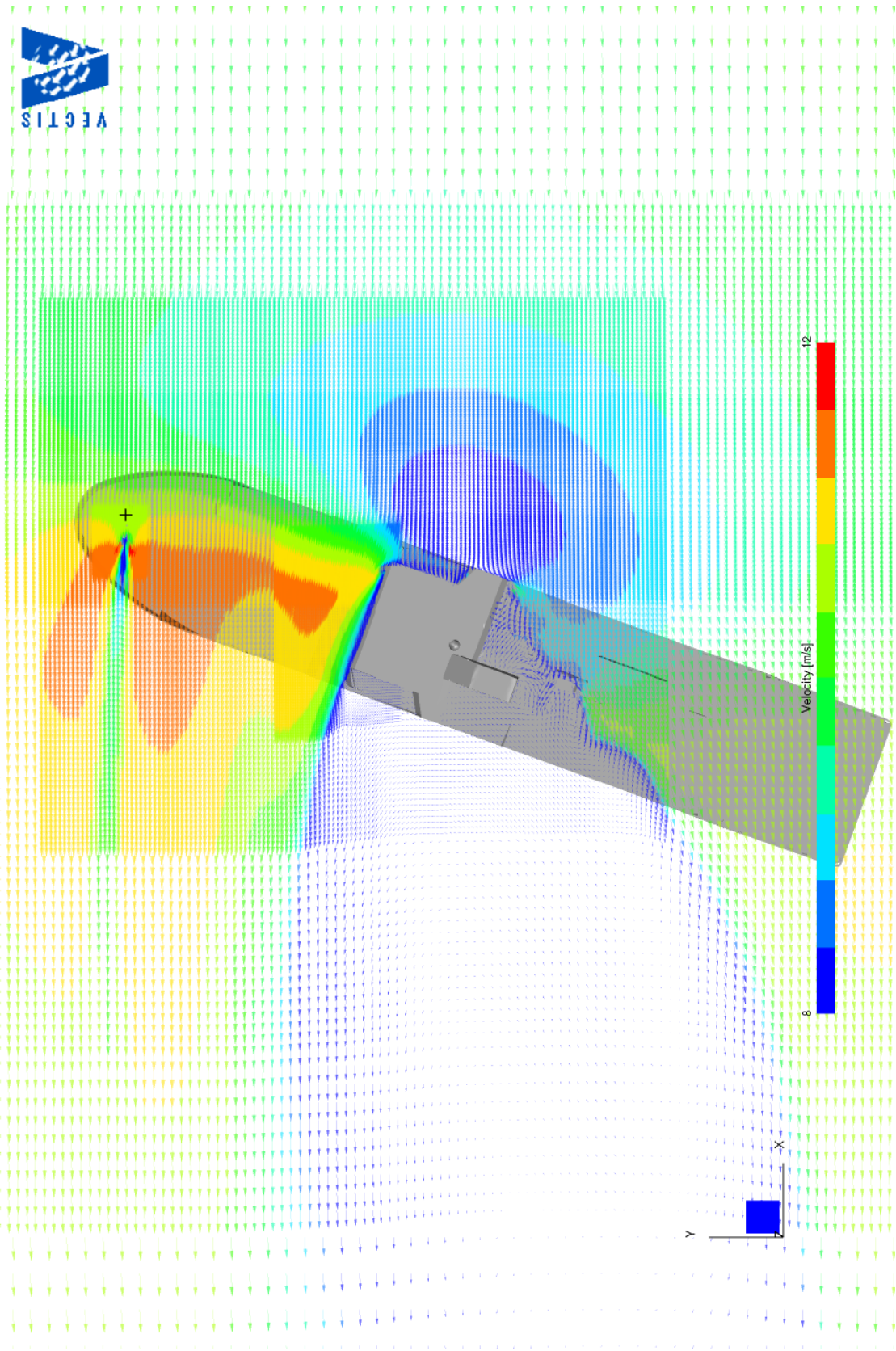


Figure A15 - 90 degree starboard flow

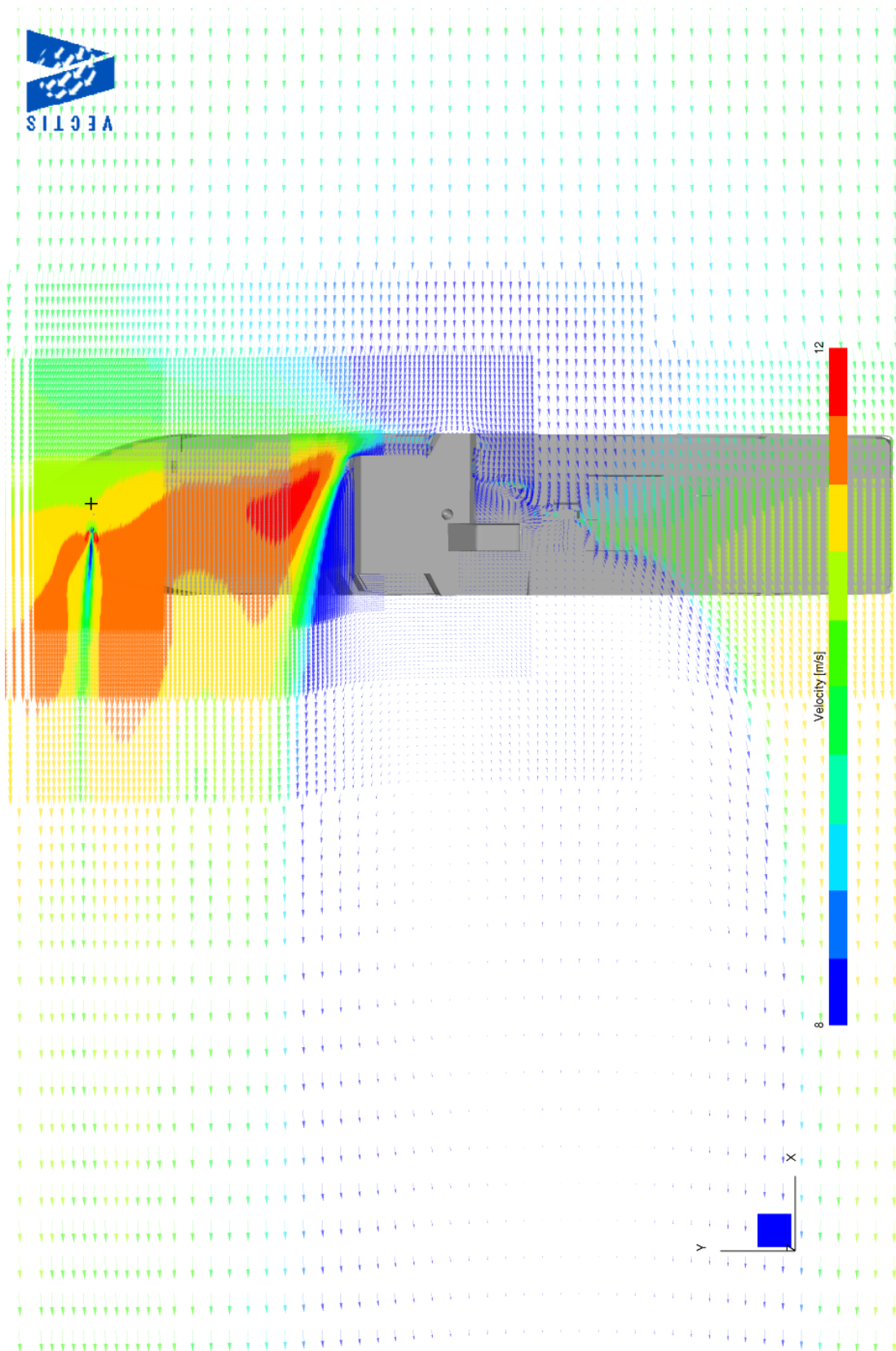


Figure A16 - 110 degree starboard flow

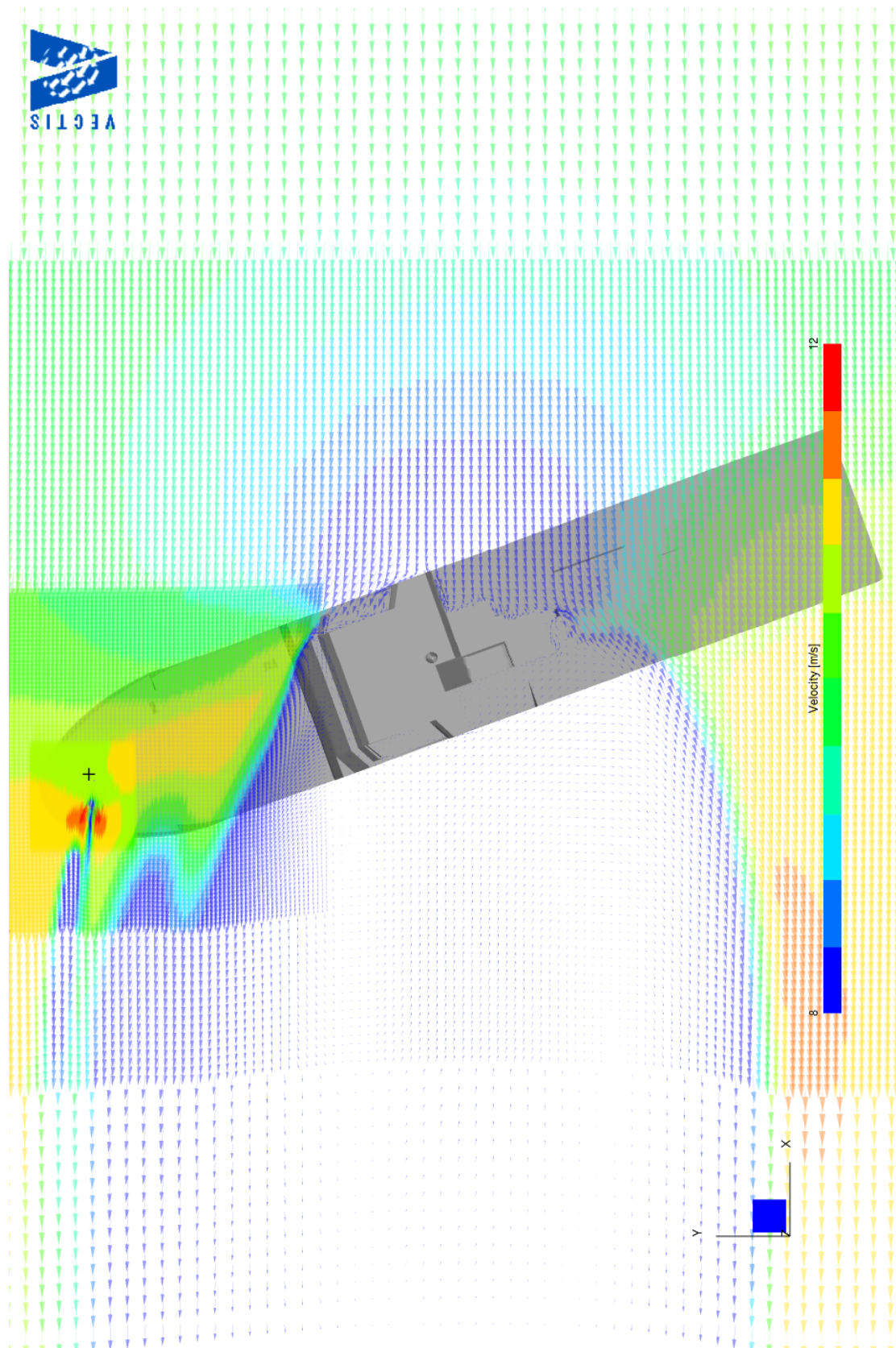


Figure A17 - 0 degree: 3 m above the monkey island

The scalar field is the wind speed and the dashed lines indicate the wind speed bias (difference from the free stream). The solid line indicates the bridge front.

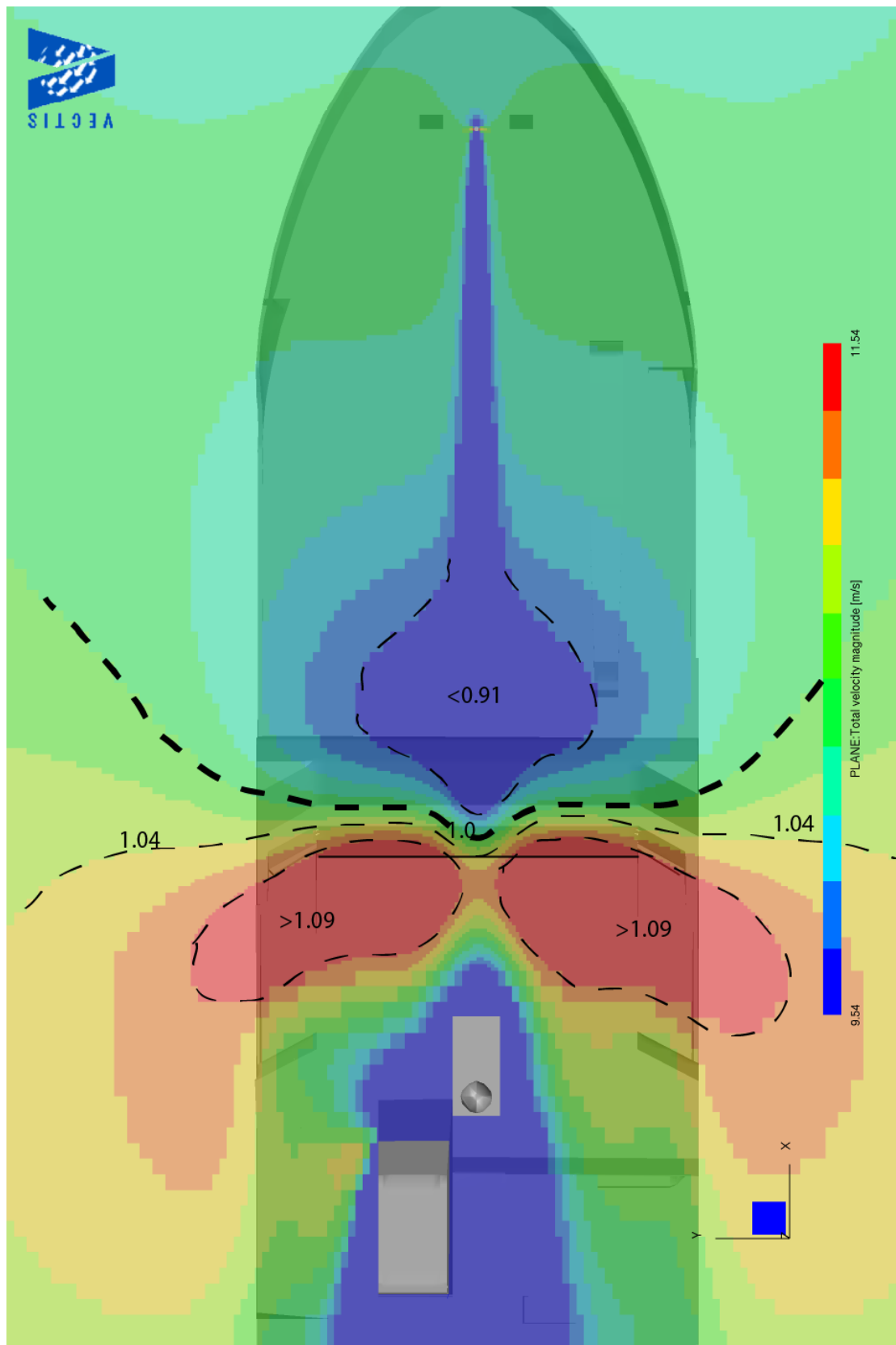


Figure A18 - 0 degree: 5 m above the monkey island

The scalar field is the wind speed and the dashed lines indicate the wind speed bias (difference from the free stream). The solid line indicates the bridge front.

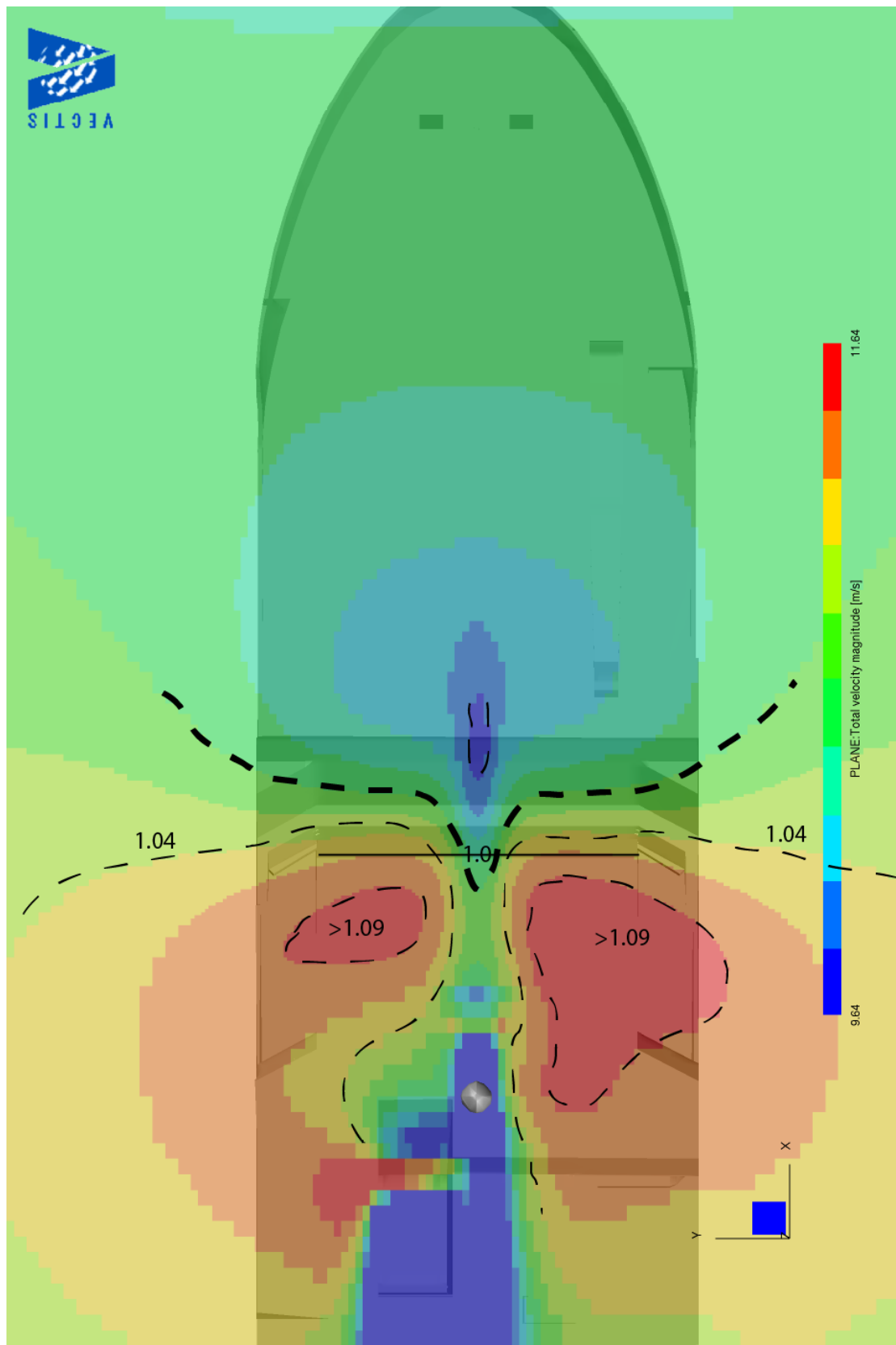


Figure A19 - 50 degree: 3 m above the monkey island

The scalar field is the wind speed and the dashed lines indicate the wind speed bias (difference from the free stream). The solid line indicates the bridge front.

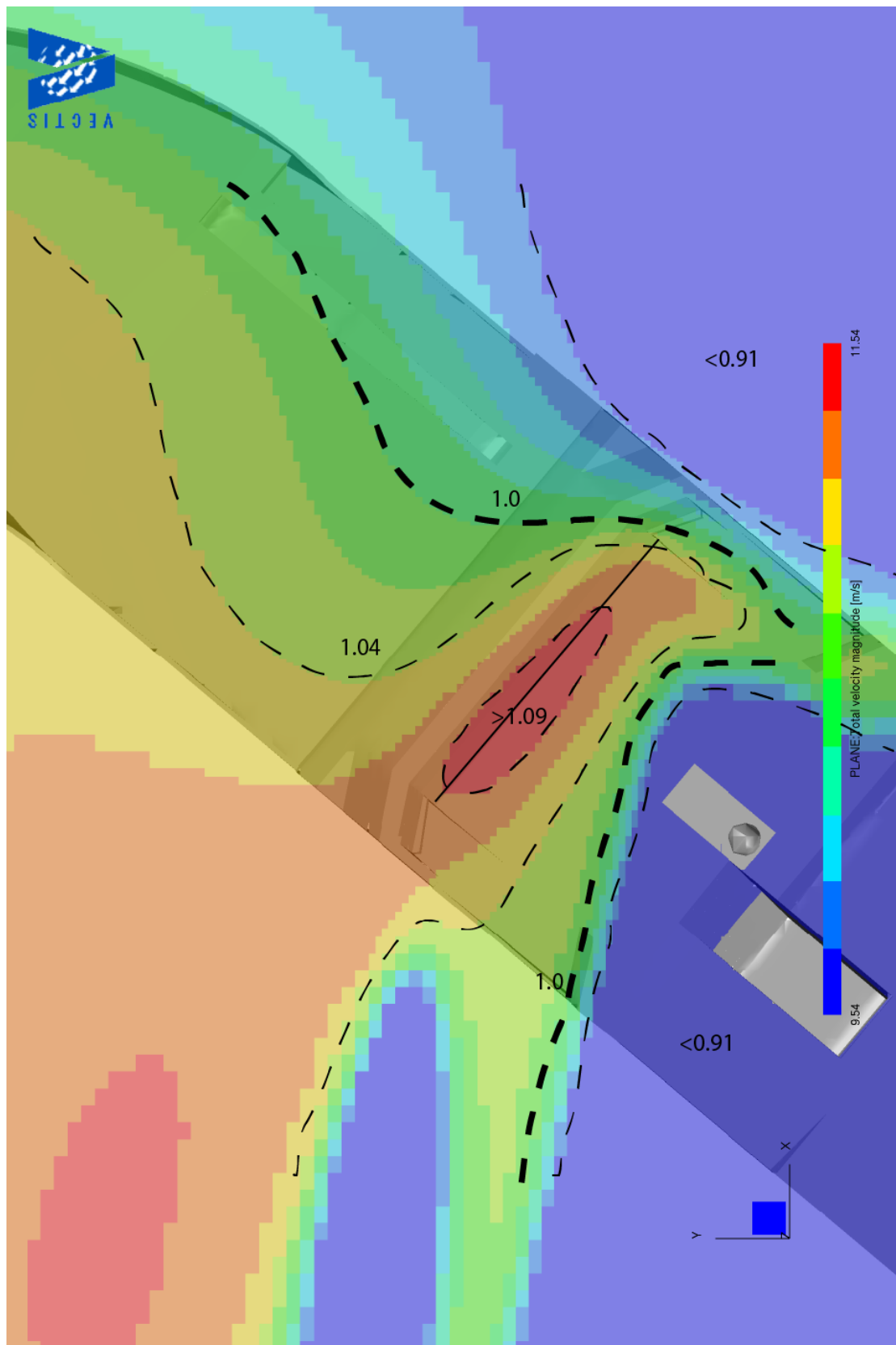


Figure A20 - 50 degree: 5 m above the monkey island

The scalar field is the wind speed and the dashed lines indicate the wind speed bias (difference from the free stream). The solid line indicates the bridge front.

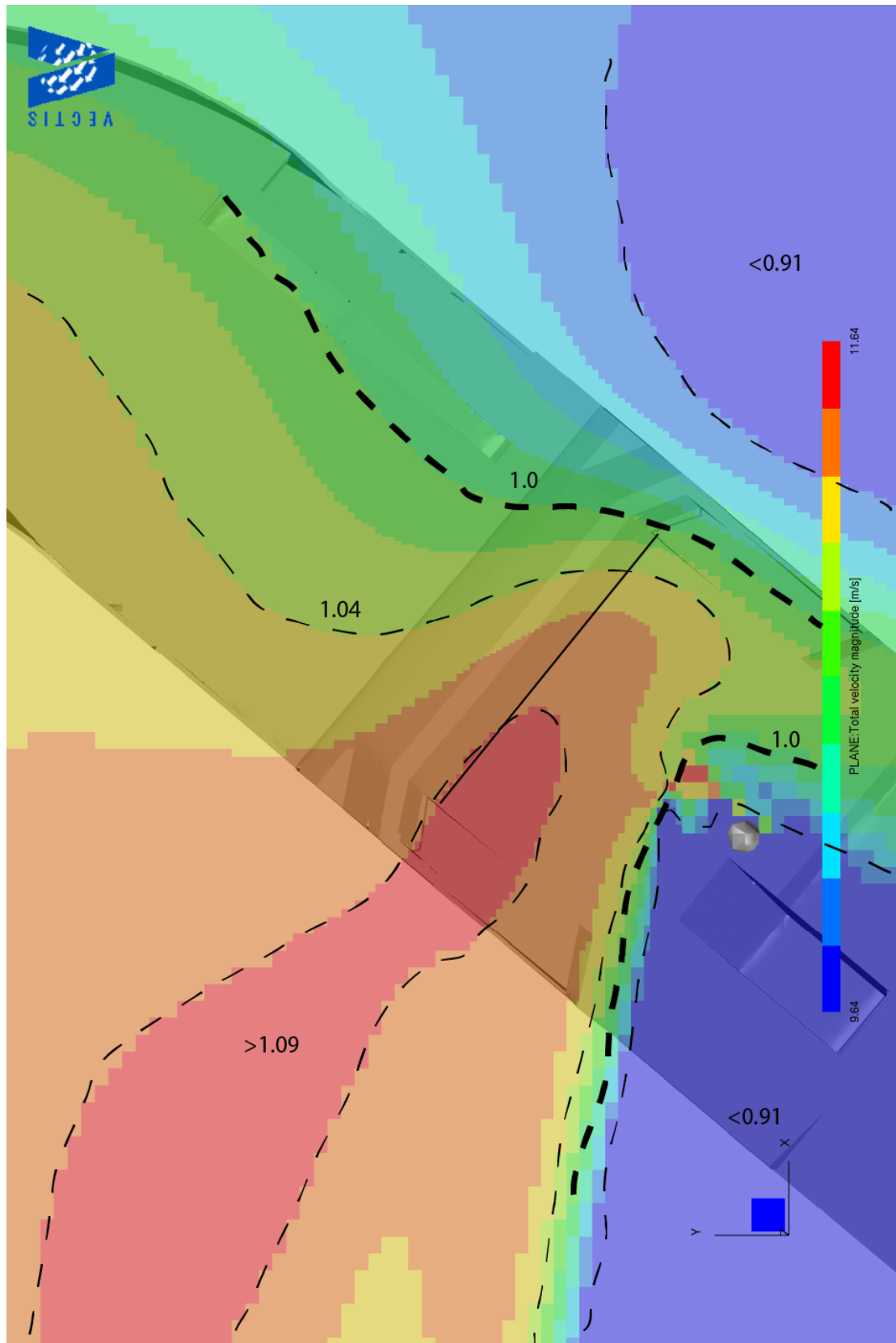


Figure A21 - 90 degree: 3 m above the monkey island

The scalar field is the wind speed and the dashed lines indicate the wind speed bias (difference from the free stream). The solid line indicates the bridge front.

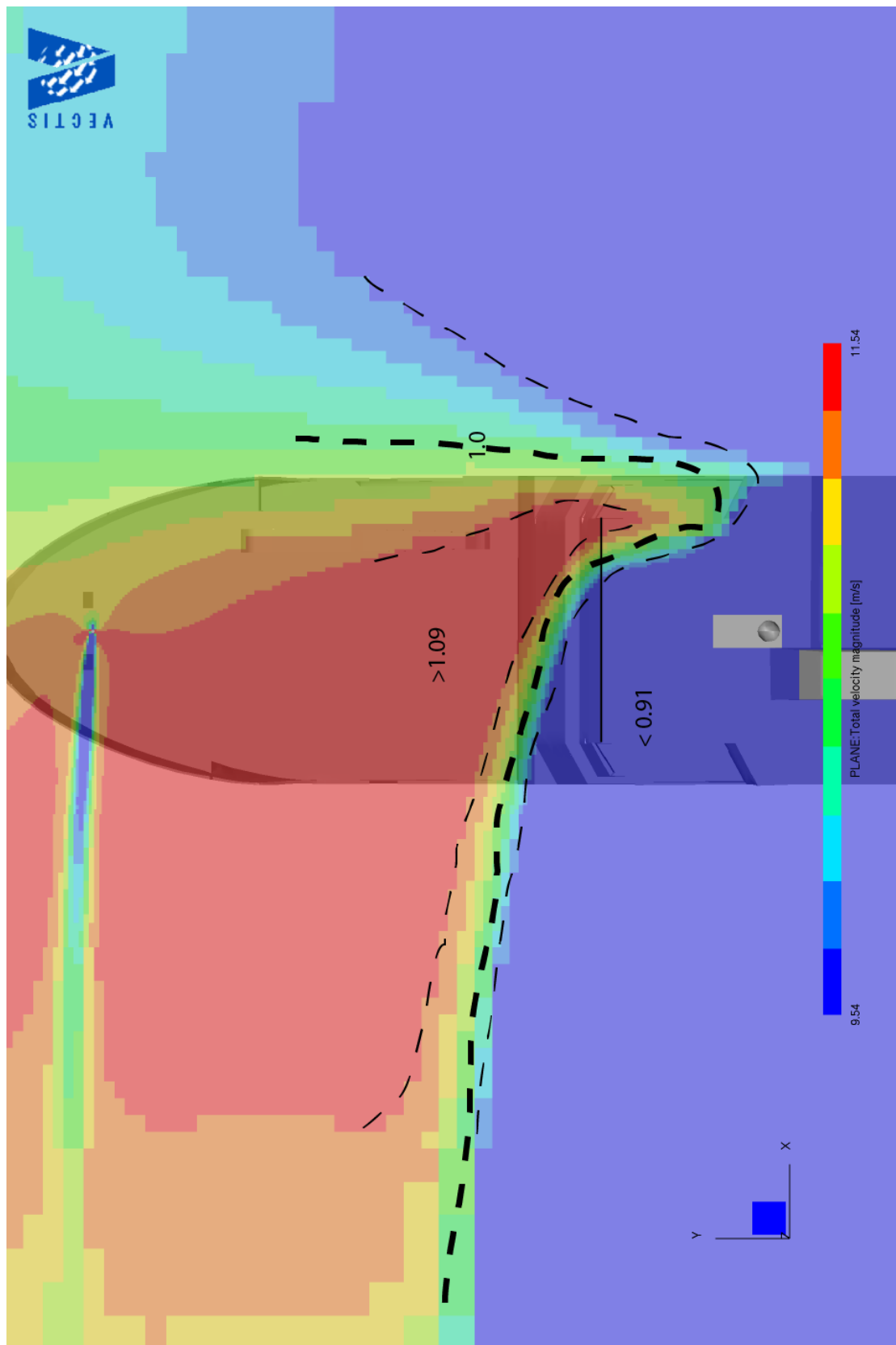


Figure A22 - 90 degree: 5 m above the monkey island

The scalar field is the wind speed and the dashed lines indicate the wind speed bias (difference from the free stream). The solid line indicates the bridge front.

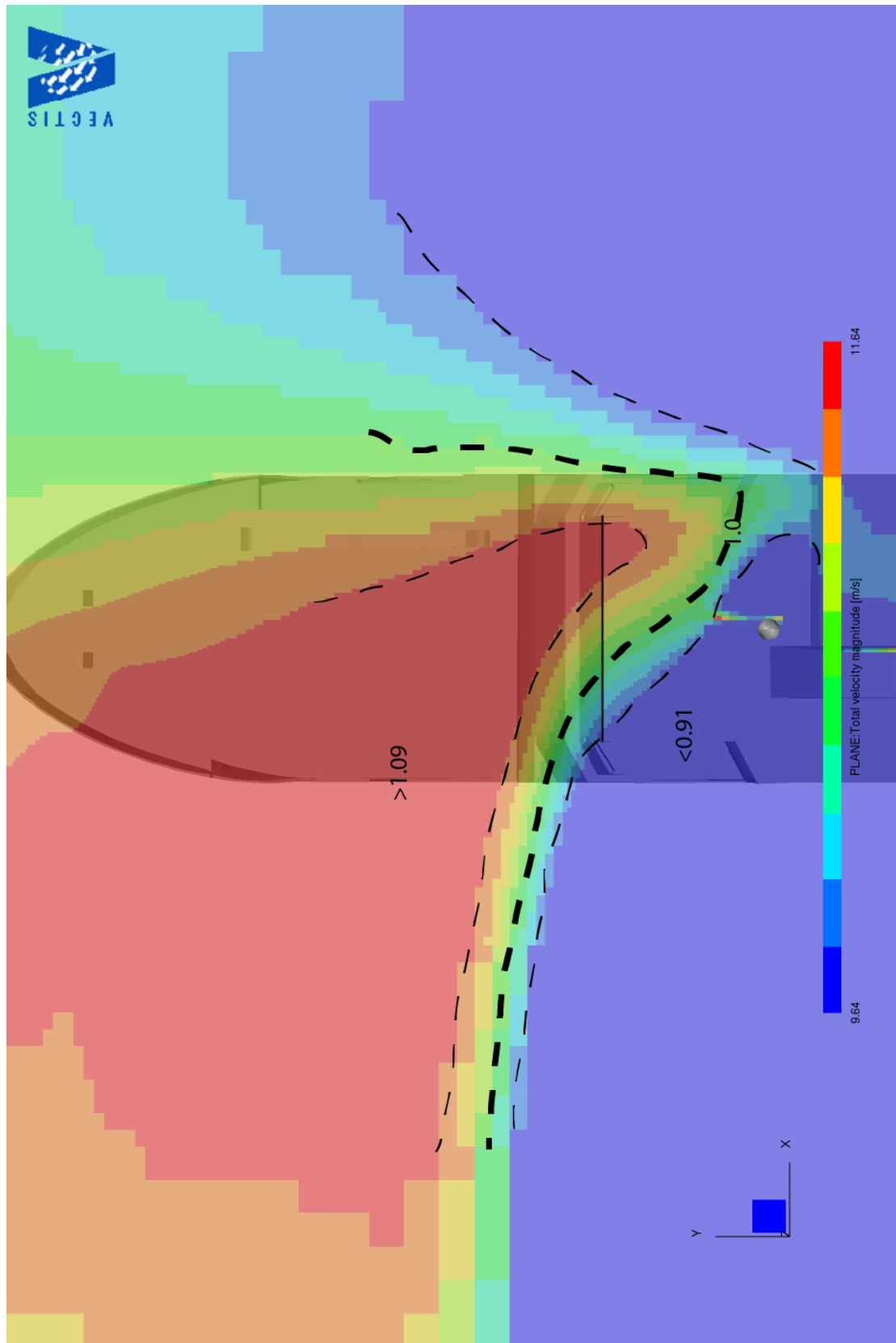


Figure A23 - 0 degree: At the front edge of the monkey island

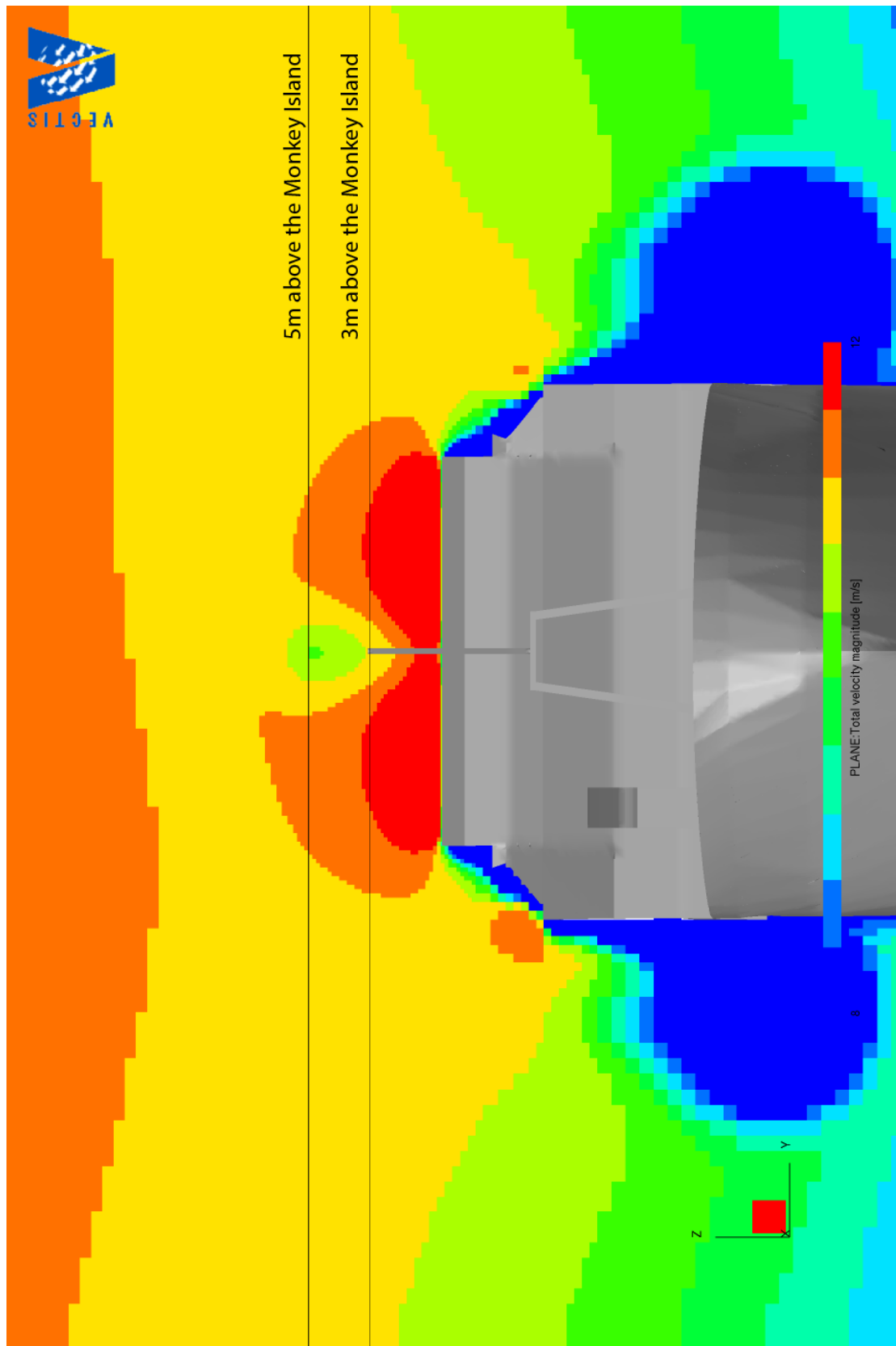


Figure A24 - 0 degree: 1 m back from the front edge of the monkey island

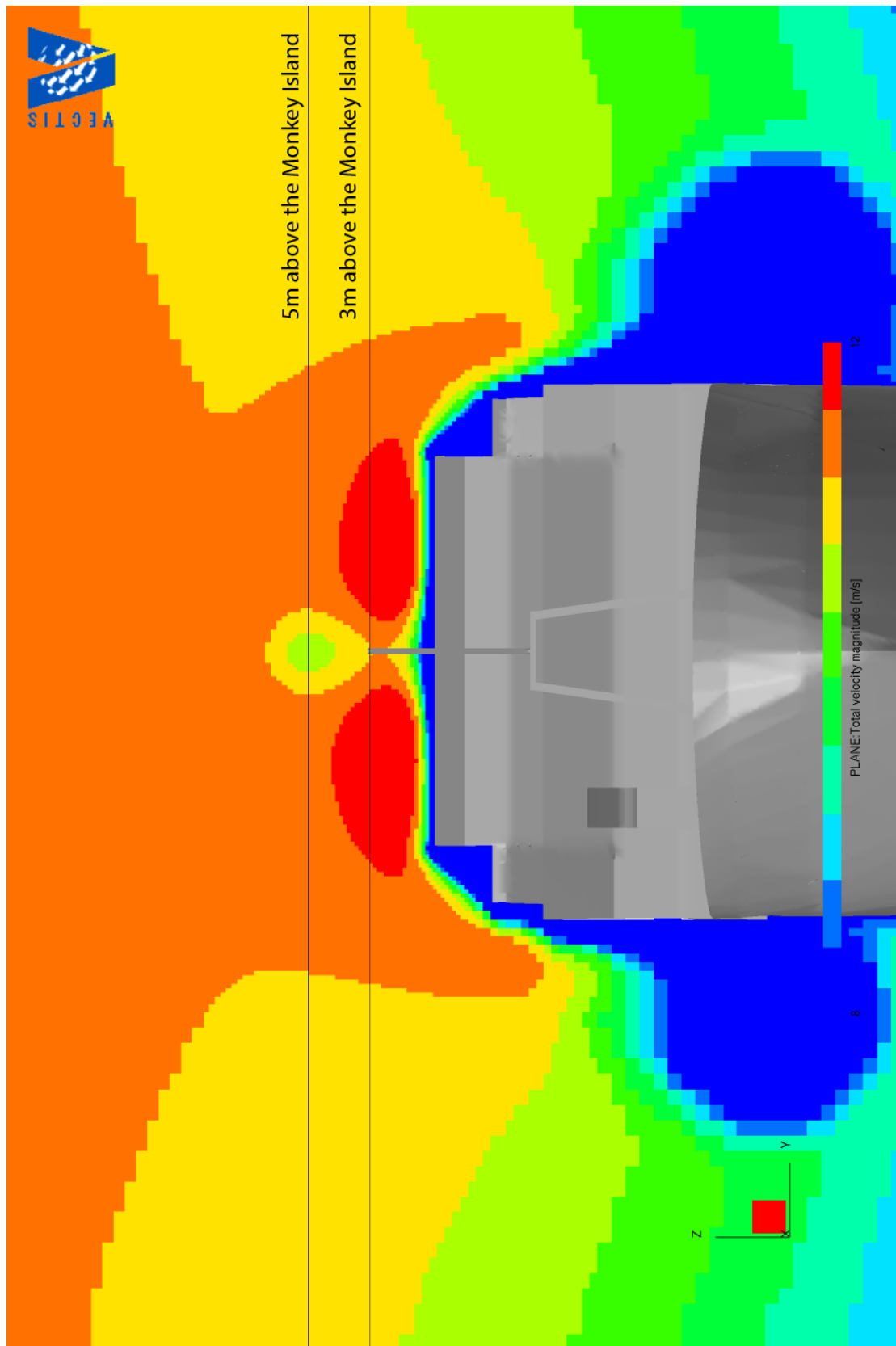


Figure A26 - 0 degree: 2 m back from the front edge of the monkey island

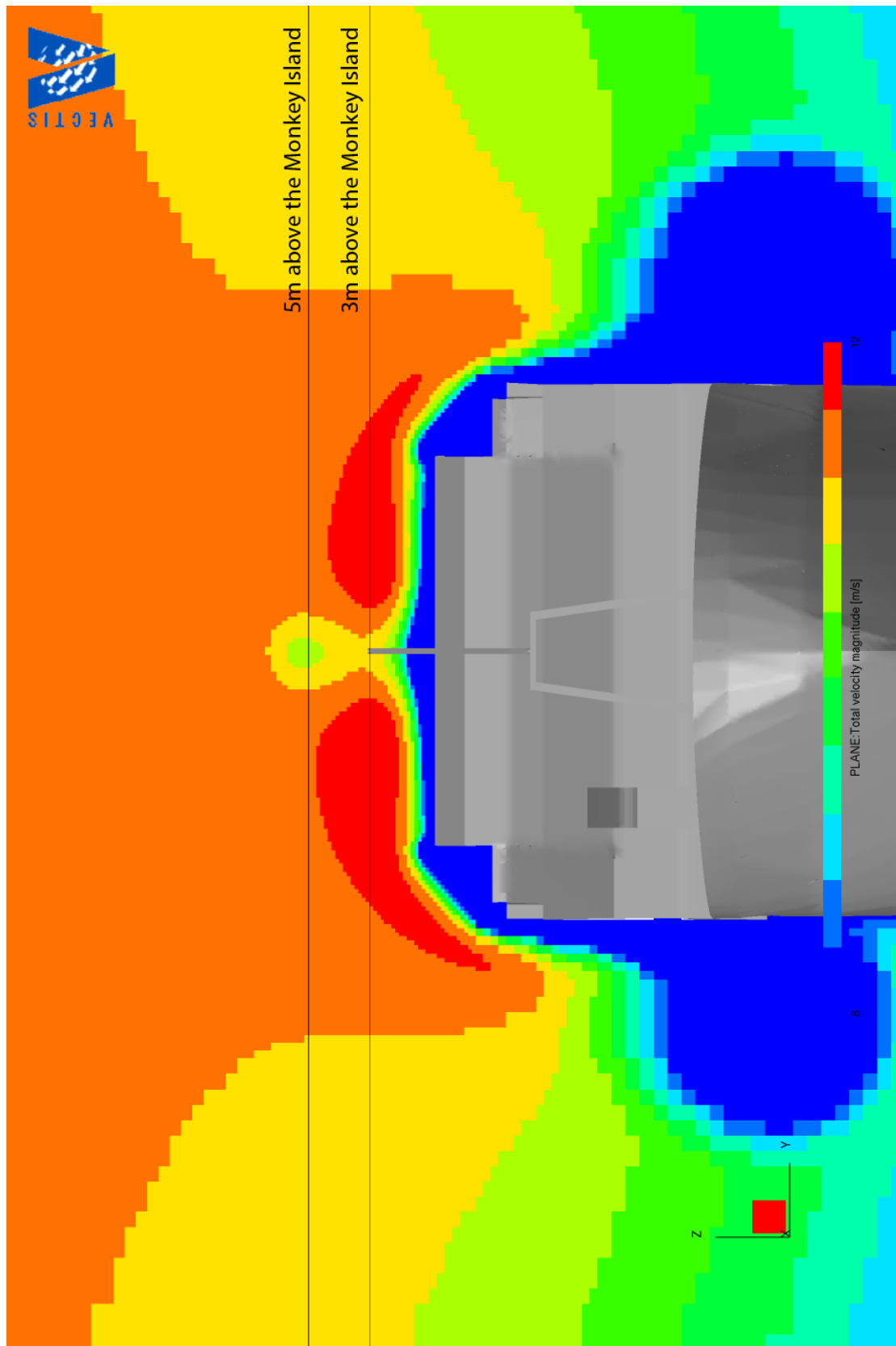
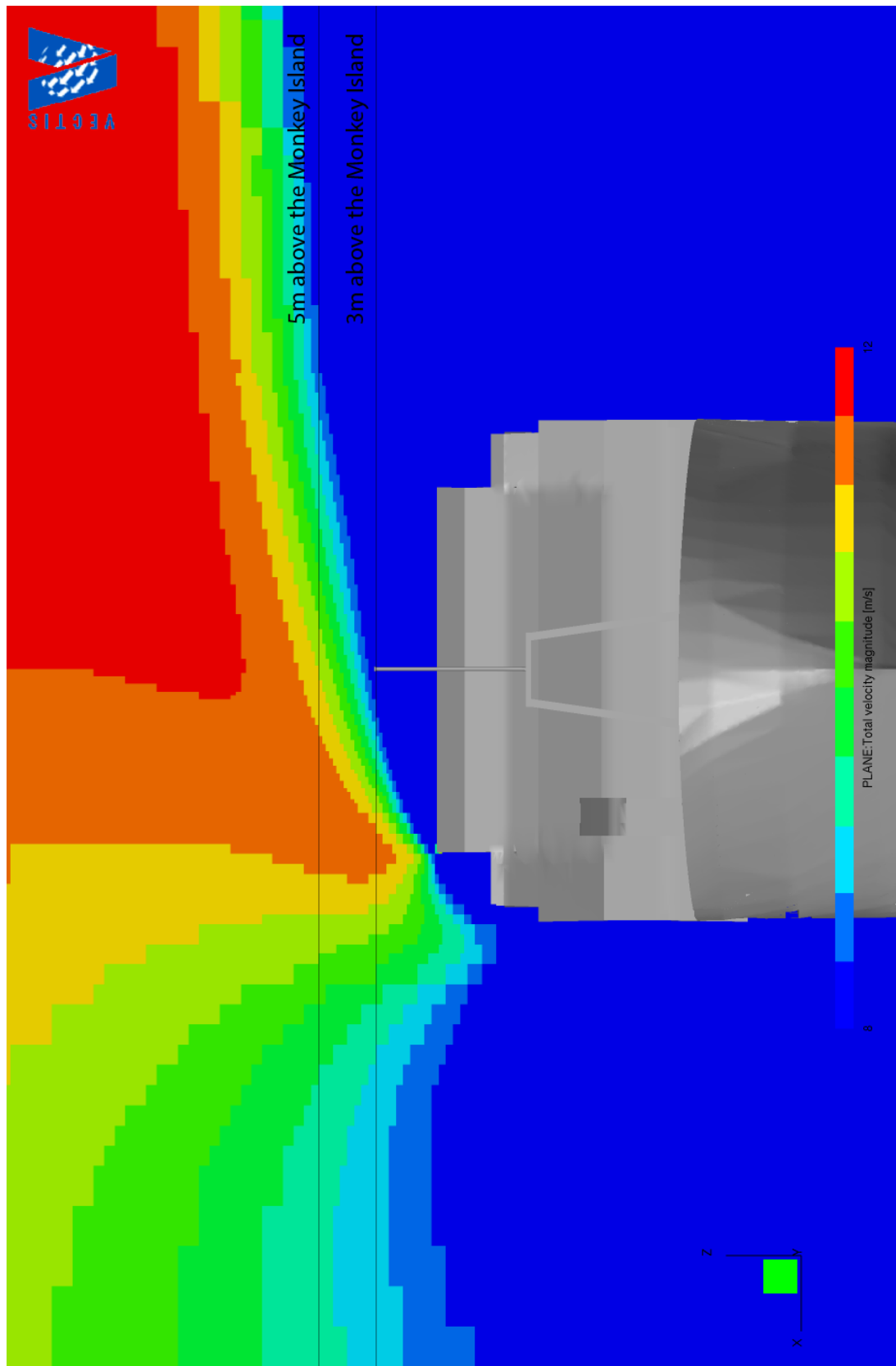


Figure A28 - 90 degree starboard beam: 2 m back from the front edge of the monkey island



10. APPENDIX B: Summary table of results for each wind direction.

Table B.1. Summary of the effects of flow distortion. The values in brackets indicate the vertical displacement and the wind speed bias using a vertical displacement calculated from 2 seconds upstream, $\Delta z_1=2$, of the anemometer site (after Yelland et al., 2002).

Instrument	Instrument height z (m)	Vertical displacement (m) Δz ($\Delta z_{t=2}$)	Velocity at instrument site (ms^{-1})	Free stream velocity at z (ms^{-1})	Free stream velocity at $z - \Delta z$ ($z - \Delta z_{t=2}$)	% velocity error at instrument site	% velocity error at instrument site at $z - \Delta z$ ($z - \Delta z_{t=2}$)	Angle of flow to the horizontal (degrees)	Horizontal twist (degrees)
110 degrees (flow over the port side)									
R3 sonic	16.02	6.92 (3.15)	7.981	10.413	9.685 (10.198)	-23.36	-17.60 (-21.74)	6.1	-3.0
ship's sonic	21.51	5.95 (2.58)	11.322	10.697	10.387 (10.570)	5.84	9.00 (7.11)	6.6	-4.8
psychrometer	18.03	11.25 (6.46)	9.096	10.522	9.152 (10.085)	-13.56	-0.62 (-9.81)	20.1	-7.8
Vaisala	17.83	11.55 (6.27)	8.89	10.511	9.014 (10.511)	-15.40	-1.34 (-11.80)	16.81	-7.5
90 degrees (flow over the port side)									
R3 sonic	16.02	5.11 (3.11)	11.228	10.309	9.833 (10.046)	8.91	14.18 (11.76)	4.9	-3.8
ship's sonic	21.51	4.18 (2.18)	11.271	10.639	10.400 (10.523)	5.94	8.38 (7.11)	5.4	-4.1
psychrometer	18.03	11.21	9.967	10.447	9.329	-4.59	6.84	22.5	-19.3
Vaisala	17.83	11.60	9.116	10.434	9.237	-12.63	-1.31	27.3	-21.9

Instrument	Instrument height z (m)	Vertical displacement Δz ($\Delta z_{t=2}$) (m)	Velocity at instrument site (ms^{-1})	Free stream velocity at z (ms^{-1})	Free stream velocity at $z - \Delta z$ ($z - \Delta z_{t=2}$)	% velocity error at instrument site	% velocity error at instrument site at $z - \Delta z$ ($z - \Delta z_{t=2}$)	Angle of flow to the horizontal (degrees)	Horizontal twist (degrees)
70 degrees (flow over the port side)									
R3 sonic	16.02	4.18 (2.79)	11.512	10.313	9.935 (10.085)	11.63	15.87 (14.15)	4.2	-6.5
ship's sonic	21.51	3.43 (1.98)	11.147	10.641	10.452 (10.537)	4.75	6.65 (5.78)	5.5	-4.8
psychrometer	18.03	10.12	11.065	10.447	9.479	5.92	16.73	25.4	-17.1
Vaisala	17.83	10.51	10.799	10.434	9.397	3.49	14.92	28.1	-17.7
50 degrees (flow over the port side)									
R3 sonic	16.02	3.12 (2.25)	11.252	10.316	10.055 (10.137)	9.07	11.91 (11.01)	4.2	-5.6
ship's sonic	21.51	2.49 (1.57)	10.876	10.643	10.510 (10.561)	2.19	3.48 (2.98)	4.4	-4.5
psychrometer	18.03	8.52	11.659	10.447	9.678	11.61	20.47	23.6	-12.9
Vaisala	17.83	9.00	11.717	10.434	9.598	12.30	22.08	26.1	-13.7
30 degrees (flow over the port side)									
R3 sonic	16.02	2.20 (1.66)	10.806	10.316	10.137 (10.185)	4.75	6.59 (6.10)	3.3	-5.8
ship's sonic	21.51	1.75 (1.18)	10.678	10.647	10.555 (10.586)	0.29	1.16 (0.86)	3.6	-3.2
psychrometer	18.03	7.84	11.494	10.444	9.743	10.05	17.96	16.4	-8.4
Vaisala	17.83	8.19	11.664	10.431	9.677	11.814	20.53	17.4	-10.5

Instrument	Instrument height z (m)	Vertical displacement Δz ($\Delta z_{t=2}$) (m)	Velocity at instrument site (ms^{-1})	Free stream velocity at z (ms^{-1})	Free stream velocity at $z - \Delta z$ ($z - \Delta z_{t=2}$)	% velocity error at instrument site	% velocity error at instrument site at $z - \Delta z$ ($z - \Delta z_{t=2}$)	Angle of flow to the horizontal (degrees)	Horizontal twist (degrees)
20 degrees (flow over the port side)									
R3 sonic	16.02	1.89 (1.44)	10.507	10.316	10.165 (10.203)	1.85	3.37 (2.98)	3.5	-4.9
ship's sonic	21.51	1.54 (1.05)	10.558	10.646	10.566 (10.592)	-0.83	-0.08 (-0.33)	3.6	-2.3
psychrometer	18.03	7.57	11.162	10.443	9.774	6.88	14.21	14.1	-4.7
Vaisala	17.83	7.87	11.063	10.430	9.715	6.06	13.88	14.6	-7.3
10 degrees (flow over the port side)									
R3 sonic	16.02	1.73 (1.35)	10.249	10.314	10.176 (10.207)	-0.63	0.72 (0.41)	4.2	-4.3
ship's sonic	21.51	1.43 (1.00)	10.506	10.646	10.571 (10.594)	-1.32	-0.62 (-0.83)	3.7	-1.1
psychrometer	18.03	7.54	11.134	10.441	9.776	6.64	13.89	11.7	0.0
Vaisala	17.83	7.89	10.821	10.423	9.710	3.77	11.45	11.4	-2.5
0 degrees (bow-on)									
R3 sonic	16.02	1.67 (1.32)	10.196	10.339	10.207 (10.235)	-1.38	-0.11 (-0.39)	4.3	-1.4
ship's sonic	21.51	1.37 (0.95)	10.489	10.668	10.598 (10.621)	-1.67	-1.03 (-1.24)	3.5	0.1
psychrometer	18.03	5.98	11.196	10.470	9.972	6.94	12.28	13.0	2.6
Vaisala	17.83	6.17	10.567	10.457	9.931	1.05	6.41	13.1	0.2

Instrument	Instrument height z (m)	Vertical displacement Δz ($\Delta z_{t=2}$) (m)	Velocity at instrument site (ms^{-1})	Free stream velocity at z (ms^{-1})	Free stream velocity at $z - \Delta z$ ($z - \Delta z_{t=2}$)	% velocity error at instrument site	% velocity error at instrument site at $z - \Delta z$ ($z - \Delta z_{t=2}$)	Angle of flow to the horizontal (degrees)	Horizontal twist (degrees)
10 degrees (flow over the starboard side)									
R3 sonic	16.02	1.76 (1.41)	10.114	10.314	10.174 (10.202)	-1.94	-0.58 (-0.86)	5.2	0.7
ship's sonic	21.51	1.39 (0.99)	10.525	10.645	10.573 (10.595)	-1.13	-0.45 (-0.66)	3.6	1.4
psychrometer	18.03	7.26	10.301	10.440	9.940	-1.33	3.64	15.8	4.4
Vaisala	17.83	7.69	9.288	10.427	9.899	-10.92	-6.17	16.4	2.5
20 degrees (flow over the starboard side)									
R3 sonic	16.02	1.98 (1.54)	10.267	10.317	10.158 (10.196)	-0.49	1.07 (0.70)	5.4	3.1
ship's sonic	21.51	1.52 (1.03)	10.589	10.647	10.567 (10.593)	-0.55	0.21 (-0.04)	3.4	2.5
psychrometer	18.03	8.54	10.814	10.442	9.660	3.56	11.95	12.6	5.5
Vaisala	17.83	8.99	10.084	10.429	9.584	-3.31	5.21	12.8	4.5
30 degrees (flow over the starboard side)									
R3 sonic	16.02	2.23 (1.76)	10.474	10.317	10.134 (10.177)	1.53	3.35 (2.92)	5.8	4.7
ship's sonic	21.51	1.77 (1.15)	10.727	10.648	10.554 (10.587)	0.74	1.64 (1.32)	3.4	3.4
psychrometer	18.03	11.24	10.497	10.442	9.302	0.53	12.84	13.4	3.9
Vaisala	17.83	12.05	9.851	10.429	9.145	-5.54	7.72	13.9	2.8

Instrument	Instrument height z (m)	Vertical displacement Δz ($\Delta z_{t=2}$) (m)	Velocity at instrument site (ms^{-1})	Free stream velocity at z (ms^{-1})	Free stream velocity at $z - \Delta z$ ($z - \Delta z_{t=2}$)	% velocity error at instrument site	% velocity error at instrument site at $z - \Delta z$ ($z - \Delta z_{t=2}$)	Angle of flow to the horizontal (degrees)	Horizontal twist (degrees)
50 degrees (flow over the starboard side)									
R3 sonic	16.02	3.09 (2.27)	10.654	10.317	10.060 (10.136)	3.26	5.91 (5.11)	7.0	6.6
ship's sonic	21.51	2.56 (1.56)	10.959	10.643	10.506 (10.561)	2.98	4.31 (3.77)	3.9	4.6
psychrometer	18.03	11.17	10.479	10.444	9.334	0.33	12.26	10.0	-1.0
Vaisala	17.83	11.49	9.978	10.431	9.259	-4.34	7.77	9.5	-1.5
70 degrees (flow over the starboard side)									
R3 sonic	16.02	3.95 (2.73)	10.581	10.314	9.960 (10.091)	2.59	6.23 (4.86)	7.5	7.7
ship's sonic	21.51	3.46 (2.00)	11.274	10.641	10.449 (10.535)	5.95	7.89 (7.01)	4.9	4.7
psychrometer	18.03	11.42	9.218	10.443	9.303	-11.73	-0.92	1.8	7.3
Vaisala	17.83	11.77	8.980	10.430	9.218	-13.90	-2.58	1.2	8.0
90 degrees (flow over the starboard side)									
R3 sonic	16.02	4.78 (2.96)	10.904	10.309	9.868 (10.064)	5.77	10.50 (8.35)	7.7	6.0
ship's sonic	21.51	4.34 (2.22)	11.361	10.639	10.390 (10.520)	6.79	9.35 (8.00)	5.0	3.9
psychrometer	18.03	4.98	4.684	10.443	9.046	-55.15	-48.22	-2.1	34.9
Vaisala	17.83	5.28	4.429	10.430	9.094	-57.53	-51.29	-2.2	36.7

Instrument	Instrument height z (m)	Vertical displacement Δz ($\Delta z_{t=2}$) (m)	Velocity at instrument site (ms^{-1})	Free stream velocity at z (ms^{-1})	Free stream velocity at $z - \Delta z$ ($z - \Delta z_{t=2}$)	% velocity error at instrument site	% velocity error at instrument site at $z - \Delta z$ ($z - \Delta z_{t=2}$)	Angle of flow to the horizontal (degrees)	Horizontal twist (degrees)
110 degrees (flow over the starboard side)									
R3 sonic	16.02	6.29 (3.06)	10.917	10.413	9.829 (10.206)	4.83	11.07 (6.97)	8.3	8.0
ship's sonic	21.51	6.22 (2.65)	11.46	10.695	10.368 (10.490)	7.15	10.53 (6.95)	6.5	4.4
psychrometer	18.03	- (-)	1.526	10.523	- (-)	-85.86	- (-)	-	-
Vaisala	17.83	- (-)	1.331	10.512	- (-)	-86.79	- (-)	-	-

11. APPENDIX C: FEMGV and VECTIS commands.

C.1 conversion of Femgv ABAQUS file (file.inp) into VECTIS format

```
abtosf -V 2013.3 -d=3 file.inp
```

```
sftovec -V 2013.3 -d=3 file.SFE
```

B.2 running phase5 using eight cores

```
phase5 -np8 -rdm8 *.INP
```